9-2010

Vibrational Spectroscopy of Intermediates of C-H Bond Activation by Transition Metal Oxide Cations

Gokhan Altinay
University of Massachusetts Amherst, altinay@chem.umass.edu

VIBRATIONAL SPECTROSCOPY OF INTERMEDIATES OF C-H BOND ACTIVATION BY TRANSITION METAL OXIDE CATIONS

A Dissertation Presented

by

GOKHAN ALTINAY

Submitted to the Graduate School of the
University of Massachusetts Amherst in partial fulfillment
of the requirements for the degree of

DOCTOR OF PHILOSOPHY

SEPTEMBER 2010

Department of Chemistry

VIBRATIONAL SPECTROSCOPY OF INTERMEDIATES OF C-H BOND ACTIVATION BY TRANSITION METAL OXIDE CATIONS

A Dissertation Presented

by

GOKHAN ALTINAY

Approved as to style and content by:

_____
Ricardo B. Metz, Chair

_____
Howard D. Stidham, Member

_____
Robert M. Weis, Member

_____
Anthony Dinsmore, Member
Department of Physics

_____
Craig Martin, Department Head
Department of Chemistry

To My Daughter Erin…

When you reach for the stars, you may not quite get one, but you won't come up with a handful of mud either.
-Leo Burnett

ACKNOWLEDGEMENTS

I still remember flying from Istanbul to Boston with mixed emotions in 2003. It was the coldest winter I had ever experienced. Entering Goessman 206 (our lab) I remember meeting Prof. Metz (Rick) who was lying on the floor fixing some instruments. He said “Hi” with his big smile, and it was not cold anymore.
I cannot say enough about Rick. Through those years, I believe I only touched on the surface. He taught me how much a person can push the boundaries and still meet success. He tried to show me how deep the rabbit hole is. A great advisor, good friend, caring brother and sometimes protecting father Rick has meant more to me than a mere major professor. Looking at things from a different angle is an invaluable tool gain I have learned from him. If I were to start my Ph.D. again today, I wouldn’t hesitate to join his group for one second.

I would like to extend my appreciation to the other members of my committee, Professors Howard D. Stidham, Robert M. Weis, and Anthony Dinsmore for their support, time and attention to my research progress. I also thank Prof. Paul Lahti for writing recommendation letters during my post-doc hunt.

In addition to the great experience as a Ph.D. student, I really feel lucky to have Jay Kerwin as a best friend in the first two years to adjust the new culture. Also thanks to the Turkish mafia; Serkan, Ilyas, Deniz, Ilke, Taner, Tansel, Ebru, Erkin, Gizem for helping me to survive my first winter.

Many thanks to family friends; Victor, Daria, Jangwong and Miyong for special dinners.

To my lab friends, Chris, Manori, Murat, Paul, Abdulkadir, Geoff, John and Lee thank you for the great experiences and memories. I specially thank Jan Daluz in the last days of submission for helping me to get correct format of the thesis. Also during the thesis preparation time, I should thank Guven, Ece, Tuba, Suphan and Huseyin who helped to make this period bearable. I shouldn't forget to thank Ada to teach Erin how to walk.

I thank my parents Cemal and Bahar Altinay for their constant and unconditional support, especially to my grandfather Ismail Balkan who played such an important role in my childhood.

Last but not least, I am grateful to my wife Cahide for supporting me during every part of the Ph.D and sacrificing her career to give me a better life forever. I also want to thank my dear daughter Erin for giving me the inspiration to be a better person.

ABSTRACT

VIBRATIONAL SPECTROSCOPY OF INTERMEDIATES OF C-H BOND ACTIVATION BY TRANSITION METAL OXIDE CATIONS

SEPTEMBER 2010

GOKHAN ALTINAY, B.Sc., BOĞAZİÇİ UNIVERSITY

Ph.D., UNIVERSITY OF MASSACHUSETTS AMHERST

Directed by: Professor Ricardo B. Metz

Direct, efficient oxidation of alkanes is a long-standing goal of catalysis. Gas phase FeO^+ can convert methane to methanol and benzene to phenol under thermal conditions. Two key intermediates of these reactions are the $[HO\text{-}Fe\text{-}R]^+$ insertion intermediate and $Fe^+(ROH)$ ($R=CH_3$ or C_6H_5) exit channel complex. This work describes measurements of the vibrational spectra of these intermediates and electronic structure theory calculations of the potential energy surfaces for the reactions. They help to characterize the mechanism for these reactions. Chapter 1 describes previous studies of methane-to-methanol and benzene-to-phenol conversion by gas-phase transition metal oxide cations.

Spectra of gas-phase reaction intermediates are obtained using photofragment spectroscopy, in which absorption of a photon leads to bond breaking. Utuilizing this technique to measure vibrational spectra is challenging, due to the low photon energies involved. Techniques used to measure vibrational spectra of ions – argon tagging, infrared multiple photon dissociation (IRMPD), vibrationally mediated photodissociation (VMP) and infrared laser assisted photodissociation spectroscopy (IRLAPS) are also detailed in chapter 1. The photofragment spectrometer and laser systems used in these studies are described in chapter 2, as is a multi-pass mirror arrangement which I implemented. This greatly improved the quality of vibrational spectra, particularly those measured using IRMPD.

Chapter 3 describes studies of the O-H and C-H stretching vibrations of two intermediates of the $FeO^+ + CH_4$ reaction. These intermediates are selectively formed by reaction of laser ablated Fe^+ with specific organic precursors and are cooled in a supersonic expansion. Vibrations of the sextet and quartet states of the $[HO\text{-}Fe\text{-}CH_3]^+$ insertion intermediate and $Fe^+(CH_3OH)$ exit channel complex are measured by IRMPD and Ar-tagging. Studies of the O-H stretching vibrations of the $[HO\text{-}Fe\text{-}C_6H_5]^+$ and $Fe^+(C_6H_5OH)$ intermediates of the $FeO^+ + C_6H_6$ reaction are discussed in chapter 4. For $Fe^+(C_6H_5OH)$, the O-H stretch is observed at 3598 cm^{-1}. Photodissociation primarily produces $Fe^+ + C_6H_5OH$. IRMPD of $[HO\text{-}Fe\text{-}C_6H_5]^+$ mainly produces $FeOH^+ + C_6H_5$ and the O-H stretch spectrum consists of a peak at ~3700 cm^{-1} with a shoulder at ~3670 cm^{-1}.

Chapter 5 compares three techniques - IRMPD, argon-tagging, and IRLAPS – in the quality of the measured vibrational spectra of $Ag^+(CH_3OH)$ ions produced under identical conditions. The sharpest spectrum is obtained using IRLAPS. The O-H stretch is observed at 3660 cm^{-1}. Monitoring loss of argon from $Ag^+(CH_3OH)(Ar)$ gives a slightly broader peak, with no significant shift. The vibrational spectrum obtained using IRMPD is shifted to 3635 cm^{-1}, is substantially broader, and is asymmetrical, tailing to the red.

TABLE OF CONTENTS

Page

LIST OF TABLES

Table Page

LIST OF FIGURES

Figure Page

CHAPTER 1

INTRODUCTION

1.1 Introduction

From practical, economic and environmental standpoints transition metal catalyzed reactions are set to dominate the chemical industry in the 21st century. Therefore, it is not surprising that the field of transition metal catalysis has been and will remain central to academic and industrial chemistry. The oxidative insertion of transition metals into the C-H bonds of hydrocarbons, a key step in many catalytic reactions, is well-documented.[1, 2] This is challenging to do for simple alkanes, especially for methane due to its very strong C-H bonds.

Methane is abundant - the energy equivalent of global natural gas reserves will soon surpass those of petroleum[3] - yet it is underutilized as a precursor for chemicals and liquid fuels due to the difficulty of transporting this permanent gas.[4] There has thus been a great deal of effort directed towards efficient conversion of methane to easily transportable and more synthetically useful liquids such as larger hydrocarbons or methanol. As a result, the direct, efficient conversion of methane to methanol been called a "holy grail" of catalysis.[5]

Isolated transition metal ions (M^+) in the gas phase have an extremely rich chemistry, activating C-H and C-C bonds in hydrocarbons at room temperature.[6, 7]

$$M^+ + C_nH_{2n+2} \rightarrow MC_nH_{2n}^+ + H_2 \qquad \text{C-H activation} \qquad (1.1)$$

$$M^+ + C_nH_{2n+2} \rightarrow MC_{n-1}H_{2n-2}^+ + CH_4 \qquad \text{C-C activation} \qquad (1.2)$$

This has led to extensive studies of the reactions of M^+ (and related reactions of metal oxide cations MO^+) by several groups.

$$MO^+ + C_nH_{2n+2} \rightarrow M^+ + C_nH_{2n+1}OH \qquad \text{oxidation} \qquad (1.3)$$

In addition to interest in the inherent reactivity, these studies are motivated by the desire to understand the chemistry of a complex condensed phase system through detailed experiments and theory on the simpler gas phase reactions. In this thesis I am going to concentrate on studies of C-H activation by MO^+.

1.2 Methane activation by MO^+

The catalytic conversion of methane to methanol by M^+/MO^+ can be written as

$$M^+ + ½\ O_2 \rightarrow MO^+ \qquad (1.4)$$

$$MO^+ + CH_4 \rightarrow M^+ + CH_3OH \qquad (1.5)$$

The early transition metals bind so strongly to oxygen that reaction of MO^+ with methane is endothermic. Some of the late transition metals bind oxygen so weakly that reaction (1.4) is endothermic.[8]

In 1990 Schröder and Schwarz reported that gas-phase FeO^+ directly converts methane to methanol under thermal conditions(at 300 K).[9] The reaction is efficient, occurring ~20% of collisions, and is quite selective, producing $Fe^+ + CH_3OH$ 40% of the time (the other major product is $FeOH^+ + CH_3$). More recent experiments reveal that NiO^+ and PtO^+ also convert methane to methanol with good efficiency and selectivity.[10] This process can be viewed as a model for alkane hydroxylation. Here, reductive elimination of methanol corresponds to a formal O-atom transfer from the metal oxide to methane.[10] Reactions of gas-phase transition metal oxides with methane are thus a simple model system for the direct conversion of methane to methanol, which

has spurred extensive experimental and computational studies.[8, 10-17] In Table 1.1, the efficiencies ϕ and the product branching ratios for reactions of several metal oxide cations with methane are summarized. [10] The reaction of FeO^+ has attracted particular interest.

1.3 Benzene activation by MO^+

Schwarz, Schröder and coworkers also showed that, under thermal conditions, several gas-phase metal oxide cations MO^+ react efficiently with benzene to produce phenol with good selectivity.[18] The reaction of FeO^+ has been particularly well-studied. This is the prototypical arene reaction. Oxidation of benzene is more exothermic than methane. The reaction efficiency and selectivity are higher as well. In Table 1.3, the efficiencies ϕ and the product branching ratios for reactions of many metal oxide cations with benzene are summarized.

MO^+	% Efficiency (ϕ)	Products		
		$M^+ + CH_3OH$	$MOH^+ + CH_3$	$MCH_2^+ + H_2O$
MnO^+	40	<1	100	-
FeO^{+a}	20	41	57	2
FeO^{+b}	9	39	61	Trace
FeO^{+c}	7	18	82	-
CoO^+	0.5	100	-	-
NiO^+	20	100	-	-
PtO^+	100	25	-	75

Table 1.1 Reaction efficiencies and selectivities of MO^+ with methane at thermal energies. Values are from ref.10,except for: (a)1990 ICR study[9]; (b) 1997 ICR study[15]; (c)1997 SIFT study[15]

MO^+	% Efficiency (ϕ)	Products			
		$M^+ + C_6H_5OH$	$MOH^+ + C_6H_5$	$MC_6H_4^+ + H_2O$	$MC_5H_6^+ + CO$
CrO^+	100	100			
MnO^+	100	67	15	18	
FeO^+	100	56		5	37
CoO^+	100	70			30
NiO^+	100	100			

Table 1.2 Reaction efficiencies and selectivities of MO^+ with benzene at thermal energies.[18, 19]

1.4 Studies of intermediates

1.4.1 Electronic spectroscopy

Our group has studied the reactants, intermediates and products of C-H bond activating reactions by MO^+. Intermediates are formed by reaction of M^+ (produced by laser ablation) with an appropriate organic precursor and subsequently cooled. In previous work, we have measured their electronic spectroscopy and photodissociation dynamics using photofragment spectroscopy in the visible and ultraviolet.[8, 14] In this technique, absorption of photons is monitored by photodissociation. Photofragment spectroscopy not only allows us to study the spectroscopy of these systems but also often gives information on the dissociation dynamics (fragmentation pathways and, in certain cases, kinetic energy release (KER)).

Electronic spectroscopy is useful for measuring positions of excited electronic states. In some cases the electronic spectrum contains resolved vibrational structure, which allows characterization of bonding in the excited state. However, electronic spectroscopy of cold molecules does not give any information on vibrations in the ground state. Also, the electronic spectrum is usually very broad and unstructured particularly for larger molecules and for non-covalent complexes with multiple ligands. Also, complexes with different metals give completely different electronic spectra, which makes it experimentally challenging to study periodic trends.

1.4.2 Vibrational spectroscopy

Obtaining the vibrational (IR) spectra of these systems will broaden our horizons to describe the bonding in the ground states of the ions. Measuring the vibrational spectrum determines the structure and bonding characteristics of the intermediates and illuminates the mechanism of ligand activation by the metal center. IR spectroscopy is advantageous over electronic spectroscopy because it is applicable to all transition metals and their compounds. This feature will increase our ability to examine different organometallic systems in our apparatus. IR spectroscopy of the reaction intermediates will enhance our chance to understand the mechanism of C-H and C-C bond activation reactions of M^+ and MO^+ in the ground electronic state.

1.5 Vibrational spectra of ions

Vibrational spectroscopy is widely used to measure structure and bonding of gas-phase ions.[14, 20-23] For most ions, low ion densities preclude direct absorption studies. As a result, photofragment spectroscopy, in which absorption of light leads to fragment ion formation (and parent ion depletion) is widely used. The primary challenge in applying photofragment spectroscopy to measure vibrational spectra is that light absorption needs to lead to bond breaking. One photon in the O-H stretching region has ~45 kJ/mol of energy, so vibrational photofragment spectroscopy requires studying weakly-bound ions or absorption of multiple photons. Popular techniques for vibrational spectra of ions include infrared multiple photon dissociation, messenger spectroscopy, and two-color techniques such as vibrationally mediated photodissociation and infrared laser assisted photodissociation spectroscopy.

1.5.1 IRMPD

Infrared multiple photon dissociation (IRMPD) can be achieved by IR radiation with high laser fluences. Photodissociation requires that the molecule sequentially absorb several photons, which provide sufficient energy to break the weakest bond, and that this energy find its way from the initially-excited vibration to the dissociation coordinate. A high density of vibrational states and efficient intramolecular vibrational redistribution (IVR) facilitate IRMPD by maintaining the resonance that would otherwise be lost due to anharmonicity and by transferring energy from the vibration excited to the dissociation coordinate.[24] Small molecules such as $Fe^+(CH_3OH)$ and $Ag^+(CH_3OH)$ have relatively high binding energies and low IVR rates, and are thus challenging to study via IRMPD. IRMPD is often more efficient for larger molecules, such as Fe^+(Phenol). Despite its simplicity, IRMPD has several disadvantages. It requires high laser fluences, which can lead to spectral broadening. Multi-passing the IR beam can help to overcome this problem. A more fundamental problem is that IRMPD preferentially dissociates hot molecules, as they require fewer photons to dissociate. This leads to spectral broadening, and often to tailing of peaks to the red.[25]

1.5.2 Argon tagging

Messenger spectroscopy avoids many of the drawbacks of IRMPD. In messenger spectroscopy, a weakly-bound atom or molecule is attached to the ion of interest. Absorption of one IR photon by the chromophore leads to loss of the messenger.[26] This allows much lower laser fluences to be used than for IRMPD. Argon is the most widely used messenger (hence the technique is often termed “argon

tagging").[26-32] Argon usually binds strongly enough that the tagged ions can be readily produced in a molecular beam source, but weakly enough that absorption of one photon leads to dissociation. Vibrational resonances observed via tagging are usually sharp. This is due to the small ion-Ar binding energies, which ensure that Ar-tagged ions are vibrationally cold. Usually, the tag only slightly perturbs the vibrational spectrum of the ion. However, there are some ions for which rare-gas tagging significantly perturbs the spectrum.[32, 33] To check for this, it is useful to measure, and use calculations to predict, spectra with varying number of argon atoms attached, and even to use another tag such as neon.[34]

1.5.3 VMP and IRLAPS

Two-color methods combine one-photon vibrational excitation with selective dissociation of vibrationally excited molecules. In vibrationally mediated photodissociation (VMP), one-photon absorption in the visible or UV promotes the vibrationally excited ions to an excited electronic state from which they dissociate.[24, 35-37] This method requires that the vibrationally excited molecules have a different electronic photodissociation spectrum than the remaining, unexcited molecules. In infrared laser assisted photodissociation spectroscopy (IRLAPS), the vibrationally excited ions absorb several photons from a second infrared laser and dissociate.[38-42] both have the potential to measure vibrational spectra of unperturbed ions with laser-limited resolution. This makes them particularly useful for studying small, strongly bound ions such as $V^+(OCO)$, $Co^+(H_2O)$ and $Ag^+(CH_3OH)$.

This thesis is organized in the following manner. Chapter 2 describes the experimental techniques employed in these studies including details of the apparatus, laser systems and data acquisition used. In Chapter 3, we investigate the potential energy surface (PES) of the reaction $FeO^+ + CH_4 \rightarrow Fe^+ + CH_3OH$ in both sextet and quartet spin states and measure the O-H and C-H stretching frequencies of the $[HO\text{-}Fe\text{-}CH_3]^+$ insertion intermediate and $Fe^+(CH_3OH)$ exit channel complex using infrared multiple photon dissociation (IRMPD) and argon-tagging techniques. In Chapter 4, we extend our vibrational spectroscopy study from the simple alkane to simple aromatic system of benzene to phenol conversion by FeO^+. We measure vibrational spectra of the $[HO\text{-}Fe\text{-}C_6H_5]^+$ insertion intermediate and the $Fe^+(C_6H_5OH)$ exit channel complex in the O-H stretching region. In Chapter 5, we compare three different techniques for vibrational spectroscopy of ions - IRMPD, Ar tagging and IRLAPS - and apply them to $Ag^+(CH_3OH)$. Finally, Chapter 6 discusses extensions and suggestions for future work.

1.6 References

1. Shilov, A. E.; Shul'pin, G. B., Activation of C-H bonds by metal complexes. *Chem. Rev.* **1997,** 97, (8), 2879-2932.
2. Hall, C.; Perutz, R. N., Transition metal alkane complexes. *Chem. Rev.* **1996,** 96, (8), 3125-3146.
3. In 2008 proven world petroleum reserves were 1258 billion barrels (bbl.); gas reserves were 1221 bbl. oil equivalent, and growing much more rapidly than petroleum reserves. Source: BP Statistical Review of World Energy, June 2009.
4. Lunsford, J. H., Catalytic Conversion of Methane to more Useful Chemicals and Fuels: a Challange for the 21st Century. *Catal. Today* **2000,** 63, 165-174.
5. Barton, D. H. R., The Invention of Chemical Reactions. *Aldrichim. Acta* **1990,** 23, 3-10.
6. Eller, K.; Schwarz, H., Organometallic Chemistry in the Gas Phase. *Chem. Rev.* **1991,** 91, 1121-1177.
7. Weisshaar, J. C., Bare Transition Metal Atoms in the Gas Phase: Reactions of M, M^+ and M^{+2} with Hydrocarbons. *Acc. Chem. Res.* **1993,** 26, 213-219.
8. Metz, R. B., Photofragment Spectroscopy of Covalently Bound Transition Metal Complexes: A Window into C-H and C-C Bond Activation by Transition Metal Ions. *Int. Rev. Phys. Chem.* **2004,** 23, (1), 79-108.
9. Schröder, D.; Schwarz, H., FeO^+ Activates Methane. *Angew. Chem. Intl. Ed. Engl.* **1990,** 29, 1433-1434.
10. Schröder, D.; Schwarz, H., C-H and C-C Bond Activation by Bare Transition-Metal Oxide Cations in the Gas Phase. *Angew. Chem. Int. Ed. Engl.* **1995,** 34, 1973-1995.
11. Schröder, D.; Schwarz, H.; Shaik, S., Characterization, Orbital Description, and Reactivity Patterns of Transition-Metal Oxo Species in the Gas Phase. *Struct. Bonding* **2000,** 97, 91-123.
12. Bohme, D. K.; Schwarz, H., Gas-Phase Catalysis by Atomic and Cluster Metal Ions: The Ultimate Single-Site Catalysts. *Angew. Chem. Int. Ed. Engl.* **2005,** 44, (16), 2336-2354.
13. Schroder, D.; Schwarz, H., Gas-phase activation of methane by ligated transition-metal cations. *Proc. Nat. Acad. Sci.* **2008,** 105, (47), 18114-18119.
14. Metz, R. B., Spectroscopy of the Potential Energy Surfaces for C-H and C-O Bond Activation by Transition Metal and Metal Oxide Cations. *Adv. Chem. Phys.* **2008,** 138, 331-373.
15. Schröder, D.; Schwarz, H.; Clemmer, D. E.; Chen, Y.; Armentrout, P. B.; Baranov, V.; Bohme, D. K., Activation of Hydrogen and Methane by Thermalized FeO^+ in the Gas Phase as Studied by Multiple Mass Spectrometric Techniques. *Int. J. Mass Spectrom. Ion Proc.* **1997,** 161, 175-191.
16. Shiota, Y.; Yoshizawa, K., Methane-to-Methanol Conversion by First-Row Transition-Metal Oxide Ions: ScO^+, TiO^+, VO^+, CrO^+, MnO^+, FeO^+, CoO^+, NiO^+, and CuO^+. *J. Am. Chem. Soc.* **2000,** 122, 12317-12326.
17. Yoshizawa, K.; Shiota, Y.; Yamabe, T., Methane-Methanol Conversion by MnO^+, FeO^+, and CoO^+: A Theoretical Study of Catalytic Activity. *J. Am. Chem. Soc.* **1998,** 120, 564-572.

18. Ryan, M. F.; Stockigt, D.; Schwarz, H., Oxidation of Benzene Mediated by First-Row Transition-Metal Oxide Cations - the Reactivity of ScO^+ through NiO^+ in Comparison. *J. Am. Chem. Soc.* **1994,** 116, (21), 9565-9570.
19. Schröder, D.; Schwarz, H., Benzene Oxidation By 'Bare' FeO^+ in the Gas Phase. *Helv. Chim. Acta* **1992,** 75, (4), 1281-1287.
20. Duncan, M. A., Frontiers in the Spectroscopy of Mass-Selected Molecular Ions. *Int. J. Mass Spectrom.* **2000,** 200, 545-569.
21. Bieske, E. J.; Dopfer, O., High-Resolution Spectroscopy of Cluster Ions. *Chem. Rev.* **2000,** 100, (11), 3963-3998.
22. MacAleese, L.; Maitre, P., Infrared spectroscopy of organometallic ions in the gas phase: From model to real world complexes. *Mass Spectrom. Rev.* **2007,** 26, (4), 583-605.
23. Oomens, J.; Sartakov, B. G.; Meijer, G.; Von Helden, G., Gas-Phase Infrared Multiple Photon Dissociation Spectroscopy of Mass-Selected Molecular Ions. *Int. J. Mass Spectrom.* **2006,** 254, (1-2), 1-19.
24. Citir, M.; Altinay, G.; Metz, R. B., Electronic and Vibrational Spectroscopy and Vibrationally Mediated Photodissociation of $V^+(OCO)$. *J. Phys. Chem. A* **2006,** 110, 5051-5057.
25. Altinay, G.; Citir, M.; Metz, R. B., Vibrational Spectroscopy of Intermediates in Methane-to-Methanol Conversion by FeO^+. *J. Phys. Chem. A* **2010,** 114, (15), 5104-5112.
26. Okumura, M.; Yeh, L. I.; Meyers, J. D.; Lee, Y. T., Infrared Spectra of the Cluster Ions $H_7O_3^+$-H_2 and $H_9O_4^+$-H_2. *J. Chem. Phys.* **1986,** 85, 2328-2329.
27. Corcelli, S. A.; Kelley, J. A.; Tully, J. C.; Johnson, M. A., Infrared Characterization of the Icosahedral Shell Closing in $Cl^-\cdot H_2O\cdot Ar_n$ ($1 \leq n \leq 13$) Clusters. *J. Phys. Chem. A* **2002,** 106, 4872-4879.
28. Duncan, M. A., Infrared Spectroscopy to Probe Structure and Dynamics in Metal Ion-molecule Complexes. *Int. Rev. Phys. Chem.* **2003,** 22, (2), 407-435.
29. Vaden, T. D.; Lisy, J. M.; Carnegie, P. D.; Pillai, E. D.; Duncan, M. A., Infrared Spectroscopy of the $Li^+(H_2O)Ar$ complex: the role of internal energy and its dependence on ion preparation. *Phys. Chem. Chem. Phys.* **2006,** 8, (26), 3078-3082.
30. Furuya, A.; Tsuruta, M.; Misaizu, F.; Ohno, K.; Inokuchi, Y.; Judai, K.; Nishi, N., Infrared photodissociation spectroscopy of $Al^+(CH_3OH)_n$ (n=1-4). *J. Phys. Chem. A* **2007,** 111, (27), 5995-6002.
31. Asmis, K. R.; Sauer, J., Mass-selective vibrational spectroscopy of vanadium oxide cluster ions. *Mass Spec. Rev.* **2007,** 26, (4), 542-562.
32. Dopfer, O., Spectroscopic and theoretical studies of CH_3^+-Rg_n clusters (Rg = He, Ne, Ar): From weak intermolecular forces to chemical reaction mechanisms. *Int. Rev. Phys. Chem.* **2003,** 22, (3), 437-495.
33. Hammer, N. I.; Diken, E. G.; Roscioli, J. R.; Johnson, M. A.; Myshakin, E. M.; Jordan, K. D.; McCoy, A. B.; Huang, X.; Bowman, J. M.; Carter, S., The Vibrational Predissociation Spectra of the $H_5O_2^+\bullet RG_n$ (RG=Ar,Ne) Clusters: Correlation of the Solvent Perturbations in the Free OH and Shared Proton Transitions of the Zundel Ion. *J. Chem. Phys.* **2005,** 122, (24), Art. No. 244301.

34. Solca, N.; Dopfer, O., Microsolvation of the Phenol Cation (Ph^+) in Nonpolar Environments: Infrared Spectra of Ph^+-L_n (L=He, Ne, Ar, N_2, CH_4). *J. Phys. Chem. A* **2001,** 105, 5637-5645.
35. Honovich, J. P.; Dunbar, R. C., Vibrational Spectroscopy and Photo-Dissociation Properties of Ions as Determined by Two-Laser Photo-Dissociation Techniques. *J. Phys. Chem.* **1983,** 87, (19), 3755-3758.
36. Crim, F. F., Vibrationally Mediated Photodissociation: Exploring Excited-State Surfaces and Controlling Decomposition Pathways. *Annu. Rev. Phys. Chem.* **1993,** 44, 397.
37. Rosenwaks, S. Z., *Vibrationally Mediated Photodissociation*. The Royal Society of Chemistry: Cambridge, 2009.
38. Yeh, L. I.; Okumura, M.; Meyers, J. D.; Price, J. M.; Lee, Y. T., Vibrational Spectroscopy of the Hydrated Hydronium Cluster Ions $H_3O^+ \cdot (H_2O)_n$ (n=1,2,3). *J. Chem. Phys.* **1989,** 91, 7319-7330.
39. Watson, C. H.; Zimmerman, J. A.; Bruce, J. E.; Eyler, J. R., Resonance-Enhanced Two-Laser Infrared Multiple Photon Dissociation of Gaseous Ions. *J. Phys. Chem.* **1991,** 95, (16), 6081-6086.
40. Boyarkin, O. V.; Settle, R. D. F.; Rizzo, T. R., Vibrational Overtone Spectra of Jet-Cooled CF_3H by Infrared-Laser Assisted Photofragment Spectroscopy. *Ber. Bunsen-Ges. Phys. Chem. Chem. Phys.* **1995,** 99, (3), 504-513.
41. Boyarkin, O. V.; Lubich, L.; Settle, R. D. F.; Perry, D. S.; Rizzo, T. R., Intramolecular energy transfer in highly vibrationally excited methanol.1. Ultrafast dynamics. *J. Chem. Phys.* **1997,** 107, (20), 8409-8422.
42. Boyarkin, O. V.; Rizzo, T. R.; Rueda, D. S.; Quack, M.; Seyfang, G., Nonlinear Intensity Dependence in the Infrared Multiphoton Excitation of Methanol Preexcited to Different Energies. *J. Chem. Phys.* **2002,** 117, 9793-9805.

CHAPTER 2

EXPERIMENTAL

2.1 Apparatus Overview and Modifications

The apparatus in which all the studies were performed is schematically illustrated in Figure 2.1 below. It is a dual Wiley-McLaren type time-of-flight mass spectrometer. It has been described in detail previously.[1, 2] I will describe each part in detail.

(A) Minilite (Continuum) ablation laser is focused onto a rotating metal rod to produce ions.

(B) Selected transition metal rod. Laser ablation of a metal rod creates a mixture of metal clusters, neutrals, and multi-charged ions in addition to the desired singly charged cations.

(C) Metal ions react with a precursor gas, which is introduced through a pulsed valve, to produce the ion of interest. Before they reach the skimmer, collisions with the bath gas cool the ions. Backing pressure of the gas mixture is generally 1-5 atm.

(D) Skimmer: It allows ions to enter the accelerator along the beam axis.

(E) Accelerator: Using a pulsed electric field ions gain 1800 V kinetic energy at this point.

(F) Re-reference the ions to ground potential before entering the field-free flight tube.

(G) Einzel Lens and **(H)** Deflectors: Focus and guide the ions through a hole into the detector chamber.

(I) Mass Gate: It selects the ions that will be photodissociated. It is the final deflector, which turns the ion beam to pass through the 5° angle through the reflectron.

(K) Reflectron: It decelerates the ions and then reaccelerates them, so that fragment ions will have different flight times from the parent.[3]Multi-pass mirrors were added in this region and will be described in section 2.2.

(J) Photodissociation Laser: Target ions are photodissociated at the turning point of the reflectron. Fundamental or frequency doubled output of a tunable Nd:YAG pumped dye or IR laser photodissociates the selected ions.

Dye Laser System: it is tunable between 220 to 900 nm with 0.08 cm^{-1} linewidth with mixing and doubling crystals.

The IR laser System: Using a combination of 532 nm OPO and 1064 nm pumped OPA system we get tunable near IR light with a range between 712 to 880 nm and mid IR from 1.35 to 5.0 microns. (2000-7400 cm^{-1})

(L) Detector: The detector consists of a stack of two 40 mm dia. micro-channel plates, which efficiently detect ions and are sufficiently large to ensure all fragments and parents are detected. We can identify the masses of both parent and fragments by their flight times. The final signal is amplified and collected on a digital oscilloscope. Using a gated integrator system we can also measure the area under the peaks. A Labview program enables us to average the signal and save as a wavelength scan format. Also, immediate identification of the dissociation channels at a given wavelength is possible

using a difference spectrum with laser on and off system. The repetition rate for the experiment is that of the ablation and fragmentation lasers, 20 Hz.

The source region (to the left of the skimmer **(D)**) is maintained at ~ 10^{-4} torr by a 6" diffusion pump; the differential region (between the skimmer and the ion optics **(G)**) is kept at ~ 10^{-6} torr by a 4" diffusion pump, and the detector **(L)** is kept at ~ 10^{-8} torr by a turbomolecular pump.

2.2 Multi-pass laser beam system

In order to maximize the photodissociation yield, particularly in infrared multiple-photon dissociation, I implemented a multipass system for the dissociation laser(s). We considered several designs, and settled on a "Perry cell." [4] This is a multipass cell with two-spherical mirrors which has also been used for molecular beam absorption spectroscopy using a laser source. It is schematically shown in Figure 2.2. This system has following features:

i) Efficient coupling to a collimated molecular beam because the rays collectively form a small, easily adjustable waist in the center of the cell.

ii) All rays nearly perpendicular to a collimated molecular beam, minimizing Doppler broadening. The pattern of reflected spots on each mirror approximates a narrow parabola.

iii) The number of passes is easily and quickly adjustable. We obtain 21 passes in our system.

iv) Off-the shelf commercial mirrors may be used.

Quantity	Symbol
Radius of curvature of the mirrors	R
Mirror spacing	L
Fractional deviation of mirror spacing from concentricity	ϵ
Height of each spot pattern on each mirror	h
Vertical waist of ray pattern in center of cell	a
Number of passes	N
Number of spots on each mirror	n
Wavelength	λ
Spot size at center	ω_o
Spot size at mirrors	ω

Table 2.1 Parameters and typical values for Perry cell. [4]

The number of passes depends on the radius of curvature of the mirrors and, very sensitively, on the distance between them. Following Kaur, et al.[4] one can analyse the Perry cell as follows (See Table 2.1 for definitions of symbols used).

The number of spots on each mirror is

$$n=2h/a \qquad (2.1)$$

The total number of passes through the cell is

$$N=2n + 1 \qquad (2.2)$$

In the concentric limit, the mirrors would be spaced by L=2R. In practice, the spacing used is very close to this value. The fractional deviation of L from the concentric value is

$$\epsilon =(2R-L)/2R \qquad (2.3)$$

typically, $\epsilon = 0.0015$. In order to maximize the number of passes, the spot size at the mirror should remain constant. The required spot size at each mirror is

$$\omega = (L \lambda /2 \pi)^{1/2} \epsilon^{-1/4} \qquad (2.4)$$

The number of spots on each mirror is

$$n= 0.25 \pi \epsilon^{-1/2} \qquad (2.5)$$

Combining equations 2.4 and 2.5,

$$\omega = (2 n L \lambda)^{1/2} / \pi \qquad (2.6)$$

Including the constraint that clipping of the input beam be minimized, one can obtain

$$n_{max} = (h^2 \pi^4 / 18 L \lambda)^{1/3} \qquad (2.7)$$

Kaur et al. obtained N=41 passes. In our experiment, the vacuum system limits the allowed spacing between the mirrors. In addition, since we wish to use standard, off-

the-shelf mirrors, this greatly limits their radius of curvature. We use 2" diameter mirrors, with a 6" radius of curvature. The mirrors are silver coated, so they are >98% reflective throughout the mid-IR. The mirrors are mounted on 3-control adjustable mirror mounts. In addition to tweaking the alignment of the mirrors, this allows us to change the distance between them. As equation 2.5 shows, this adjustment is critical in maximizing the number of passes. Equation 2.4 implies that the light entering the Perry cell is not collimated. Rather, it focuses just before the first reflection. In our system, the light enters the vacuum chamber through an anti-reflection coated ZnSe lens with a focal length of ~12." As the IR laser beam is not visible to the naked eye, we overlap the IR beam with a visible HeNe laser beam, which we use for alignment. The beams are combined using a ZnSe flat, which is placed at Brewster's angle to the IR laser beam. The HeNe is reflected off the top surface of the ZnSe flat. We find that it is very easy to obtain 3-4 spots on each mirror (~8 passes), but that obtaining more passes requires carefully tuning the separation of the mirrors. We can obtain (and maintain) 10 spots (21 passes) without too much effort. The spots get slowly, but consistently larger. Obtaining more passes would likely require adjusting the focal length of the lens. After 20 passes, assuming 98% reflectivity, the incident beam retains 67% of its initial intensity.

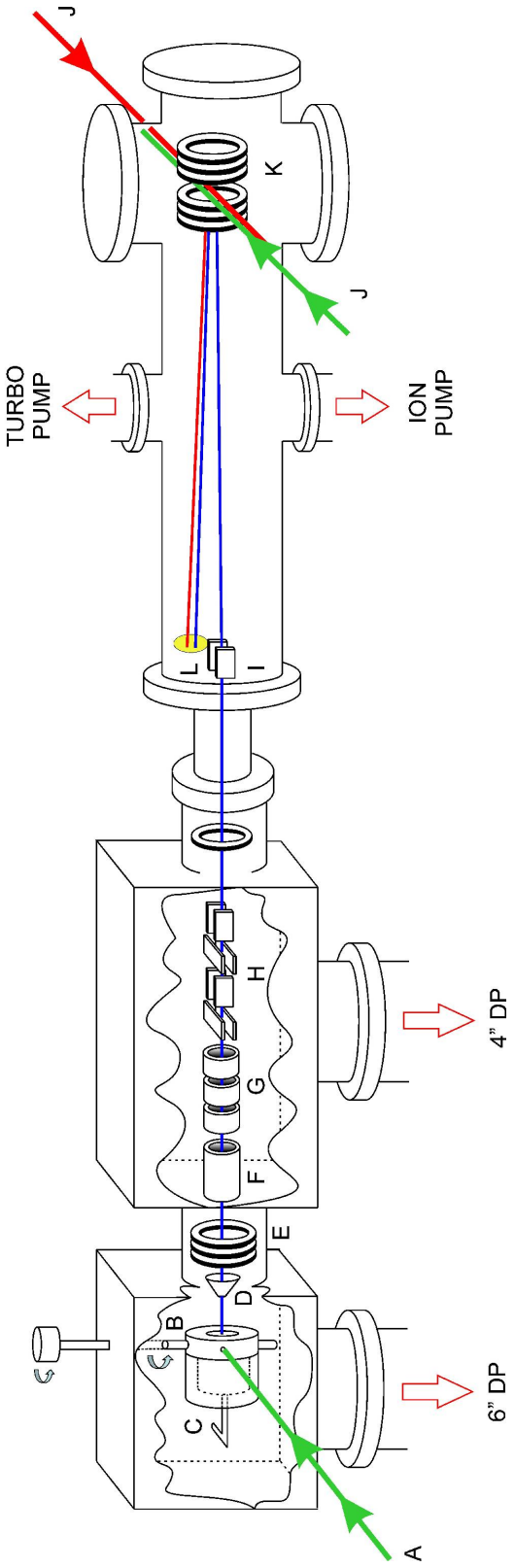

Figure 2.1 Schematic view of the Dual Time-of-Flight Reflectron Mass Spectrometer. Labels are described in the text.

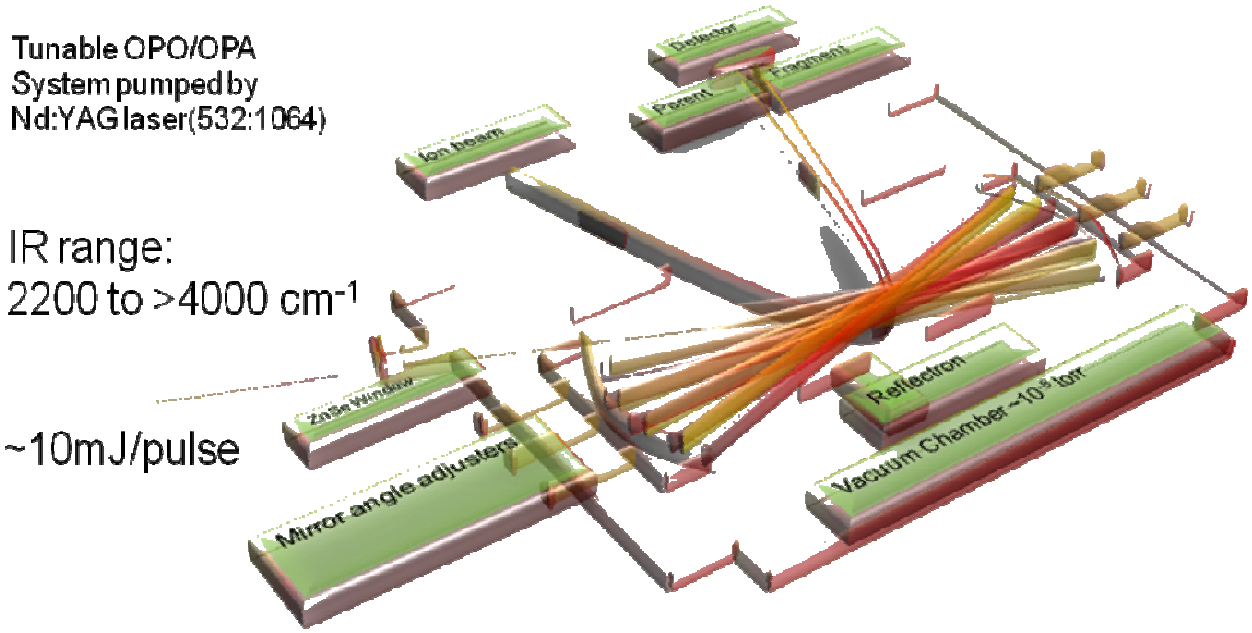

Figure 2.2 **Perry-type multipass mirror setup.**

2.3 Laser Systems

These studies employed two Nd:YAG lasers (Continuum Powerlite 8020 and Minilite II), a custom-made tunable Nd:YAG-pumped IR laser (LaserVision), and a pulsed, tunable CO_2 laser (Infralight SP) in these studies. The Nd:YAG lasers will be briefly described. Due to installation of the new IR laser system and first time use, It will be discussed in detail in section 2.3.2.

2.3.1 Nd:YAG Lasers

Powerlite 8020 and Surelite I series are high energy Q-switched Nd-YAG lasers; the lasing medium is a Nd:YAG rod (Nd^{+3} ion at low concentration in yttrium aluminum garnet) excited by the discharge of energy from high voltage flashlamps. The aim of Q-switching is to achieve a large population inversion in the absence of the resonant cavity, then to force the population-inverted medium into a cavity, and hence to obtain a sudden pulse of radiation. In practice, Q-switching gives pulses of about 5 ns duration. The technique allows the production of light pulses with extremely high peak power, much higher than would be produced by the same laser if it were operating in a continuous wave mode.

The Powerlite 8020 can produce >l J/pulse output at 1064 nm, ~ 550 mJ/pulse at 532 nm, and ~ 300 mJ/pulse at 355 nm. We can use a maximum of 550 mJ/pulse at 1064 nm to pump the IR laser system. The linewidth is ~0.7 cm^{-1} at 1064 nm. In addition, the oscillator can be injection seeded, reducing the linewidth to ~ 0.001 cm^{-1}. This is useful in mixing the Nd:YAG fundamental with the dye laser output, or for pumping a narrow band optical parametric oscillator (OPO) such as our IR laser system.

The Surelite I-20 produces ~420 mJ/pulse at 1064 nm, ~160 mJ/pulse at 532 nm, and ~60 mJ/pulse at 355 nm. The Minilite laser is used for ablation of the metal rod. Usually, 15 mJ power per pulse at 532 nm is enough for vaporization. All Nd:YAG lasers operate at 20 Hz repetition rate. The ablation laser flash lamps are triggered by a digital delay generator. The Q-switch is internally clocked to fire ~ 150 µs later. Because of the experimental need for precise timing of the dissociation lasers, the flashlamps and Q-switch are separately and externally triggered by the pulse generator. This timing is particularly important for the vibrationally mediated photodissociation experiments, where the delay between the IR and visible lasers is ~40 ns.

2.3.2 IR Laser

The IR laser system used in our experiment is a two-stage nonlinear device designed to convert the fixed-frequency output of a Nd:YAG laser system into tunable radiation in the mid-infrared. Using a combination of a 532 nm pumped optical parametric oscillator (OPO) and a 1064 nm pumped optical parametric amplifier (OPA), the system will produce an output that is tunable from 712 to 880 nm and from 1.35 to 5.0 microns using a single set of nonlinear crystals.

The system is pumped by an injection seeded Powerlite 8020 Nd:YAG laser producing roughly 550 mJ/pulse at 1064 nm. A beamsplitter divides the horizontally polarized incoming 1064 nm pump into two separate beam lines. One beam is frequency doubled in KTP to provide the 532 nm pump light for the OPO while the second is directed through a delay before recombination with the idler output of the first

stage. The combined beams are then directed into a 1064 nm pumped OPA stage for difference-frequency generation.

In both the 532 and 1064 nm stages, pairs of crystals of equal length are used and counter-rotated to compensate for beam displacement. Two KTP crystals are used in the 532 nm pumped oscillator stage. The OPO "divides" light at 532 nm (18797 cm^{-1}) into a visible signal beam (tunable from 710 nm to 880 nm, or 11364 – 14085 cm^{-1}) and a complementary near-IR idler beam (2.1 – 1.35 microns, or 7433 – 4712 cm^{-1}). The OPO uses a grazing incidence grating cavity design, which reduces the bandwidth of the visible output to ~0.2 cm^{-1}. The OPA uses four KTA crystals to produce the near-IR difference between the 1064 nm (9398 cm^{-1}) pump beam and the idler beam, nominally producing light from 1965 to 4686 cm^{-1} (2.1 – 5.1 microns). In practice, the IR laser can produce 5 mJ/pulse from 712 to 880 nm, 12 mJ/pulse for the range 1.5 to 3.5 microns, 7 mJ/pulse at 3.7 microns, 4.5 mJ/pulse at 4.0 microns, 3 mJ/pulse at 4.5 microns, and 0.5 mJ/pulse at 4.9 microns. The drop in power at longer wavelength is due to absorption by the KTA. If the IR laser is pumped by a seeded Nd:YAG laser, the linewidth in the mid-IR is determined by the grating and is ~0.2 cm^{-1}. If an unseeded Nd:YAG is used for pumping, the linewidth is ~0.7 cm^{-1} (the linewidth of the Nd:YAG fundamental). For survey scans, a mirror can be used instead of the grating, which also leads to ~ 1 cm^{-1} linewidth, but gives higher power.

The wavelength is controlled by a servo motor; the crystal angles are each controlled by a servo, as the optimum crystal angle depends quite strongly on wavelength. All OPO and OPA crystals are controlled through a Microsoft Windows

based program running on a personal computer. Calibration of the IR laser system is discussed in section 2.5.

2.3.3 CO_2 Laser

The CO_2 laser is a custom-made short pulse, tunable laser made by Optosystems, Ltd. Most CO_2 lasers operate either continuously, or in pulsed mode, with millisecond pulses. In our experiments, the ion packet is in the reflectron for such a short time that any light lasting longer than ~200 ns does not overlap the ion beam. Our CO_2 laser produces short pulses by using platinum electrodes (rather than nickel) and by using a gas mixture of 15% CO_2 and 4% N_2 in helium. The typical gas mixture used in longer-pulse CO_2 lasers is 5% CO_2 and 15% N_2 in helium.

The CO_2 laser is line-tunable over the P and R branches of two bands. The available wavelengths and powers are shown in table 2.2. The relationship between the grating angle and the wavelength is given by the grating equation:

$$\lambda = A \sin(\Theta + \Theta_o) \qquad (2.8)$$

where λ is in microns. To calibrate the laser, one fires the beam through a bag containing some ammonia; a loud "snap" is heard if the CO_2 laser line is coincident with an NH_3 absorption (photoacoustic effect). In this way one identifies a few lines in each band. For our laser, A=13.36922 microns and Θ_o = 124.78º. The known and predicted line positions are shown in table 2.2.

Line #	Position deg.sec	Position deg.	Line	µm	cm^{-1}	Energy mJ/pulse	predict cm^{-1}	Diff. cm^{-1}
1	1.36	1.600	10P36	10.764	929.02	50	929.060	0.040
2	1.46	1.767	10P34	10.741	931.01	80	931.059	0.049
3	1.55	1.917	10P32	10.719	932.92	50	932.872	-0.048
4	2.05	2.083	10P30	10.696	934.93	360	934.903	-0.027
5	2.15	2.250	10P28	10.675	936.77	110	936.951	0.181
6	2.24	2.400	10P26	10.653	938.7	100	938.808	0.108
7	2.33	2.550	10P24	10.632	940.56	440	940.679	0.119
8	2.41	2.683	10P22	10.611	942.42	495	942.354	-0.066
9	2.49	2.817	10P20	10.591	944.2	470	944.040	-0.160
10	2.58	2.967	10P18	10.571	945.98	300	945.950	-0.030
11	3.07	3.117	10P16	10.551	947.78	190	947.875	0.095
12	3.15	3.250	10P14	10.532	949.49	140	949.597	0.107
13	3.23	3.383	10P12	10.513	951.2	140	951.332	0.132
14	3.3	3.500	10P10	10.494	952.93	180	952.858	-0.072
15	3.38	3.633	10P8	10.476	954.56	190	954.614	0.054
16	3.45	3.750	10P6	10.459	956.11	120	956.160	0.050
17	4.36	4.600	10R8	10.334	967.68	240	967.698	0.018
18	4.48	4.800	10R12	10.303	970.59	430	970.484	-0.106
19	4.54	4.900	10R14	10.289	971.91	130	971.888	-0.022
20	5	5.000	10R16	10.274	973.33	350	973.299	-0.031
21	5.05	5.083	10R18	10.260	974.66	490	974.480	-0.180
22	5.11	5.183	10R20	10.247	975.9	200	975.904	0.004
23	5.22	5.367	10R24	10.220	978.47	260	978.532	0.062
24	5.27	5.450	10R26	10.207	979.72	390	979.735	0.015
25	5.32	5.533	10R28	10.195	980.87	350	980.943	0.073
26	5.37	5.617	10R30	10.182	982.13	270	982.156	0.026

Table 2.2 CO_2 laser line assignment and calibration

27	5.41	5.683	10R32	10.170	983.28	190	983.131	-0.149
28	5.46	5.767	10R34	10.159	984.35	100	984.353	0.003
29	5.51	5.850	10R36	10.147	985.51	50	985.580	0.070
30	8.51	8.850	9P34	9.675	1033.59	60	1033.401	-0.189
31	9.05	9.083	9P30	9.639	1037.45	300	1037.437	-0.013
32	9.18	9.300	9P26	9.604	1041.23	250	1041.229	-0.001
33	9.25	9.417	9P24	9.588	1042.97	455	1043.288	0.318
34	9.31	9.517	9P22	9.569	1045.04	320	1045.063	0.023
35	9.37	9.617	9P20	9.552	1046.9	50	1046.848	-0.052
36	9.48	9.800	9P16	9.520	1050.42	160	1050.143	-0.277
37	9.55	9.917	9P14	9.504	1052.19	176	1052.257	0.067
38	10	10.000	9P12	9.488	1053.96	130	1053.775	-0.185
39	10.06	10.100	9P10	9.473	1055.63	60	1055.604	-0.026
40	10.54	10.900	9R8	9.342	1070.43	20	1070.594	0.164
41	10.58	10.967	9R10	9.329	1071.93	220	1071.872	-0.058
42	11.02	11.033	9R12	9.317	1073.31	310	1073.154	-0.156
43	11.07	11.117	9R14	9.306	1074.58	110	1074.764	0.184
44	11.11	11.183	9R16	9.294	1075.96	467	1076.056	0.096
45	11.15	11.250	9R18	9.282	1077.35	340	1077.354	0.004
46	11.19	11.317	9R20	9.271	1078.63	60	1078.655	0.025
47	11.22	11.367	9R22	9.261	1079.8	50	1079.635	-0.165
48	11.27	11.450	9R24	9.250	1081.08	230	1081.273	0.193
49	11.3	11.500	9R26	9.240	1082.25	280	1082.259	0.009
50	11.34	11.567	9R28	9.230	1083.48	280	1083.578	0.098
51	11.38	11.633	9R30	9.220	1084.63	210	1084.902	0.272
52	11.41	11.683	9R32	9.210	1085.74	190	1085.898	0.158
53	11.44	11.733	9R34	9.201	1086.84	50	1086.897	0.057

Line #	Position deg.sec	Position deg.	Line	µm	cm^{-1}	Energy mJ/pulse	predict cm^{-1}	Diff. cm^{-1}

Table 2.2, Continued CO_2 laser line assignment and calibration

2.4 Photofragment Spectroscopy

Photodissociation requires the absorption of a photon with sufficient energy to break a bond; furthermore, bond cleavage must occur on a time scale faster than that for fluorescence. In photofragment spectroscopy, monitoring fragment yield at a single wavelength produces a time of flight mass spectrum, identifying the dissociation products and corresponding branching ratios. If over a series of runs the area under one fragment peak is integrated with respect to a varying wavelength, then a photodissociation spectrum will be produced showing those molecules which absorb a photon to give a particular fragment.

After each run (each time the dissociation laser is fired, at a particular wavelength, and fragments are detected), a conventional time-of-flight mass spectrum is produced. Measuring a mass spectrum with the laser ON and subtracting one obtained with the laser OFF give a difference mass spectrum, see figure 2.3. This measurement immediately reveals the percent dissociation of the parent. It also gives information on the masses of the fragment ions produced, and their branching ratios.

Monitoring the yield of a particular fragment ion as a function of laser wavelength gives the photodissociation spectrum. This is the product of the absorption spectrum and the photodissociation quantum yield. The photodissociation spectrum is measured using a gated integrator for each fragment of interest, and one for the parent, for normalization. In some cases, monitoring different fragments gives different photodissociation spectra, as is observed in chapters 3.3.3.1 and 4.3.2.

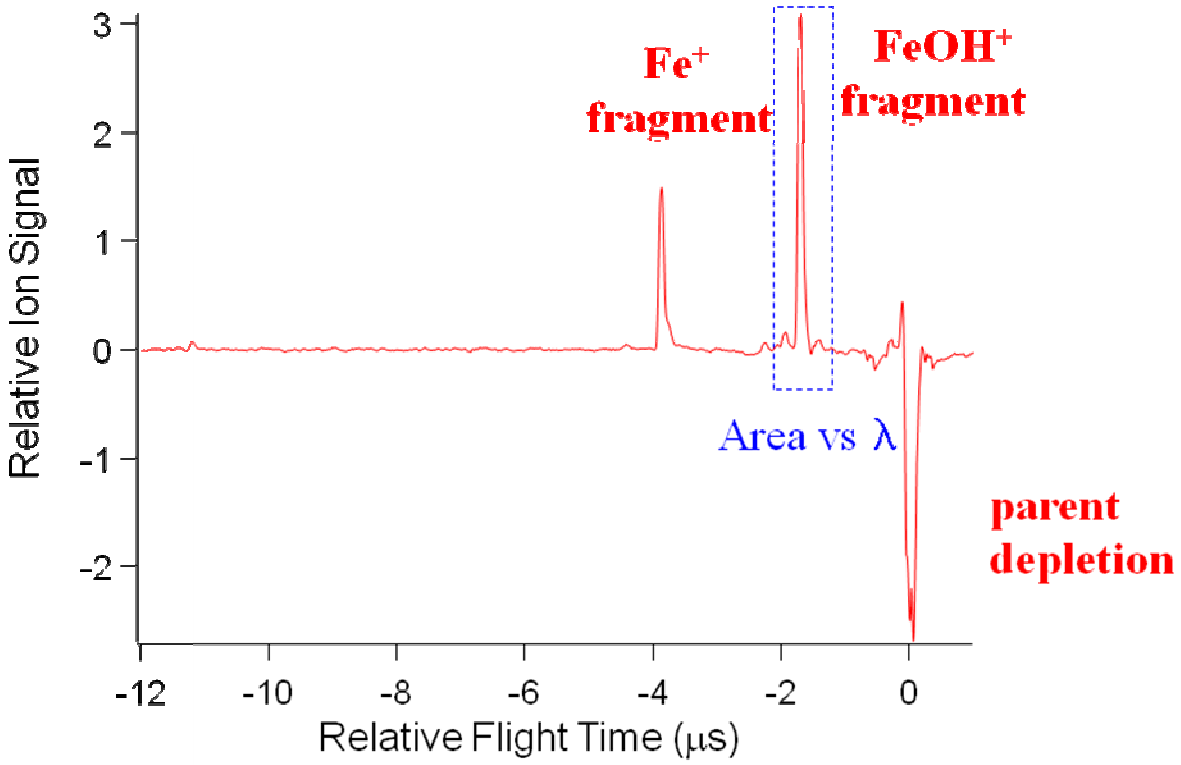

Figure 2.3 Difference mass spectrum obtained from photodissociating $[HO\text{-}Fe\text{-}CH_3]^+$ at 300 nm.

2.5 Laser Calibration

Calibration of the wavelengths of our laser systems is essential for the assignment of the peaks in the spectra and to ensure accurate spectroscopy. There are two fundamental methods of determining the wavelength of a laser, *spectroscopic calibration* and *instrumental measurement*.[5] Instrumental measurement of is very difficult for pulsed lasers, so we use spectroscopic calibration.

Recording standard spectra is the simplest way to measure laser wavelength. In each spectroscopic region, this can be achieved by absorption spectra of simple, well-characterized systems. The choice of species depends entirely on the region of the spectrum under study, but in general small, stable molecules are employed.[6] To record the absorption spectra we typically use the photoacoustic technique. For calibration in the mid-IR, we typically use water and methane. A small portion of calibration spectra in two regions are shown in figure 2.4.

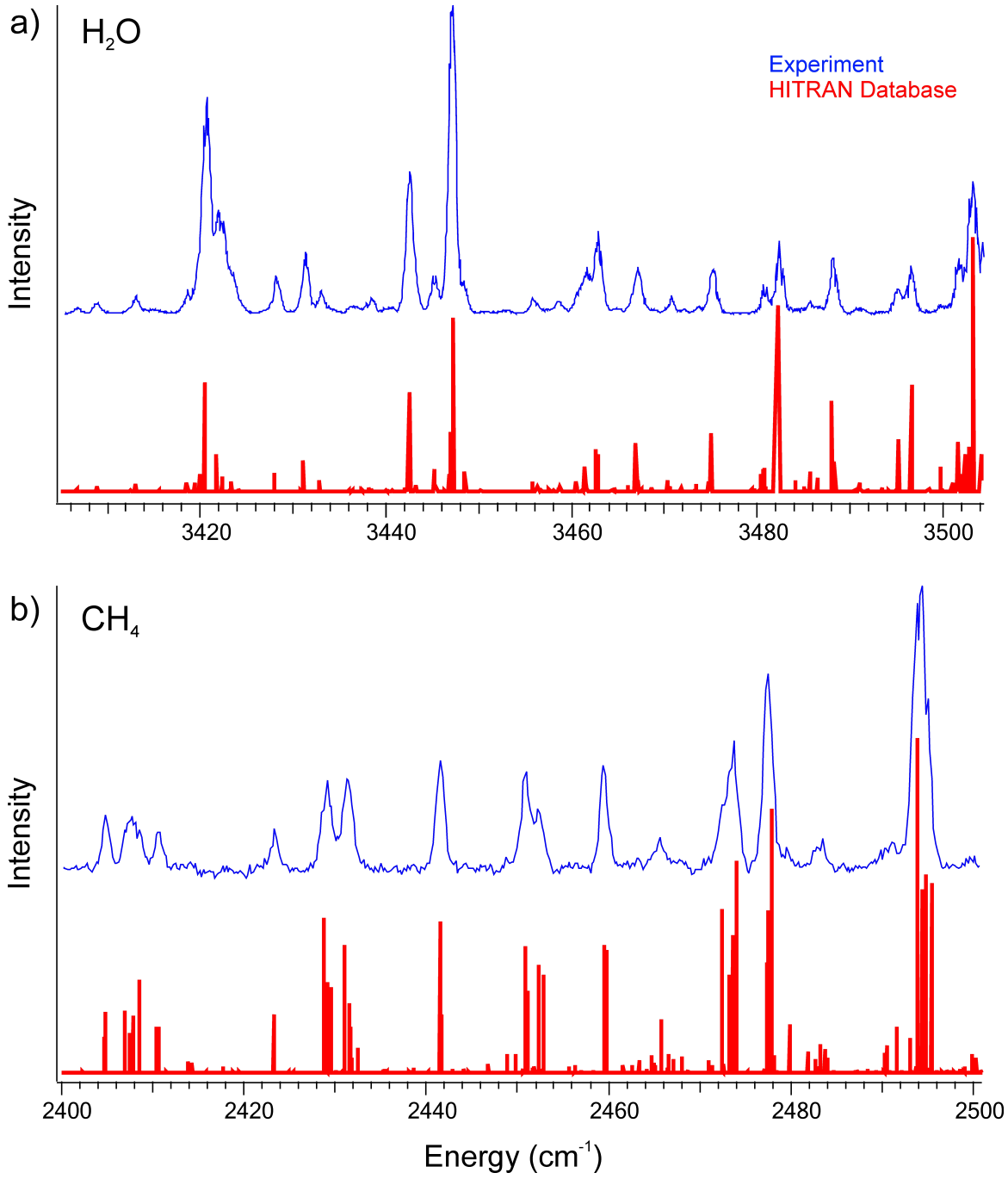

Figure 2.4 Calibration of the IR laser. Photoacoustic spectra are compared to tabulated intensities (HITRAN database). [7]

2.6 References:

1. Husband, J.; Aguirre, F.; Ferguson, P.; Metz, R. B., Vibrationally Resolved Photofragment Spectroscopy of FeO^+. *J. Chem. Phys.* **1999,** 111, 1433-1437.
2. Aguirre, F.; Husband, J.; Thompson, C. J.; Metz, R. B., Gas-Phase Photodissociation of $AuCH_2^+$: the Dissociation Threshold of Jet-Cooled and Rotationally Thermalized Ions. *Chem. Phys. Lett.* **2000,** 318, 466-470.
3. Cornett, D. S.; Peschke, M.; Laitting, K.; Cheng, P. Y.; Willey, K. F.; Duncan, M. A., Reflectron Time-of-Flight Mass Spectrometer for Laser Photodissociation. *Rev. Sci. Instrum.* **1992,** 63, 2177.
4. Kaur, D.; Desouza, A. M.; Wanna, J.; Hammad, S. A.; Mercorelli, L.; Perry, D. S., Multipass Cell for Molecular-Beam Absorption-Spectroscopy. *Appl. Optics* **1990,** 29, (1), 119-124.
5. Demtröder, W., *Laser Spectroscopy : Basic Concepts and Instrumentation*. third ed.; Springer: Berlin ; New York, **2003**.
6. Andrews, D. L.; Demidov, A. A., *An Introduction to Laser Spectroscopy* second ed.; Kluwer Academic/Plenum Publishers: New York, **2002**.
7. Rothman, L. S.; Jacquemart, D.; Barbe, A.; Benner, D. C.; Birk, M.; Brown, L. R.; Carleer, M. R.; Chackerian, C.; Chance, K.; Coudert, L. H.; Dana, V.; Devi, V. M.; Flaud, J. M.; Gamache, R. R.; Goldman, A.; Hartmann, J. M.; Jucks, K. W.; Maki, A. G.; Mandin, J. Y.; Massie, S. T.; Orphal, J.; Perrin, A.; Rinsland, C. P.; Smith, M. A. H.; Tennyson, J.; Tolchenov, R. N.; Toth, R. A.; Vander Auwera, J.; Varanasi, P.; Wagner, G., The HITRAN 2004 molecular spectroscopic database *J. Quant. Spec. Radiat. Transfer* **2005,** 96, 139.

CHAPTER 3

VIBRATIONAL SPECTROSCOPY OF INTERMEDIATES IN METHANE-TO-METHANOL CONVERSION BY FeO^+

3.1 Introduction

Methanol, one of the top 25 chemicals produced worldwide, is mainly used as a primary feedstock for the chemical industry. It has been proposed as the basis for a new energy economy by developing its utility as a liquid fuel.[1] Currently, commercial methane to methanol production is via the indirect synthesis gas (syn-gas) route:

$$CH_4 + O_2 \rightarrow CO + 2H_2 \rightarrow CH_3OH \qquad (3.1)$$

The main drawback of this method is the large energy requirement of the first, highly endothermic step. Methanol production via *direct* partial oxidation of methane is exothermic and thus has the potential to be significantly more economical and energy efficient than the syn-gas process. An efficient method for direct methane to methanol conversion is thus highly desirable.[2-5]

In nature, efficient conversion of methane to methanol at moderate temperatures is observed in *methanotrophs*, bacteria which obtain all the energy and carbon they need for life from methane.[2] The reaction is catalyzed by the enzyme methane mono-oxygenase (MMO), which contains non-heme iron centers in the active site.[6, 7] Although chemists have yet to develop a direct, efficient methane-methanol conversion process, significant advances have been made using iron-containing catalysts. An

$FePO_4$ catalyst with N_2O and H_2/O_2 as the oxidizing agents shows high catalytic selectivity for direct oxidation of methane to methanol at temperatures below 400 °C, but the reaction yield is low.[4, 8] Other promising approaches include direct oxidation to a methyl ester using a platinum catalyst[9] and direct methane-methanol conversion using an iron-doped zeolite.[10] Also noteworthy is the recent report of synthetically useful oxidation of unactivated C-H bonds using an iron-based catalyst with H_2O_2 as the oxidant.[11]

As we mentioned in the introduction chapter, in 1990 Schröder and Schwarz reported that gas-phase FeO^+ directly converts methane to methanol under thermal conditions. [12] In later experiments, they compared the efficiency and selectivity of the methane to methanol conversion by using different transition metal oxide cations. [13]

The key intermediates in the reaction are the $OFe^+(CH_4)$ entrance channel complex, $[HO\text{-}Fe\text{-}CH_3]^+$ insertion intermediate and $Fe^+(CH_3OH)$ exit channel complex. Vibrational spectra of intermediates of the *neutral* MO + CH_4 reaction have been measured in inert gas matrices for several transition metals.[14-16] For HO-Fe-CH_3, the O-H stretch is at 3744.8 cm^{-1} and the Fe-O stretch at 687.5 cm^{-1} in solid argon.[14, 15]

Our group has studied the electronic spectroscopy of intermediates of the FeO^+ + CH_4 reaction in the visible and near-UV region. By using specific ion-molecule reactions, the key insertion intermediate $[HO\text{-}Fe\text{-}CH_3]^+$ of the FeO^+ + CH_4 reaction was prepared. Photoexcitation of $[HO\text{-}Fe\text{-}CH_3]^+$ near 320 nm produces $FeOH^+$ + CH_3 and also activates the "half-reaction" to yield Fe^+ + CH_3OH. The photodissociation spectrum has well-resolved vibrational structure, with progressions in the Fe-C stretch (478 cm^{-1}) and shorter progressions in the Fe-O stretch (861 cm^{-1}) and O-Fe-C bend

(132 cm^{-1}).[17] These experiments give us information about the vibrations of the molecule in its excited electronic state. However, as no vibrational hot bands are observed, they don't provide information on vibrations in the ground electronic state. In this work we measure vibrational spectra of intermediates of methane to methanol oxidation by FeO^+ in the C-H and O-H stretching regions.

3.2 Experimental and Theoretical Methods

Vibrational spectra are measured using a dual time-of-flight reflectron photofragment spectrometer. The instrument is described in chapter 2.[18, 19] Iron cations are generated by laser ablation of an iron rod (Sigma-Aldrich, 99.8% pure). Fe^+ cations react with a suitable organic precursor diluted in a carrier gas (He, Ar, or a mixture) to produce the target molecule. The choice of precursors is guided by the collisional activation (CA) studies of Schröder et al.[20] and by our electronic spectroscopy studies of this system.[17] Details of the precursors used and characterization of the intermediates produced are discussed in section 3.3.2. Ions produced in the source expand supersonically into vacuum and cool to a rotational temperature of ~10 K.[21] Ions are accelerated to 1800 V kinetic energy, then re-referenced to ground potential before entering the field-free flight tube. Mass-selected ions are photodissociated at the turning point of the reflectron. Energetically, photodissociation of $[HO\text{-}Fe\text{-}CH_3]^+$ requires at least three photons in the O-H stretching region. So, vibrational spectra are obtained using infrared multiple photon dissociation (IRMPD) of $[HO\text{-}Fe\text{-}CH_3]^+$ and $Fe^+(CH_3OH)$ and IR resonance enhanced photodissociation (IR-REPD) of argon tagged molecules $[HO\text{-}Fe\text{-}CH_3]^+(Ar)_n$ and $Fe^+(CH_3OH)(Ar)$. The photodissociation efficiency

is greatly improved by using a multi-pass mirror arrangement[22, 23] in which the laser makes 21 passes through the ion cloud (see chapter 2). The light source is a Nd:YAG pumped optical parametric oscillator which is tunable from 2 to 5 μm, producing ~10 mJ/pulse near 3600 cm^{-1}. The IR beam path is purged with nitrogen to minimize absorptions by water vapor. The laser wavelength is calibrated using H_2O and CH_4 absorptions. Fragment ions and undissociated parent ions are detected by a dual micro-channel plate detector.

The ion signal is amplified, collected on a digital oscilloscope or a gated integrator, and averaged with a LabView based program. The photodissociation products are identified using a *difference spectrum*, which is generated by subtracting time-of-flight spectra collected at a specific wavelength with the dissociation laser blocked from when it is unblocked. The *photodissociation spectrum* is obtained by monitoring the yield of the fragment ion of interest as a function of wavelength and normalizing to parent ion signal and laser fluence. The photodissociation spectrum is the product of the absorption spectrum and the photodissociation quantum yield.

Computations are carried out with the Gaussian 2003 program package.[24] Optimized geometries of the reactants, intermediates, transition states and products are calculated using the Becke Lee-Yang-Parr hybrid HF/DFT method (B3LYP). Complementary density functional calculations were also carried out using the PBEPBE functional. For iron, the basis set is the SDD basis and relativistic effective core potential, as partially uncontracted by Dolg et al.[25] The large aug-cc-pVTZ basis set is used for the remaining atoms. Vibrational frequencies are computed to ensure that all optimized geometries correspond to a local minimum or a first-order saddle point (for

transition states). Energies were also calculated the coupled clusters singles and doubles with perturbative triples (CCSD(T)) method and the complete basis set (CBS-QB3) procedure.[26, 27]

3.3 Results and Discussion

This section is organized as follows. First, the calculated potential energy surface (PES) and mechanism of the $FeO^+ + CH_4$ reaction will be presented. Then, precursors and source conditions used to generate specific reaction intermediates and their identification will be discussed. Finally, vibrational spectroscopy will be used to characterize the O-H and C-H stretches of the intermediates.

3.3.1 Mechanism of the $FeO^+ + CH_4$ Reaction

Several groups have examined the mechanism for the $FeO^+ + CH_4$ reaction, characterizing the potential energy surface (PES) at various levels of theory.[17, 20, 28-30] Schröder et al. studied the intermediates using second order Møller-Plesset perturbation theory (MP2).[20] Later, Yoshizawa and co-workers calculated the geometries and relative energies of reactants, products, intermediates, and the transition states between them for methane to methanol conversion by all of the first-row transition metal oxide cations using B3LYP hybrid density functional theory.[28, 29] Our group also examined the $FeO^+ + CH_4$ PES using the B3LYP method.[17] Here, we use CCSD(T) and CBS-QB3 methods to obtain more accurate energies, as B3LYP calculations have been found to underestimate reaction barriers.[31, 32]

Figure 3.1 shows the potential energy surface for the $FeO^+ + CH_4$ reaction calculated using the CBS-QB3 method. Methanol production occurs in a two-step

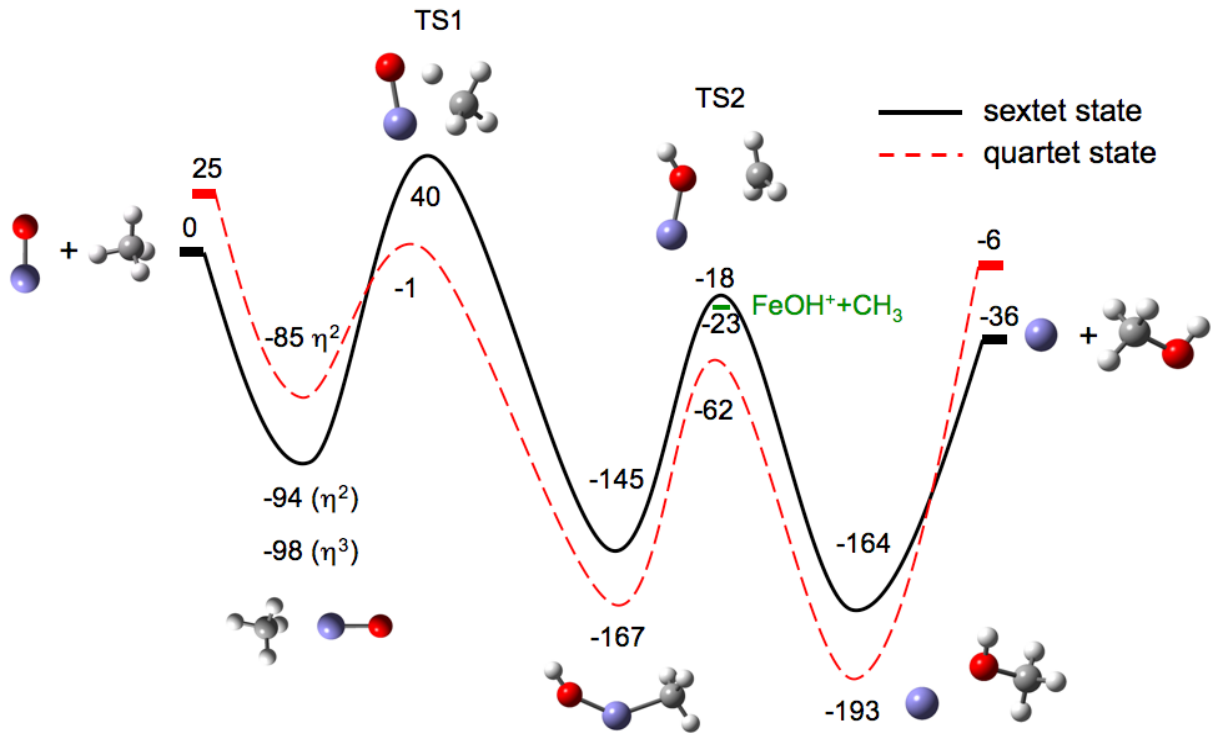

Figure 3.1 Schematic potential energy surface for the $FeO^+ + CH_4 \rightarrow Fe^+ + CH_3OH$ reaction and structures of intermediates and transition states. Energies (in kJ/mol) are calculated at the CBS-QB3 level of theory. The solid line represents the sextet and dashed line the quartet surface.

concerted manner through the formation of the hydroxy intermediate $[HO\text{-}Fe\text{-}CH_3]^+$. The minimum energy path involves first producing the $OFe^+(CH_4)$ entrance channel complex. Hydrogen abstraction via TS1 leads to the key $[HO\text{-}Fe\text{-}CH_3]^+$ insertion intermediate. The FeO^+ reactant and Fe^+ product have sextet ground states.[21] However, sextet TS1 lies significantly above the reactants. Thus, at thermal energies the reaction proceeds via low-spin, quartet TS1. This "two-state" reactivity is a fundamental feature of many organometallic reactions and has been examined in detail by Shaik and co-workers for the $FeO^+ + CH_4$ and related $FeO^+ + H_2$ reactions[33-35] and by Yoshizawa and co-workers for the FeO^+, NiO^+ and $CoO^+ + CH_4$ systems.[28, 36] The overall reaction *efficiency* is determined by the probability that reactants will cross TS1, which is determined by the energy of quartet TS1 and by how readily the initially formed sextet entrance channel complex undergoes a spin change to the quartet state. Once produced, the $[HO\text{-}Fe\text{-}CH_3]^+$ insertion intermediate can dissociate to $FeOH^+ + CH_3$ or isomerize via TS2 to form the $Fe^+(CH_3OH)$ exit channel complex, which subsequently dissociates to $Fe^+ + CH_3OH$. The *selectivity* to produce methanol rather than methyl radical is primarily determined by the relative energies of TS2 and methyl radical products. Methyl radical is produced by simple bond fission, so it is entropically favored over methanol production, which occurs via the tight transition state TS2. If TS2 is at an energy close to or above methyl radical products, then $MOH^+ + CH_3$ products dominate, as is observed for MnO^+.[13, 28] For $FeO^+ + CH_4$, TS2 lies somewhat below methyl radical products, so both pathways have similar yields at thermal energies, but higher translational energy strongly favors methyl radical formation.[37]

To establish the accuracy of the computational methods used, we compare calculated and accurate experimental results for the sextet-quartet energy splitting in Fe^+, the Fe^+-O bond enthalpy, and the overall exothermicity of the $FeO^+ + CH_4 \rightarrow Fe^+ + CH_3OH$ reaction (Table 3.1). Experimentally, the ground state of Fe^+ is ^6D ($3d^6$ 4s), with the ^4F ($3d^7$) state 23.9 kJ/mol higher. Calculations at the B3LYP/6-311+G(d,p) level incorrectly predict a quartet ground state, 19.8 kJ/mol below the sextet state. This is a well known failure of the B3LYP method with this type of basis set.[38, 39] The corresponding calculation with the SDD basis set correctly predicts the energy ordering of the Fe^+ states, as do CCSD(T) calculations. The CCSD(T) method is less sensitive to the quality of the reference wave function than other single reference *ab initio* methods. This makes the method quite attractive for transition metals since multi-reference methods are often prohibitively expensive for such systems due to the large active space which is required for an adequate multi-reference treatment.[38] Unfortunately, CCSD(T) results often converge very slowly with increasing basis set size, as can be seen in Table 3.1. An attractive alternative to rigorous (and expensive) CCSD(T) calculations are hybrid methods developed for accurate thermochemistry, such as the complete basis set CBS-QB3 approach.[26, 27] In CBS-QB3, one first optimizes the geometry and calculates harmonic frequencies at the B3LYP level. Then, from a series of single point energy calculations at various levels of theory and with different basis sets, one extrapolates the result of a large basis set calculation at a very high level of theory. CBS-QB3 thermodynamics have similar accuracy to an extrapolated series of CCSD(T) calculations with very large basis sets, and are significantly more accurate than a single CCSD(T) calculation with a modest basis set.[40] CBS-QB3 calculations also correctly

	B3LYP 6-311+G(d,p)	B3LYP SDD;aug-cc-pVTZ	CCSD(T) 6-311+G(d,p)	CCSD(T) 6-311+G(3df,p)	CBS-QB3	Expt.
$Fe^+(^6D\text{-}^4F)$	-19.8	12.6	32.5	17.3	28.2	23.9
$D_0(Fe^+\text{-}O)$	327.3	320.5	277.4	308.5	337.8	340±2[41] 335±5[42]
ΔH_{rxn}	-22.6	-41.0	-51.2	-45.8	-40.6	-31±2

Table 3.1 Experimental and calculated values of thermodynamic quantities related to the $FeO^+ + CH_4 \rightarrow Fe^+ + CH_3OH$ reaction. All values are in kJ/mol, at 0 K. CCSD(T) values are at the B3LYP/6-311+G(d,p) geometry, with zero-point energy at the B3LYP/6-311+G(d,p) level. The experimental ΔH_{rxn} is based on $D_o(FeO^+)$[41] and ΔH_f^o of O, CH_4 and CH_3OH.

predict the ordering of the Fe^+ states, with the quartet 28.2 kJ/mol above the sextet. The B3LYP calculations slightly underestimate the dissociation enthalpy of FeO^+; this is consistent with previous B3LYP calculations on FeO^+.[39]

The CCSD(T) value is low, but improves significantly for the larger basis set. The CBS-QB3 calculations are in excellent agreement with experiment.[41, 42] For the $FeO^+ + CH_4 \rightarrow Fe^+ + CH_3OH$ reaction enthalpy, all the methods are in good agreement with experiment. Table 3.1 shows that, overall, CBS-QB3 calculations most accurately predict atomic excitation energies and bond strengths of reactants and products.

The potential energy surface for the $FeO^+ + CH_4$ reaction at the CCSD(T)/6-311+G(3df,p) level (Table 3.2) is similar to the CBS-QB3 result. One key difference is that the CCSD(T) calculations predict that quartet FeO^+ lies 45 kJ/mol above the sextet; 20 kJ/mol higher than the CBS-QB3 prediction. The relatively higher energies for the quartet states persist from the reactants through TS2. As a result, the CCSD(T) calculations predict that quartet TS1 is 12 kJ/mol above reactants, which is inconsistent with the observed reaction rate at thermal energies.[12, 37] The use of a larger basis set in the CCSD(T) calculations would likely improve the results, but significantly larger calculations are prohibitively expensive.

The potential energy surface in Figure 3.1 is similar to previous B3LYP results by Yoshizawa and co-workers.[28, 29] However, there is one significant difference. The specific basis set used for iron in their B3LYP calculations predicts that quartet Fe^+ lies 89 kJ/mol above sextet Fe^+. This substantial (65 kJ/mol) error leads to the incorrect prediction that reaction to form quartet $Fe^+ + CH_3OH$ is endothermic. In a detailed

	CCSD(T)/6-311+G(d,p)		CCSD(T)/6-311+G(3df,p)	
Species	Quartet	Sextet	Quartet	Sextet
$FeO^+ + CH_4$	50	0	45	0
$OFe^+(CH_4)$	-51	-92	-63	-99
TS1	34	59	12	60
$[HO\text{-}Fe\text{-}CH_3]^+$	-139	-153	-153	-159
TS2	-30	-9	-44	-16
$Fe^+(CH_3OH)$	-185	-174	-197	-210
$Fe^+ + CH_3OH$	-21	-54	-31	-49

Table 3.2 Calculated CCSD(T)/6-311+G(d,p) and CCSD(T)/6-311+G(3df,p) energies of stationary points for the $FeO^+ + CH_4 \rightarrow Fe^+ + CH_3OH$ reaction. All energies are at the B3LYP/6-311+G(d,p) geometry and include zero-point energy at B3LYP/6-311+G(d,p). Energies are in kJ/mol.

examination of spin changes in the $FeO^+ + CH_4$ reaction, Shiota and Yoshizawa find that the spin-orbit coupling decreases during the course of the reaction, from 133.6 cm^{-1} for $OFe^+(CH_4)$, to 21.4 cm^{-1} for $[HO\text{-}Fe\text{-}CH_3]^+$ and 0.3 cm^{-1} for $Fe^+(CH_3OH)$. As a result, in the thermal reaction, the spin changes from sextet to quartet in the entrance channel region, but is unlikely to revert to sextet, so quartet $Fe^+ + CH_3OH$ is produced.[28, 36]

3.3.2 Synthesis and Characterization of $[HO\text{-}Fe\text{-}CH_3]^+$ and $Fe^+(CH_3OH)$

Our group has studied the electronic spectroscopy of intermediates of the $FeO^+ + CH_4$ reaction in the visible and near-UV.[17] The photodissociation spectrum of $[HO\text{-}Fe\text{-}CH_3]^+$ has well-resolved vibrational structure, with progressions in the Fe-C stretch, Fe-O stretch and O-Fe-C bend. These experiments give us information on the vibrations of the molecule in its excited electronic state but they do not provide information on vibrations in the ground electronic state. This motivated the present study of the vibrational spectroscopy of the intermediates.

A major challenge in these studies is to find suitable precursors and reaction conditions to selectively produce specific intermediates. In our earlier study, $[HO\text{-}Fe\text{-}CH_3]^+$ was synthesized by reacting ablated Fe^+ with methanol, isopropanol or acetic acid. In this work, we find that reaction with methanol produces $[HO\text{-}Fe\text{-}CH_3]^+$ and $Fe^+(CH_3OH)$, with the relative amounts depending on the source conditions. Measuring the types of fragment ions produced by UV photodissociation is a fast, convenient method to optimize source conditions to most selectively produce different

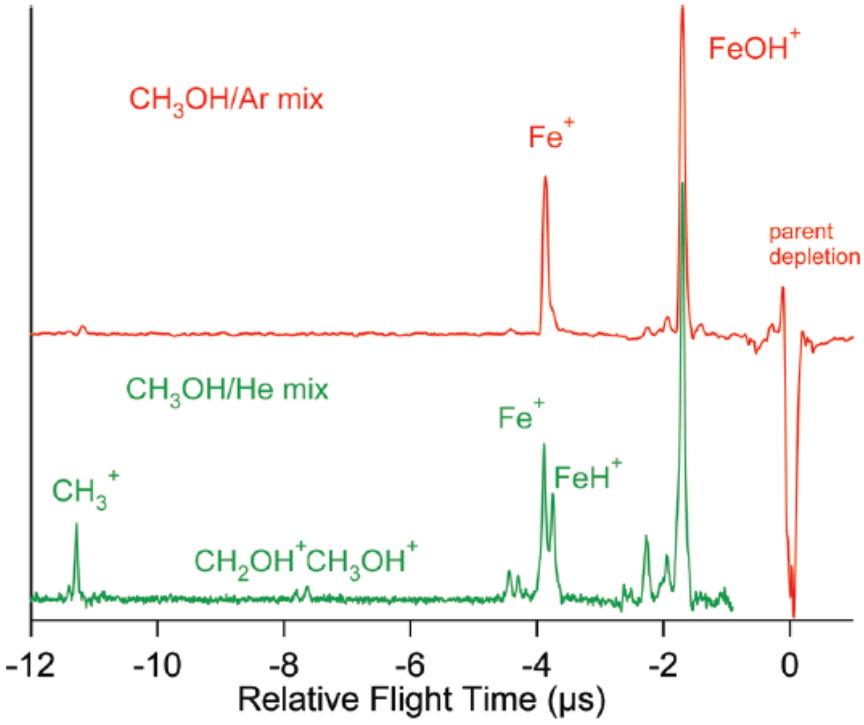

Figure 3.2 Difference spectra at 320 nm of $[FeCH_4O]^+$ ions formed by reacting Fe^+ with methanol in argon (top) and in helium (bottom). Reaction in argon produces $[HO\text{-}Fe\text{-}CH_3]^+$, while the FeH^+, CH_3^+ and CH_3OH^+ fragments indicate that reaction in helium also forms $Fe^+(CH_3OH)$.

intermediates. The intermediates are then identified based on the fragments found in UV photodissociation and infrared multiple photon dissociation, as well as by their vibrational and electronic photodissociation spectra. Figure 3.2 (top) shows a difference mass spectrum obtained by UV photodissociation of ions with stoichiometry $[FeCH_4O]^+$ made by reacting Fe^+ with 0.5% methanol in argon. The Fe^+ and $FeOH^+$ fragments observed indicate dissociation of the $[HO\text{-}Fe\text{-}CH_3]^+$ insertion intermediate. They are the only photofragments observed in our earlier electronic spectroscopy study of $[HO\text{-}Fe\text{-}CH_3]^+$. They are also the dominant fragment ions detected when $[HO\text{-}Fe\text{-}CH_3]^+$ ions are accelerated to 8 keV and collide with helium in the collisional activation (CA) studies of Schröder et al.[20] In contrast, photodissociation of $[FeCH_4O]^+$ ions produced using 0.5% methanol in helium reveals several additional fragments: CH_3^+, CH_2OH^+, CH_3OH^+ and FeH^+ (Figure 3.2, bottom). Collisional activation studies show that these additional channels are characteristic of the $Fe^+(CH_3OH)$ exit channel complex.[20] CH_3OH^+ and CH_3^+ are also major products in the UV photodissociation of $Zn^+(CH_3OH)$.[43] Hydrogen abstraction occurs from the carbon, as confirmed by observation of FeD^+ and no FeH^+ in photodissociation of $Fe^+(CD_3OH)$. Under these conditions, the source produces a mixture of $Fe^+(CH_3OH)$ and $[HO\text{-}Fe\text{-}CH_3]^+$. From 290 to 330 nm, the photodissociation spectrum of $Fe^+(CH_3OH)$ (obtained by monitoring FeH^+, CH_3^+, or CH_3OH^+) is broad and structureless. The relative CH_3^+ yield increases at longer wavelength, while the CH_3OH^+ yield decreases. This is in contrast to the spectrum of $[HO\text{-}Fe\text{-}CH_3]^+$, which has well-resolved vibronic features.[17] Although our previous study was also carried out in helium, we did not observe $Fe^+(CH_3OH)$,

presumably because much higher methanol concentrations were used (11% *vs* 0.5%), as well as a lower stagnation pressure (1 atm *vs.* 4 atm).

3.3.3 Vibrational Spectroscopy of the $[HO\text{-}Fe\text{-}CH_3]^+$ Insertion Intermediate and $Fe^+(CH_3OH)$ Exit Channel Complex

Vibrational spectra of $[HO\text{-}Fe\text{-}CH_3]^+$ and $Fe^+(CH_3OH)$ were measured using photofragment spectroscopy. A challenge in obtaining vibrational spectra using photofragment spectroscopy is that absorption of a photon needs to lead to bond breaking. One photon in the O-H stretching region only has ~43 kJ/mol of energy, so photodissociation of $[HO\text{-}Fe\text{-}CH_3]^+$ or $Fe^+(CH_3OH)$ requires at least three photons. As a result, vibrational spectra were measured using infrared multiple photon dissociation (IRMPD) and by IR resonance enhanced photodissociation (IR-REPD) of argon-tagged molecules $[HO\text{-}Fe\text{-}CH_3]^+(Ar)_n$ (n=1,2) and $Fe^+(CH_3OH)(Ar)$. These techniques have been discussed in chapter 1.

3.3.3.1 IRMPD of Insertion Intermediate and Exit Channel Complex

The UV photodissociation results show that reacting Fe^+ with methanol in *argon* produces $[HO\text{-}Fe\text{-}CH_3]^+$. Infrared multiple photon dissociation of these ions in the O-H stretching region produces $Fe^+ + CH_3OH$ and $FeOH^+ + CH_3$ in a 45:55 ratio, with little wavelength dependence. The photodissociation spectrum obtained by monitoring $FeOH^+$ has an asymmetrical peak at 3623 cm^{-1}, with a shoulder at 3576 cm^{-1} (Fig. 3.3, black trace; a deconvolution showing the two components is shown in Fig. 3.4). The UV photodissociation studies show that reacting Fe^+ with methanol in *helium* produces

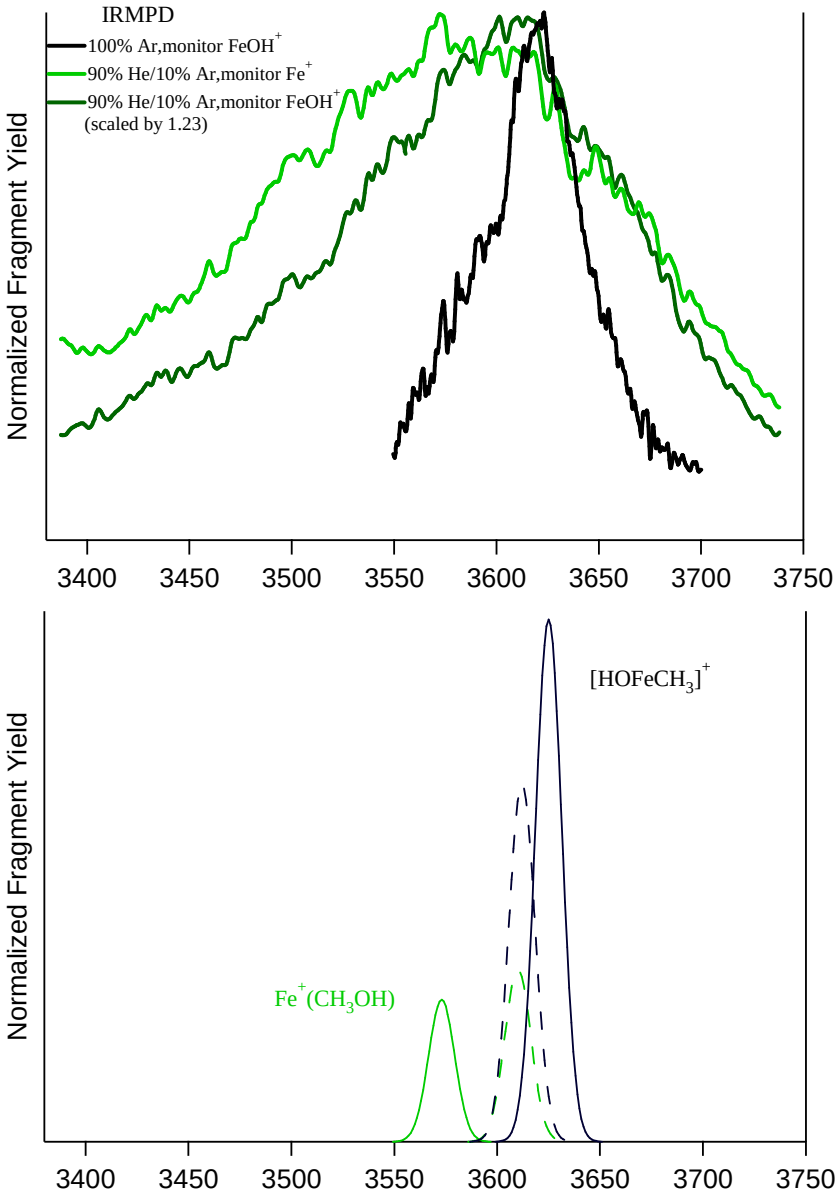

Figure 3.3 Experimental (top) and calculated (bottom) vibrational spectra of $[FeCH_4O]^+$ in the O-H stretching region. Vibrational spectra are obtained by IRMPD of $[FeCH_4O]^+$ produced by reacting Fe^+ with CH_3OH in 100% Ar, monitoring $FeOH^+$ (black) and by reacting Fe^+ with CH_3OH in 90% He/10% Ar and monitoring Fe^+ (light green) and $FeOH^+$ (dark green). Dissociation of $[HO\text{-}Fe\text{-}CH_3]^+$ peaks at 3623 cm^{-1} and primarily produces $FeOH^+$. Dissociation of $Fe^+(CH_3OH)$ primarily produces Fe^+ and is responsible for the increased intensity from 3400 to 3570 cm^{-1}. Calculated spectra are at the B3LYP/SDD;aug-cc-pVTZ level, with frequencies scaled by 0.956. For the simulations, solid lines represent sextet and dashed lines quartet states.

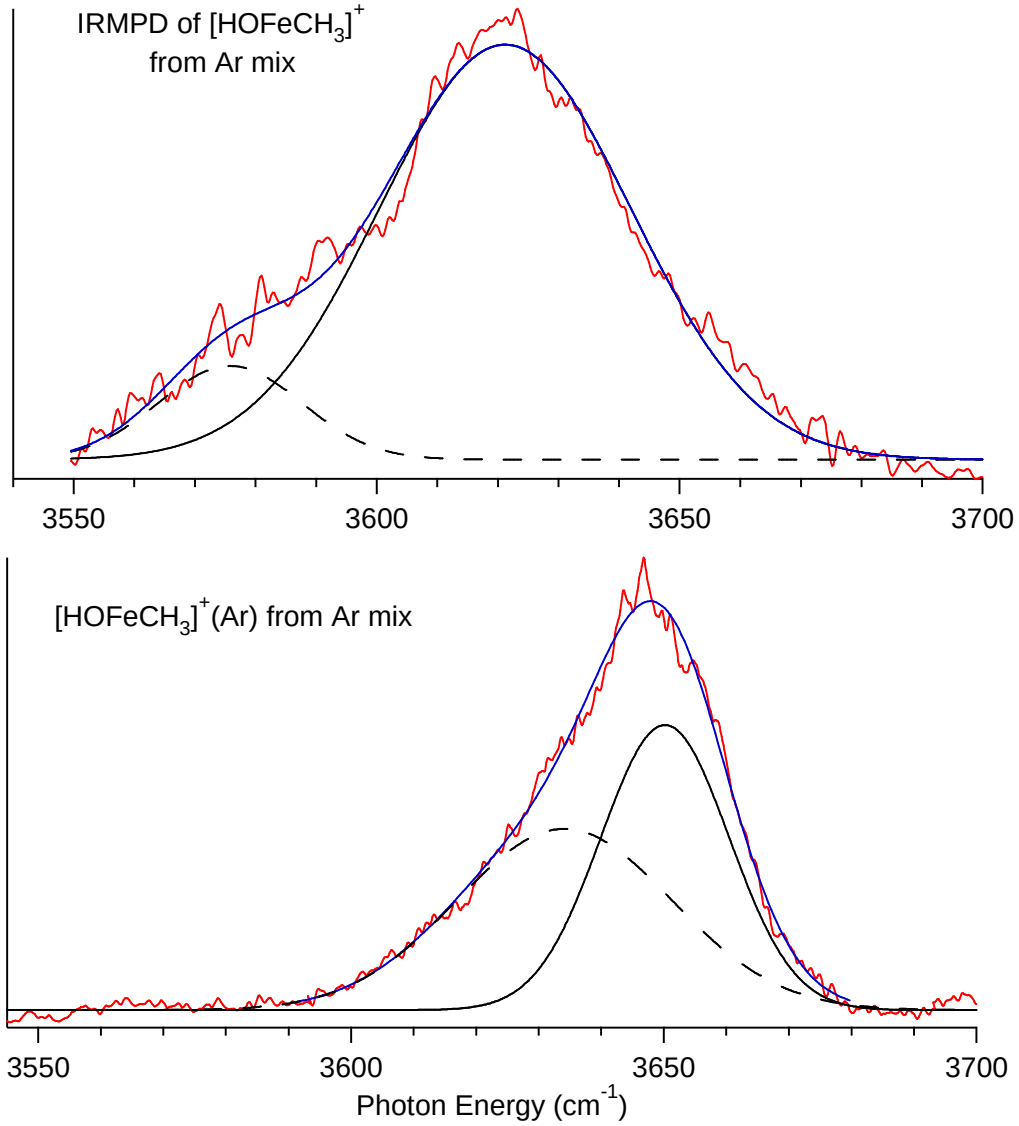

Figure 3.4 Spectra of $[HO\text{-}Fe\text{-}CH_3]^+$ (top) and $[HO\text{-}Fe\text{-}CH_3]^+(Ar)$ (bottom), along with fits to sum of two Gaussians and contributions from each Gaussian. Fitting parameters : peak (FWHM) in cm^{-1}:

$[HO\text{-}Fe\text{-}CH_3]^+$: 3576 (28); 3621 (49)

$[HO\text{-}Fe\text{-}CH_3]^+(Ar)$: 3632 (40); 3647 (24)

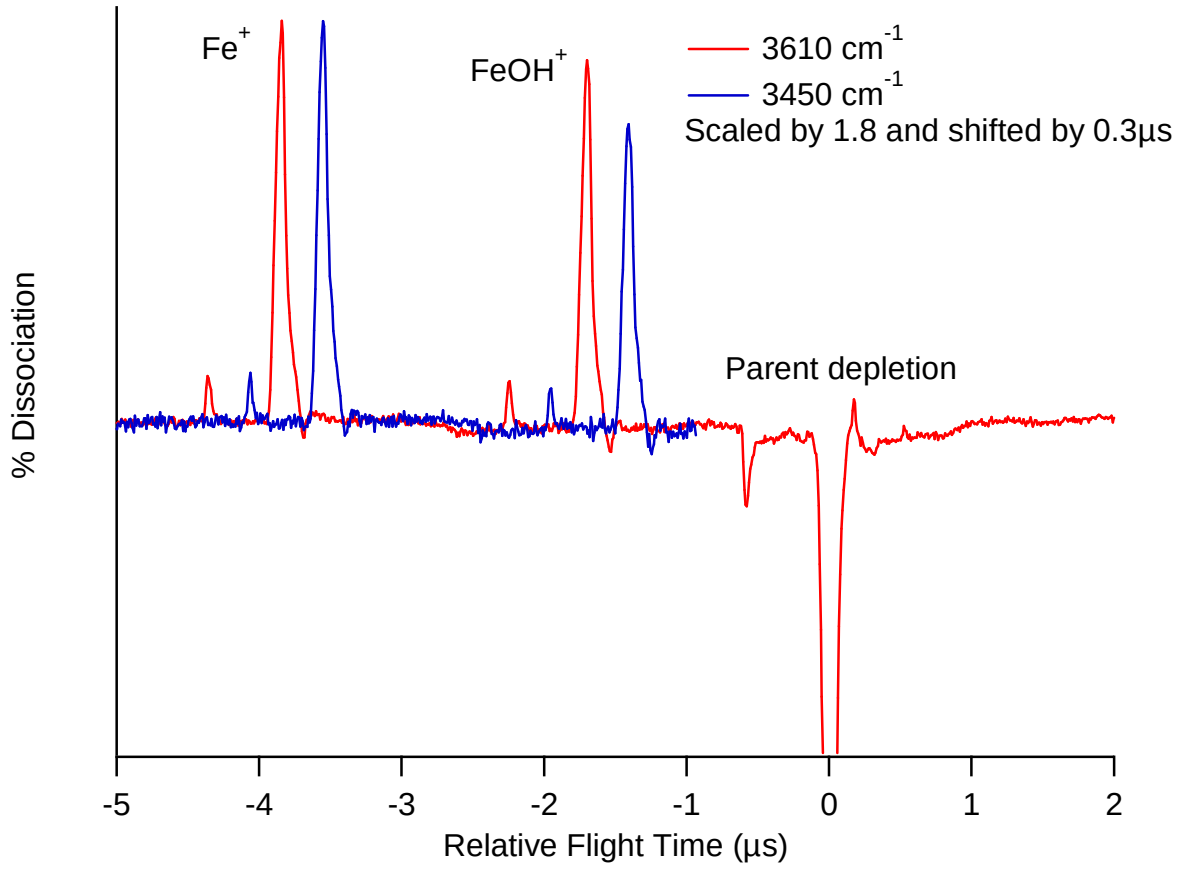

Figure 3.5 Difference spectra of $[FeCH_4O]^+$ from CH_3OH/90% He /10% mix at 3610 cm^{-1} and 3450 cm^{-1}. The small peaks ~0.7 µs before each major peak are due to the iron-54 isotopomer.

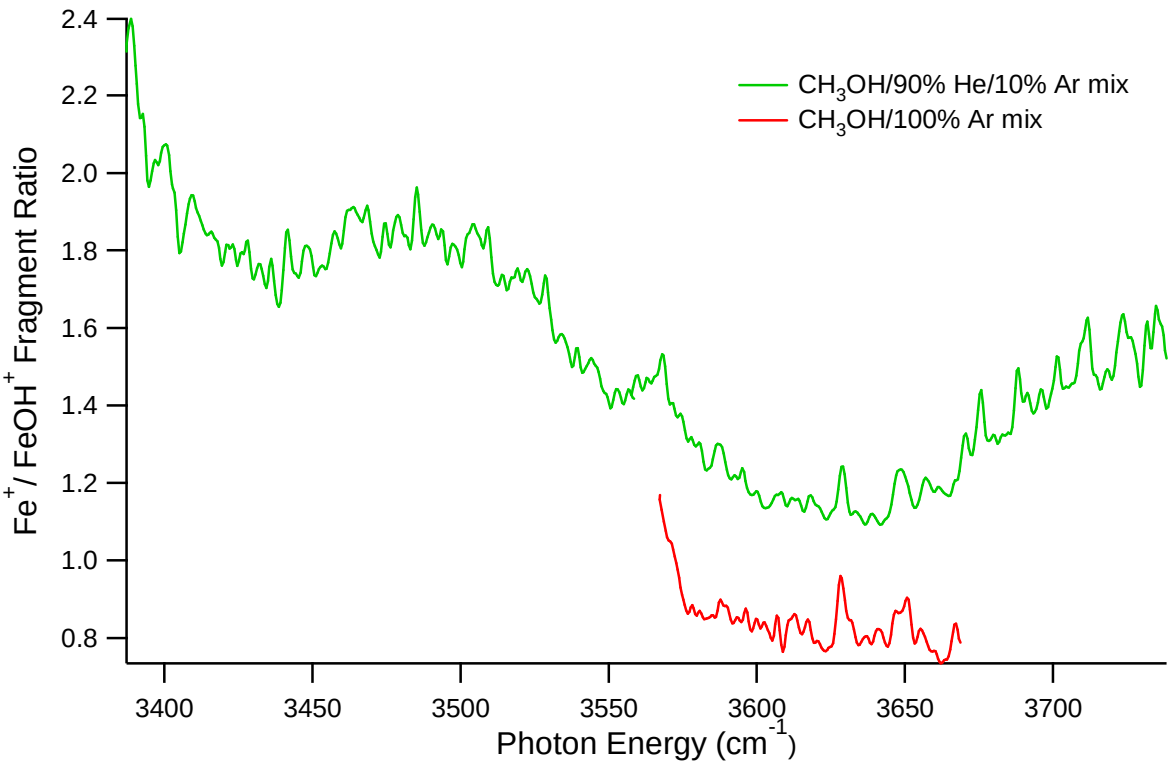

Figure 3.6 $Fe^+/FeOH^+$ fragment ratios from IRMPD of $[FeCH_4O]^+$ produced by reacting Fe^+ with methanol in argon (red) and 90% helium/10% argon (green). IRMPD of $Fe^+(CH_3OH)$ predominately produces Fe^+, while dissociation of $[HO\text{-}Fe\text{-}CH_3]^+$ primarily forms $FeOH^+$.

$[HO\text{-}Fe\text{-}CH_3]^+$ and $Fe^+(CH_3OH)$. The infrared studies use a 90% He/10% Ar mixture rather than pure helium, so that spectra of argon-tagged and untagged molecules can be measured under the same conditions. IRMPD of these ions also gives Fe^+ and $FeOH^+$, but with a very different, wavelength-dependent ratio ranging from 52:48 at ~3620 cm^{-1}, near the $[HO\text{-}Fe\text{-}CH_3]^+$ peak, to 65:35 near 3450 cm^{-1}. IRMPD difference spectra and branching ratios are shown in figures 3.5 and 3.6. The photodissociation spectra obtained by monitoring Fe^+ and $FeOH^+$ in the same scan are shown in figure 3.3 (light and dark green traces). Disentangling the contributions from the insertion intermediate and the exit channel complex is difficult, as the two spectra overlap, and both dissociate to Fe^+ and $FeOH^+$, although the insertion intermediate primarily produces $FeOH^+$ while the exit channel complex mostly forms Fe^+. Monitoring $FeOH^+$ gives a similar, but broader spectrum to the $[HO\text{-}Fe\text{-}CH_3]^+$ spectrum obtained using argon. The broadening is likely due to overlapping spectra due to quartet and sextet states of the insertion and exit channel intermediates, as well as to preferential photodissociation of vibrationally hot molecules produced in the source. Figure 3.3 shows that monitoring Fe^+ gives additional intensity from 3400 to 3570 cm^{-1}. This is due to photodissociation of $Fe^+(CH_3OH)$.

3.3.3.2 Vibrational Spectroscopy: Argon-Tagged Insertion Intermediate and Exit Channel Complex

Photodissociation spectra obtained by IRMPD tend to emphasize contributions from vibrationally excited ions, which leads to broadening, especially to lower photon

energy. Photodissociation spectra obtained from argon-tagged molecules are often narrower, as only one photon is required to dissociate the complex and the low argon binding energy ensures that argon-tagged molecules are vibrationally cold. Argon-tagged $[HO\text{-}Fe\text{-}CH_3]^+$ and $Fe^+(CH_3OH)$ are produced with the same gas mixtures and source conditions as for the respective IRMPD experiments. Argon binding energies have not been measured for these molecules, but they should be similar to that of Fe^+-Ar (900±600 cm^{-1}).[53] Our B3LYP/SDD;aug-cc-pVTZ calculations predict that argon binds quite strongly to the quartet ground state of $Fe^+(CH_3OH)$ (3500 cm^{-1}), while it binds weakly to the sextet, excited, state (500 cm^{-1}). Argon binding energies to $[HO\text{-}Fe\text{-}CH_3]^+$ are similar for the two spin states: 2700 cm^{-1} for the first argon and 1300 cm^{-1} for the second (Table 3.3). Absorption of one photon in the O-H stretching region should readily lead to dissociation, and we observe much higher dissociation yields than for untagged molecules, with loss of argon the only dissociation pathway. The photodissociation spectrum of $[HO\text{-}Fe\text{-}CH_3]^+(Ar)$ consists of a sharp peak at 3647 cm^{-1} with a shoulder at 3632 cm^{-1} (Fig. 3.7, and Fig. 3.8, top, blue trace; a deconvolution of the spectrum into two components is shown in Fig. 3.4). The small peak near 3700 cm^{-1} is likely due to a combination band of the O-H and Fe-Ar stretches. The photodissociation spectrum of $[FeCH_4O]^+(Ar)$ from the 90% He/10% Ar mix (brown trace, Fig. 3.7) extends substantially further to the red. This is due to absorption from $Fe^+(CH_3OH)(Ar)$ at ~3620 cm^{-1}. This is 60 cm^{-1} red shifted from the O-H stretch in bare methanol (3681 cm^{-1}).[54]

Figure 3.8 compares the spectra of $[HO\text{-}Fe\text{-}CH_3]^+(Ar)_n$ (n=0,1,2) obtained using argon carrier gas. The shoulders to the red of the main peaks in the n=0 and 1 spectra

	B3LYP/6-311+G(d,p)	B3LYP/6-311+G(3df,p)
$[HO\text{-}Fe\text{-}CH_3]^+$- Ar sextet	22.2	28.2
$[HO\text{-}Fe\text{-}CH_3]^+$- Ar quartet	23.9	29.6
$[HO\text{-}Fe\text{-}CH_3]^+$Ar-Ar sextet	15.2	18.9
$[HO\text{-}Fe\text{-}CH_3]^+$Ar-Ar quartet	14.8	17.7
$Fe^+(CH_3OH)$-Ar sextet	3.3	5.6
$Fe^+(CH_3OH)$-Ar quartet	36	42.5

Table 3.3 Calculated argon binding energies. All energies are at the B3LYP/6-311+G(d,p) geometry and include zero-point energy at B3LYP/6-311+G(d,p). All energies are 0 Kelvin values, in kJ/mol.

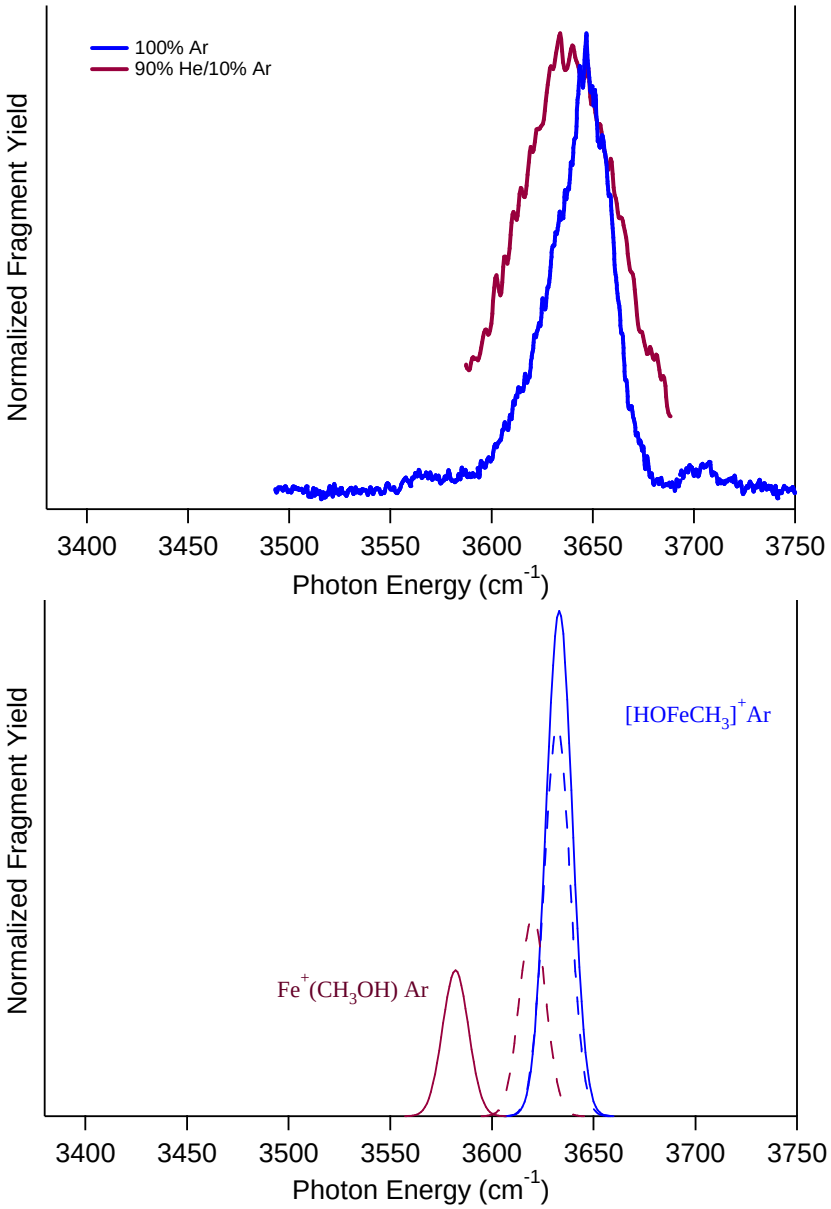

Figure 3.7 Experimental (top) and calculated (bottom) vibrational spectra of $[FeCH_4O]^+(Ar)$ in the O-H stretching region. Spectra are measured by monitoring argon loss. A 100% argon mix (blue) produces $[HO\text{-}Fe\text{-}CH_3]^+(Ar)$ while the 90% He/10% Ar mix (brown) also produces $Fe^+(CH_3OH)(Ar)$, which leads to enhanced absorption near 3620 cm^{-1}. Calculated spectra (right axis) are at the B3LYP/SDD;aug-cc-pVTZ level, with frequencies scaled by 0.956. For the simulations, solid lines represent sextet and dashed lines quartet states.

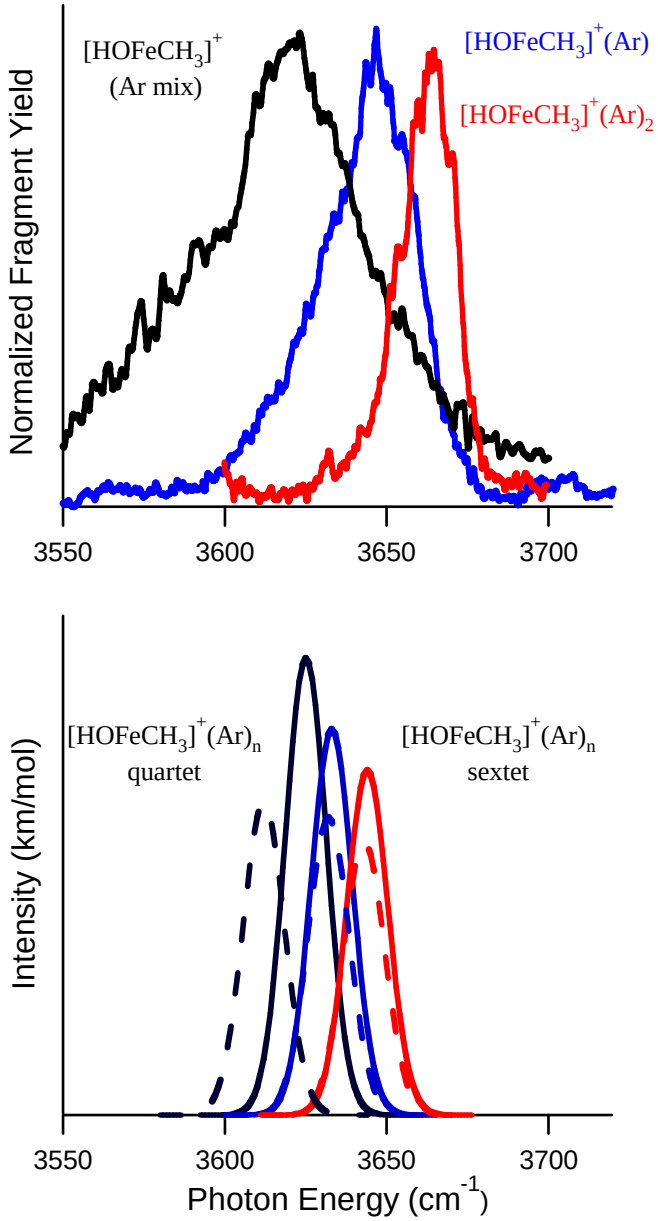

Figure 3.8 Experimental (top) and calculated (bottom) vibrational spectra of $[HO\text{-}Fe\text{-}CH_3]^+(Ar)_n$ (n=0-2) in the O-H stretching region. The spectrum of $[HO\text{-}Fe\text{-}CH_3]^+$ was obtained by IRMPD, monitoring $FeOH^+$; those of $[HO\text{-}Fe\text{-}CH_3]^+(Ar)_n$ (n=1,2) were measured by argon loss. Spectra were calculated at the B3LYP/SDD;aug-cc-pVTZ level and frequencies scaled by 0.956. Spectra of $[HO\text{-}Fe\text{-}CH_3]^+(Ar)_n$ are in black, blue and red for n=0, 1, 2, respectively. For the simulations, solid lines represent sextet states and dashed lines quartet states.

suggest that two spin states or isomers of the molecule contribute to the spectrum. The same $[HO\text{-}Fe\text{-}CH_3]^+(Ar)$ spectrum is obtained using acetic acid, which previous studies[17, 20] have shown produces $[HO\text{-}Fe\text{-}CH_3]^+$. This again confirms that we are studying $[HO\text{-}Fe\text{-}CH_3]^+$ rather than $Fe^+(CH_3OH)$, and that the peak and shoulder are likely due to the sextet and quartet states of $[HO\text{-}Fe\text{-}CH_3]^+(Ar)_n$. In addition, spectra obtained with the two precursors, and under varying source conditions, show the same relative intensity of the shoulder. This suggests that the two spin states are in equilibrium in our source, which implies that the sextet and quartet states are at similar energies and that they can interconvert readily. This is consistent with the calculated[36] 21 cm^{-1} spin-orbit coupling between sextet and quartet $[HO\text{-}Fe\text{-}CH_3]^+$. The evolution of the $[HO\text{-}Fe\text{-}CH_3]^+(Ar)_n$ (n=0,1,2) spectra is very informative. Adding one Ar leads to a 24 cm^{-1} blue shift in the main O-H stretching peak, and a second Ar causes an additional shift of 15 cm^{-1}. For the shoulders, the spectral shifts are larger, with addition of one Ar leading to a 56 cm^{-1} shift. As a result, the separation between the shoulder and main peak decreases with increasing n, until for $[HO\text{-}Fe\text{-}CH_3]^+(Ar)_2$ a 20 cm^{-1} FWHM peak at 3662 cm^{-1} with no shoulder is observed.

To better characterize the quartet and sextet states of the insertion intermediate, we measured the photodissociation spectra of $[HO\text{-}Fe\text{-}CH_3]^+(Ar)_n$ (n=1,2) in the C-H stretching region. Of the three C-H stretches, calculations predict that the lowest frequency, symmetric vibration near 2850 cm^{-1} is the most intense. Measuring this vibration is very challenging, as it is calculated to be an order of magnitude weaker than the O-H stretch. As a result, we were unable to measure the IRMPD spectrum of

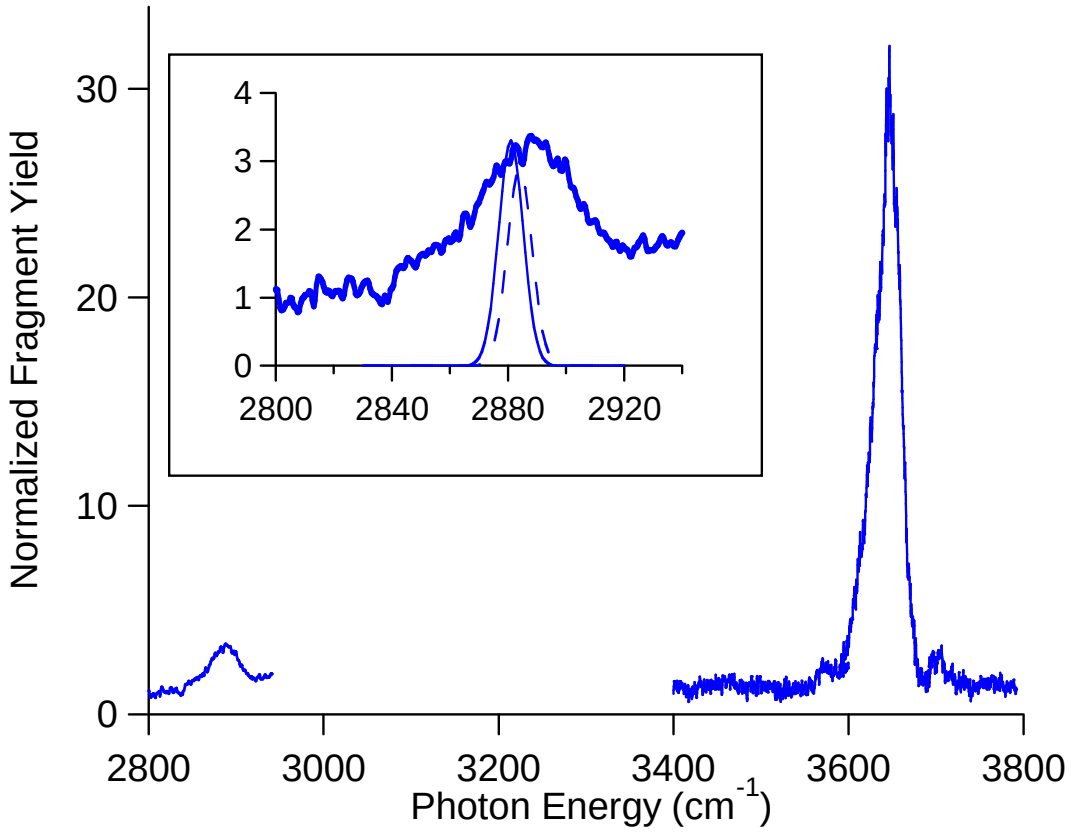

Figure 3.9 IR photodissociation spectrum of $[HO\text{-}Fe\text{-}CH_3]^+(Ar)$ in the C-H and O-H stretching regions; the Ar loss channel is detected. The inset shows an expanded view of the C-H stretching region, along with simulated spectra for the sextet (solid) and quartet (dashed) states at the B3LYP/SDD;aug-cc-pVTZ level, with the vibrational frequency scaled by 0.956.

.

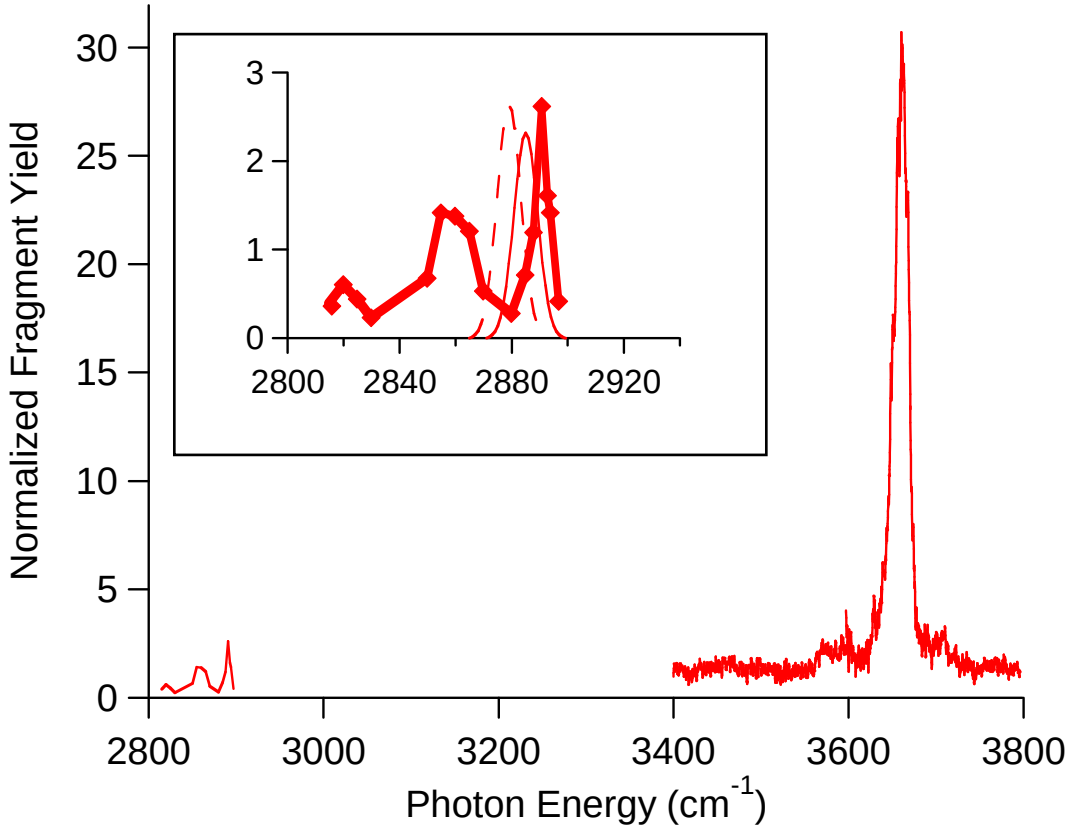

Figure 3.10 IR photodissociation spectrum of $[HO\text{-}Fe\text{-}CH_3]^+(Ar)_2$ in the C-H and O-H stretching regions; the Ar loss channel is detected. The inset shows an expanded view of the C-H stretching region, along with simulated spectra for the sextet (solid) and quartet (dashed) states at the B3LYP/SDD;aug-cc-pVTZ level, with the vibrational frequency scaled by 0.956

$[HO\text{-}Fe\text{-}CH_3]^+$ in this region. The photodissociation spectra of $[HO\text{-}Fe\text{-}CH_3]^+(Ar)$ and $[HO\text{-}Fe\text{-}CH_3]^+(Ar)_2$ are shown in Figures 3.9 and 3.10. The C-H stretch is much less intense than the O-H stretch, so it is magnified in the insets. In this region, the spectrum of $[HO\text{-}Fe\text{-}CH_3]^+(Ar)$ consists of a single, broad peak at 2888 cm^{-1} with 35 cm^{-1} FWHM. Due to low signal levels, the spectrum of $[HO\text{-}Fe\text{-}CH_3]^+(Ar)_2$ was measured by integrating the area under difference spectra taken at ~5 cm^{-1} intervals. The $[HO\text{-}Fe\text{-}CH_3]^+(Ar)_2$ spectrum shows two, narrow peaks in this region: at 2855 cm^{-1} (15 cm^{-1} FWHM) and 2891 cm^{-1} (6 cm^{-1} FWHM).

To help assign the spectra, we calculated geometries, energies and harmonic frequencies of the quartet and sextet states of $[HO\text{-}Fe\text{-}CH_3]^+(Ar)_n$ and $Fe^+(CH_3OH)(Ar)_n$ (n=0-2). Calculations were carried out using the B3LYP hybrid density functional with the SDD basis set on Fe and aug-cc-pVTZ on the remaining atoms. Calculated harmonic frequencies are scaled by 0.956, which is the average ratio of the experimental to calculated C-H and O-H stretching frequencies in bare methanol. The calculations predict that the geometries of sextet and quartet $[HO\text{-}Fe\text{-}CH_3]^+$ differ in the O-Fe-C angle (138º vs 111º) and slightly in the Fe-O bond length (1.738 Å vs 1.703 Å), see Table 3.4. Calculated, scaled C-H and O-H frequencies and intensities for bare and argon-tagged insertion intermediates are shown in Table 3.5. Anharmonic calculations are shown in Table 3.6. In principle these should be more accurate than scaled harmonic frequencies, as they include anharmonicity by calculating third derivatives. However, for this system spin contamination leads to small energy shifts that cause substantial error in the third derivatives, and hence in the anharmonic frequencies. Complementary calculations using smaller basis sets with the B3LYP and

the PBEPBE density functional were also carried out to assess the robustness of the computational results. Frequencies at the PBEPBE/SDD;aug-cc-pVTZ level are given in Table 3.7. While the computed frequencies vary slightly with functional and basis set, the calculations consistently make several predictions: the O-H stretch of quartet $[HO\text{-}Fe\text{-}CH_3]^+$ lies below that of the sextet state; argon-tagging shifts both to higher energy, but the shift is larger for the quartet state, so that the quartet-sextet gap decreases with sequential addition of argon. Our assignment of spectra in the O-H stretching region is based on the agreement between these predictions and experiment. In addition, spectra obtained using helium expansions contain contributions from the $Fe^+(CH_3OH)$ complex, which is not present in argon expansions.

Figures 3.3, 3.7 and 3.8 show simulated O-H stretching spectra for sextet and quartet states of bare and argon-tagged $[HO\text{-}Fe\text{-}CH_3]^+$ and $Fe^+(CH_3OH)$. Exit channel complexes are predicted to have the lowest O-H stretching frequencies, with very small shifts on argon-tagging. The IRMPD spectra measured using a 90% He/10% Ar mix extend significantly to the red of the other spectra measured. The calculations predict that this is due to dissociation of sextet $Fe^+(CH_3OH)$. The remaining breadth of this peak is likely due to contributions from quartet $Fe^+(CH_3OH)$ and $[HO\text{-}Fe\text{-}CH_3]^+$, as well as to preferential dissociation of vibrationally excited ions.

The IRMPD spectrum of $[HO\text{-}Fe\text{-}CH_3]^+$, obtained using argon carrier gas, has a distinct shoulder, indicating contributions from two species. The calculations predict that the O-H stretching frequency of quartet $[HO\text{-}Fe\text{-}CH_3]^+$ is lower than that of the sextet, suggesting that the main peak is due to the sextet and the shoulder to the quartet. This assignment is supported by the argon-tagging results. Argon-tagging sequentially

	r(O-H) Å	r(C-H) Å	r(Fe-C) Å	r(Fe-O) Å	r(C-O) Å	Θ(O-Fe-C) degrees
CH_3OH	0.961	1.090 1.097 1.097	-	-	1.42	-
$[HO\text{-}Fe\text{-}CH_3]^+$ Sextet	0.967	1.095 1.094 1.094	1.987	1.742	-	137.83
$[HO\text{-}Fe\text{-}CH_3]^+$ Quartet	0.968	1.108 1.088 1.088	1.967	1.707	-	109.30
$[HO\text{-}Fe\text{-}CH_3]^+(Ar)$ Sextet	0.967	1.095 1.094 1.094	1.990	1.751	-	133.04
$[HO\text{-}Fe\text{-}CH_3]^+(Ar)$ Quartet	0.966	1.099 1.088 1.088	1.994	1.709	-	102.92
$[HO\text{-}Fe\text{-}CH_3]^+(Ar)_2$ Sextet	0.966	1.094 1.093 1.093	2.001	1.757	-	129.00
$[HO\text{-}Fe\text{-}CH_3]^+(Ar)_2$ Quartet	0.966	1.098 1.087 1.087	1.994	1.717	-	102.48
$Fe^+(CH_3OH)$ Sextet	0.969	1.088 1.088 1.087	-	2.06	1.48	-
$Fe^+(CH_3OH)$ Quartet	0.966	1.089 1.089 1.087	-	1.98	1.47	-
$Fe^+(CH_3OH).(Ar)$ Sextet	0.969	1.088 1.088 1.087	-	2.06	1.48	-
$Fe^+(CH_3OH).(Ar)$ Quartet	0.966	1.089 1.089 1.086	-	1.971	1.47	-

Table 3.4 Geometries of bare and argon tagged $[HO\text{-}Fe\text{-}CH_3]^+$ and $Fe^+(CH_3OH)$ calculated at the B3LYP/6-311+G(d,p) level.

	O-H stretch (cm^{-1})	C-H stretches (cm^{-1})
CH_3OH	3660***(31)***	2972***(24)***, 2906***(53)***, 2862***(63)***
$[HO\text{-}Fe\text{-}CH_3]^+$ quartet	3612***(313)***	3055***(7)***, 2988***(5)***, 2800***(34)***
$[HO\text{-}Fe\text{-}CH_3]^+$ sextet	3625***(456)***	2984***(8)***, 2977***(9)***, 2878***(34)***
$[HO\text{-}Fe\text{-}CH_3]^+(Ar)$ quartet	3633***(297)***	3054***(4)***, 2995***(1)***, 2884***(21)***
$[HO\text{-}Fe\text{-}CH_3]^+(Ar)$ sextet	3633***(385)***	2980***(5)***, 2979***(3)***, 2881***(24)***
$[HO\text{-}Fe\text{-}CH_3]^+(Ar)_2$ quartet	3643***(273)***	3055***(3)***, 3000***(1)***, 2880***(19)***
$[HO\text{-}Fe\text{-}CH_3]^+(Ar)_2$ sextet	3644***(344)***	2986***(2)***, 2981***(2)***, 2885***(16)***
$Fe^+(CH_3OH)$ quartet	3610***(151)***	3045***(1)***, 3029***(0.2)***, 2939***(4)***
$Fe^+(CH_3OH)$ sextet	3574***(124)***	3035***(1)***, 3028***(0.1)***, 2935***(2)***
$Fe^+(CH_3OH)(Ar)$ quartet	3620***(152)***	3044***(1)***, 3025***(1)***, 2937***(6)***
$Fe^+(CH_3OH)(Ar)$ sextet	3582***(111)***	3030***(0.3)***, 3030***(1),*** 2935***(3)***

Table 3.5 Harmonic vibrational frequencies for bare and argon-tagged intermediates at the B3LYP/SDD; aug-cc-pVTZ level. IR intensities (km/mol) in parentheses. Frequencies are scaled by 0.956

	O-H stretch	C-H stretches
CH_3OH	3697***(30)***	2992***(27)***, 2919***(64)***, 2873***(68)***
$[HO\text{-}Fe\text{-}CH_3]^+$ quartet	3640***(394)***	2993***(19)***, 2968***(6)***, 2818***(38)***
$[HO\text{-}Fe\text{-}CH_3]^+$ sextet	3642***(543)***	2974***(7)***, 2965***(9)***, 2878***(33)***
$[HO\text{-}Fe\text{-}CH_3]^+(Ar)$ quartet	3642***(337)***	3044***(3)***, 2994***(1)***, 2874***(20)***
$[HO\text{-}Fe\text{-}CH_3]^+(Ar)$ sextet	3654***(461)***	2972***(5)***, 2970***(3)***, 2881***(24)***
$[HO\text{-}Fe\text{-}CH_3]^+(Ar)_2$ quartet	3651***(319)***	3052***(3)***, 2999***(0.4)***, 2884***(18)***
$[HO\text{-}Fe\text{-}CH_3]^+(Ar)_2$ sextet	3674***(420)***	2977***(2)***, 2968***(2)***, 2885***(17)***

Table 3.6 Anharmonic vibrational frequencies for bare and argon-tagged insertion intermediates at the B3LYP/6-311+G(d,p) level, in cm^{-1}. IR intensities (km/mol) in parentheses.

	O-H stretch (cm^{-1})	C-H stretches (cm^{-1})
$[HO\text{-}Fe\text{-}CH_3]^+$ quartet	3640***(394)***	2993***(19)***, 2968***(6)***, 2818***(38)***
$[HO\text{-}Fe\text{-}CH_3]^+$ sextet	3642***(543)***	2974***(7)***, 2965***(9)***, 2878***(33)***
$[HO\text{-}Fe\text{-}CH_3]^+(Ar)$ quartet	3642***(337)***	3044***(3)***, 2994***(1)***, 2874***(20)***
$[HO\text{-}Fe\text{-}CH_3]^+(Ar)$ sextet	3654***(461)***	2972***(5)***, 2970***(3)***, 2881***(24)***
$[HO\text{-}Fe\text{-}CH_3]^+(Ar)_2$ quartet	3651***(319)***	3052***(3)***, 2999***(0.4)***, 2884***(18)***
$[HO\text{-}Fe\text{-}CH_3]^+(Ar)_2$ sextet	3674***(420)***	2977***(2)***, 2968***(2)***, 2885***(17)***

Table 3.7 Harmonic vibrational frequencies for bare and argon-tagged intermediates at the PBEPBE/SDD;aug-cc-pVTZ level in cm^{-1}. IR intensities (km/mol) in parentheses. Frequencies are scaled by 0.986

blue-shifts the spectrum, as shown in figure 3.8. The blue shift on argon binding is predicted to be larger for the quartet state. This agrees with the observation that the separation between the shoulder and main peak decreases with added argon. The peak at 3623 cm^{-1} in the IRMPD spectrum is thus assigned to the O-H stretch of sextet $[HO\text{-}Fe\text{-}CH_3]^+$, while the O-H stretch of the quartet is at 3576 cm^{-1}. In the ion source, ground-state, sextet Fe^+ can insert into the C-O bond in methanol to produce sextet $[HO\text{-}Fe\text{-}CH_3]^+$. This can convert to the quartet state via intersystem crossing or collisions with the argon buffer gas. Spectra obtained with different source conditions (timing and backing pressures) and different precursors (methanol and acetic acid) are very similar, with the shoulder having the same relative intensity. This suggests that sextet and quartet $[HO\text{-}Fe\text{-}CH_3]^+$ are in equilibrium in the ion source, so they are at similar energies and can interconvert readily.

Compared to bare methanol,[54] ν_{OH}=3681 cm^{-1}, the O-H stretching frequencies of $[HO\text{-}Fe\text{-}CH_3]^+$ are 58 and 105 cm^{-1} red-shifted for the sextet and quartet states, respectively. This correlates with the O-H bond lengths, which are calculated to be ~0.006 Å longer for the insertion intermediates than for methanol. Also, the calculations predict that the observed blue shift on argon binding is due to partial charge transfer to argon, reducing the charge of the $[HO\text{-}Fe\text{-}CH_3]^+$ core. Mulliken population analysis predicts that the charge on the $[HO\text{-}Fe\text{-}CH_3]^+$ moiety in $[HO\text{-}Fe\text{-}CH_3]^+(Ar)_n$ is +0.89 for n=1 and only +0.82 for n=2. This is supported by the observation that the O-H stretch in *neutral*[14, 15] $HO\text{-}Fe\text{-}CH_3$ shows a substantial additional blue shift, to 3744.8 cm^{-1}.

Of the three C-H stretches, the symmetric C-H stretch is predicted to be by far the most intense, and lies at lowest wavenumbers. For bare $[HO\text{-}Fe\text{-}CH_3]^+$, the symmetric C-H stretching frequencies of sextet and quartet states are predicted to differ by ~80 cm^{-1}. Unfortunately, signal levels for IRMPD of the insertion intermediate in the C-H stretching region are too low to measure its spectrum directly. Instead, we measure C-H stretching spectra of Ar-tagged molecules. However, binding to argon lengthens the Fe-C and contracts the C-H bonds in quartet $[HO\text{-}Fe\text{-}CH_3]^+$, which leads to a ~80 cm^{-1} blue shift in the calculated symmetric C-H stretch. The perturbation is much smaller for the sextet state. As a result, the calculations predict very similar symmetric C-H stretch frequencies for sextet and quartet argon-tagged insertion intermediates. For $[HO\text{-}Fe\text{-}CH_3]^+(Ar)$, both spin states contribute to the broad peak at 2888 cm^{-1} (Fig. 3.9, inset). For $[HO\text{-}Fe\text{-}CH_3]^+(Ar)_2$, two narrow peaks are observed (Fig. 3.10, inset). The calculations consistently predict that the symmetric C-H stretching frequency of quartet $[HO\text{-}Fe\text{-}CH_3]^+(Ar)_2$ is lower than that of the sextet state. However, the calculated difference is small. We thus tentatively assign the peak at 2855 cm^{-1} to the quartet state and the 2891 cm^{-1} peak to the sextet state. These values are slightly blue-shifted from the lowest C-H stretch in bare methanol, 2844 cm^{-1}, consistent with slightly shorter calculated C-H bond lengths.

It is interesting that reaction of laser-ablated Fe^+ with methanol produces $Fe^+(CH_3OH)$ and $[HO\text{-}Fe\text{-}CH_3]^+$, depending on source conditions. Both products have been seen in previous studies. In an early ion cyclotron resonance mass spectrometry (ICR) study, Allison and Ridge observed that Fe^+ inserts into the C-O bond in methanol, even under very gentle conditions.[55] They reacted $FeCO^+$ with CH_3OH. The

$[FeCH_4O]^+$ product was isolated, then reacted with CD_3OH. They produce $[FeCH_2D_3O_2]^+ + CH_3$ and do not observe loss of CD_3. This indicates that the two methyl groups are not equivalent and that reaction of $FeCO^+$ with CH_3OH produces $[HO\text{-}Fe\text{-}CH_3]^+$ rather than $Fe^+(CH_3OH)$. At higher pressure in a chemical ionization source, Schröder et al. conclude that the $Fe^+ + CH_3OH$ reaction primarily produces $Fe^+(CH_3OH)$, based on collision-induced dissociation of the products.[20] Production of $[HO\text{-}Fe\text{-}CH_3]^+$ rather than $Fe^+(CH_3OH)$ is determined by competition between insertion into the C-O bond via TS2 (the reverse of the reaction shown in Fig. 3.1) and collisional cooling of the initially-formed, internally excited $[Fe^+(CH_3OH)]^*$. Quartet Fe^+ should readily insert into the C-O bond, due to the low quartet barrier over TS2. However, the calculations predict that, for the sextet state, TS2 lies above $Fe^+ + CH_3OH$. As a result, production of $[HO\text{-}Fe\text{-}CH_3]^+$ requires sufficient translational energy to overcome the barrier, which could occur in a laser ablation source, or a spin change to the quartet state, which is unlikely for $[Fe^+(CH_3OH)]^*$, which should have small spin-orbit coupling.[36] Our observation that production of $[HO\text{-}Fe\text{-}CH_3]^+$ dominates under certain source conditions suggests that the calculations overestimate the barrier for sextet TS2. Ideally, one would like to study the $Fe^+ + CH_3OH$ reaction under single-collision conditions as a function of collision energy, as has been done by Armentrout and coworkers for the $Co^+ + CH_3OH$ reaction.[56]

3.4 Summary and Conclusions

Vibrational spectra of two intermediates of the gas-phase $FeO^+ + CH_4 \rightarrow Fe^+ + CH_3OH$ reaction have been measured. Spectra of the quartet and sextet states of

$[HO\text{-}Fe\text{-}CH_3]^+$, the key insertion intermediate, are obtained from IRMPD of the bare ion and from resonance-enhanced photodissociation of argon-tagged ions in the C-H and O-H stretching regions. $[HO\text{-}Fe\text{-}CH_3]^+$ is produced using argon carrier gas. Based on the IRMPD spectrum, sextet $[HO\text{-}Fe\text{-}CH_3]^+$ has ν_{OH}=3623 cm^{-1} while quartet $[HO\text{-}Fe\text{-}CH_3]^+$ has $\nu_{OH}\approx$3576 cm^{-1}. Using 90% helium/10% argon rather than pure argon as the carrier gas also produces the $Fe^+(CH_3OH)$ exit channel complex, whose O-H stretch is measured using IRMPD. Photodissociation produces both Fe^+ and $FeOH^+$, and the ratio depends on wavelength. $[HO\text{-}Fe\text{-}CH_3]^+$ primarily dissociates to $FeOH^+$, while $Fe^+(CH_3OH)$ mainly forms Fe^+. The O-H stretching frequencies of sextet and quartet $[HO\text{-}Fe\text{-}CH_3]^+(Ar)_n$ become more similar with increasing n. For the sextet, ν_{OH}=3647 cm^{-1} for $[HO\text{-}Fe\text{-}CH_3]^+(Ar)$ and 3662 cm^{-1} for $[HO\text{-}Fe\text{-}CH_3]^+(Ar)_2$. The photodissociation spectrum of $[FeCH_4O]^+(Ar)$ produced using 90% He/10% Ar extends to the red of the spectrum of $[HO\text{-}Fe\text{-}CH_3]^+(Ar)$, implying that $Fe^+(CH_3OH)(Ar)$ has $\nu_{OH}\approx$3620 cm^{-1}.

Hybrid density functional theory calculations aid in assigning the spectra. They correctly predict the direction, but slightly underestimate the magnitude, of the frequency shift due to adding argon to sextet and quartet $[HO\text{-}Fe\text{-}CH_3]^+$. An improved potential energy surface for the $FeO^+ + CH_4$ reaction is developed based on calculations at the complete basis set (CBS-QB3) and coupled clusters (CCSD(T)) levels. The calculations predict that the reaction proceeds through the initial formation of a $OFe^+(CH_4)$ complex followed by isomerization over TS1 to the $[HO\text{-}Fe\text{-}CH_3]^+$ insertion intermediate. The insertion intermediate can dissociate to produce $FeOH^+ + CH_3$ products or isomerize via TS2 to the $Fe^+(CH_3OH)$ exit channel complex, which then

dissociates to $Fe^+ + CH_3OH$. Although the reactant and product ground states are sextets, at thermal energies the reaction requires a spin change from sextet to quartet to overcome the barrier at TS1. Production of quartet $Fe^+ + CH_3OH$ is energetically allowed. The calculations predict that sextet and quartet $[HO\text{-}Fe\text{-}CH_3]^+$ are at similar energies, and our experiments suggest that they can interconvert. This mechanism agrees with the results of kinetics and spectroscopic experiments, by several groups.

3.5 References

1. Olah, G. A.; Goeppert, A.; Prakash, G. K. S., *Beyond Oil and Gas: The Methanol Economy*. Wiley: Weinheim, 2006.
2. Crabtree, R. H., Aspects of Methane Chemistry. *Chem. Rev.* **1995,** 95, 987-1007.
3. Lunsford, J. H., Catalytic Conversion of Methane to more Useful Chemicals and Fuels: a Challange for the 21st Century. *Catal. Today* **2000,** 63, 165-174.
4. Otsuka, K.; Wang, Y., Direct Conversion of Methane into Oxygenates. *Appl. Catal. A* **2001,** 222, 145.
5. Olah, G. A., Electrophilic Methane Conversion. *Acc. Chem. Res.* **1987,** 20, 422.
6. Baik, M. H.; Newcomb, M.; Friesner, R. A.; Lippard, S. J., Mechanistic Studies on the Hydroxylation of Methane by Methane Monooxygenease. *Chem. Rev.* **2003,** 103, 2385.
7. Lieberman, R. L.; Rosenzweig, A. C., Crystal Structure of a Membrane-Bound Metalloenzyme that Catalyses the Biological Oxidation of Methane. *Nature* **2005,** 434, (7030), 177-182.
8. Wang, Y.; Otsuka, K., Catalytic Oxidation of Methane to Methanol Initiated in a Gas Mixture of Hydrogen and Oxygen. *J. Chem. Soc. Chem. Commun.* **1994**, 2209.
9. Periana, R. A.; Taube, D. J.; Gamble, S.; Taube, H.; Satoh, T.; Fujii, H., Platinum Catalysts for the High-Yield Oxidation of Methane to a Methanol Derivative. *Science* **1998,** 280, 560-564.
10. Raja, R.; Ratnasamy, P., Direct Conversion of Methane to Methanol. *Appl. Catal. A General* **1997,** 158, L7-L15.
11. Chen, M. S.; White, M. C., A predictably selective aliphatic C-H oxidation reaction for complex molecule synthesis. *Science* **2007,** 318, 783-787.
12. Schröder, D.; Schwarz, H., FeO^+ Activates Methane. *Angew. Chem. Intl. Ed. Engl.* **1990,** 29, 1433-1434.
13. Schröder, D.; Schwarz, H., C-H and C-C Bond Activation by Bare Transition-Metal Oxide Cations in the Gas Phase. *Angew. Chem. Int. Ed. Engl.* **1995,** 34, 1973-1995.
14. Park, M.; Hauge, R. H.; Kafafi, Z. H.; Margrave, J. L., Activation of O-H and C-O Bonds of Methanol by Photoexcited Iron Atoms. *J. Chem. Soc. Chem. Comm.* **1985**, 1570-1571.
15. Wang, G. J.; Chen, M. H.; Zhou, M. F., Matrix Isolation Infrared Spectroscopic and Theoretical Studies on the Reactions of Manganese and Iron Monoxides with Methane. *J. Phys. Chem. A* **2004,** 108, (51), 11273-11278.
16. Wang, G. J.; Zhou, M. F., Probing the intermediates in the $MO + CH_4$ --> $M + CH_3OH$ reactions by matrix isolation infrared spectroscopy. *Int. Rev. Phys. Chem.* **2008,** 27, (1), 1-25.
17. Aguirre, F.; Husband, J.; Thompson, C. J.; Stringer, K. L.; Metz, R. B., Electronic Spectroscopy of Intermediates Involved in the Conversion of Methane to Methanol by FeO^+. *J. Chem. Phys.* **2002,** 116, 4071-4078.
18. Metz, R. B., Photofragment Spectroscopy of Covalently Bound Transition Metal Complexes: A Window into C-H and C-C Bond Activation by Transition Metal Ions. *Int. Rev. Phys. Chem.* **2004,** 23, (1), 79-108.

19. Husband, J.; Aguirre, F.; Ferguson, P.; Metz, R. B., Vibrationally Resolved Photofragment Spectroscopy of FeO^+. *J. Chem. Phys.* **1999,** 111, 1433-1437.
20. Schröder, D.; Fiedler, A.; Hrusák, J.; Schwarz, H., Experimental and Theoretical Studies Toward a Characterization of Conceivable Intermediates Involved in the Gas-Phase Oxidation of Methane by Bare FeO^+. Generation of Four Distinguishable $[Fe,C,H_4,O]^+$ Isomers. *J. Am. Chem. Soc.* **1992,** 114, 1215-1222.
21. Aguirre, F.; Husband, J.; Thompson, C. J.; Stringer, K. L.; Metz, R. B., The Low-Lying Electronic States of FeO^+: Rotational Analysis of the Resonance Enhanced Photodissociation Spectra of the $^6\Pi_{7/2} <-- {}^6\Sigma^+$ System. *J. Chem. Phys.* **2003,** 119, (19), 10194-10201.
22. Kaur, D.; Desouza, A. M.; Wanna, J.; Hammad, S. A.; Mercorelli, L.; Perry, D. S., Multipass Cell for Molecular-Beam Absorption-Spectroscopy. *Appl. Optics* **1990,** 29, (1), 119-124.
23. Altinay, G.; Metz, R. B., Vibrational Spectroscopy of Intermediates in Benzene-to-Phenol Conversion by FeO^+. *J. Am. Soc. Mass Spectrom.* **2010,** 21, 750-757.
24. Frisch, M. J.; Trucks, G. W.; Schlegel, H. B.; Scuseria, G. E.; Robb, M. A.; Cheeseman, J. R.; Montgomery Jr., J. A.; Vreven, T.; Kudin, K. N.; Burant, J. C.; Millam, J. M.; Iyengar, S. S.; Tomasi, J.; Barone, V.; Mennucci, B.; Cossi, M.; Scalmani, G.; Rega, N.; Petersson, G. A.; Nakatsuji, H.; M.Hada; Ehara, M.; Toyota, K.; Fukuda, R.; Hasegawa, J.; Ishida, M.; Nakajima, T.; Honda, Y.; Kitao, O.; Nakai, H.; Klene, M.; Li, X.; Knox, J. E.; Hratchian, H. P.; Cross, J. B.; Adamo, C.; Jaramillo, J.; Gomperts, R.; Stratmann, R. E.; Yazyev, O.; Austin, A. J.; Cammi, R.; Pomelli, C.; Ochterski, J. W.; Ayala, P. Y.; Morokuma, K.; Voth, G. A.; Salvador, P.; Dannenberg, J. J.; Zakrzewski, V. G.; Dapprich, S.; Daniels, A. D.; Strain, M. C.; Farkas, O.; Malick, D. K.; Rabuck, A. D.; Raghavachari, K.; Foresman, J. B.; Ortiz, J. V.; Cui, Q.; Baboul, A. G.; Clifford, S.; Cioslowski, J.; Stefanov, B. B.; Liu, G.; Liashenko, A.; Piskorz, P.; Komaromi, I.; Martin, R. L.; Fox, D. J.; Keith, T.; Al-Laham, M. A.; Peng, C. Y.; Nanayakkara, A.; Challacombe, M.; Gill, P. M. W.; Johnson, B.; Chen, W.; Wong, M. W.; Gonzalez, C.; Pople, J. A. *Gaussian 03*, Gaussian, Inc.: Pittsburgh PA, Wallingford CT, 2004.
25. Dolg, M.; Wedig, U.; Stoll, H.; Preuss, H., Abinitio Pseudopotential Study of the 1st Row Transition-Metal Monoxides and Iron Monohydride. *J. Chem. Phys.* **1987,** 86, (4), 2123-2131.
26. Montgomery Jr, J. A.; Frisch, M. J.; Ochterski, J. W.; Petersson, G. A., A complete basis set model chemistry. VI. Use of density functional geometries and frequencies. *J. Chem. Phys.* **1999,** 110, (6), 2822-2827.
27. Montgomery Jr, J. A.; Frisch, M. J.; Ochterski, J. W.; Petersson, G. A., A complete basis set model chemistry. Use of the minimum population localization method. *J. Chem. Phys.* **2000,** 112, 6532-6542.
28. Shiota, Y.; Yoshizawa, K., Methane-to-Methanol Conversion by First-Row Transition-Metal Oxide Ions: ScO^+, TiO^+, VO^+, CrO^+, MnO^+, FeO^+, CoO^+, NiO^+, and CuO^+. *J. Am. Chem. Soc.* **2000,** 122, 12317-12326.
29. Yoshizawa, K.; Shiota, Y.; Yamabe, T., Methane-Methanol Conversion by MnO^+, FeO^+, and CoO^+: A Theoretical Study of Catalytic Activity. *J. Am. Chem. Soc.* **1998,** 120, 564-572.

30. Kulik, H. J.; Marzari, N., A self-consistent Hubbard U density-functional theory approach to the addition-elimination reactions of hydrocarbons on bare FeO+. *J. Chem. Phys.* **2008,** 129, (13), 134314.
31. Abusen, R.; Bennett, F. R.; Cox, S. G.; McNab, I. R.; Sharp, D. N.; Shiell, R. C.; Smith, F. E.; Walley, J. M., Hyperfine-resolved spectrum of the molecular dication DCl^{2+}. *Phys. Rev. A* **2000,** 61, (5), 050501.
32. Glukhotsev, M.; Bach, R. D.; Pross, A.; Radom, L., *Chem. Phys. Lett.* **1996,** 260, 558-564.
33. Danovich, D.; Shaik, S., Spin-orbit coupling in the oxidative activation of H-H by FeO+. Selection rules and reactivity effects. *J. Am. Chem. Soc.* **1997,** 119, 1773.
34. Schröder, D.; Shaik, S.; Schwarz, H., Two-State Reactivity as a New Concept in Organometallic Chemistry. *Acc. Chem. Res.* **2000,** 33, 139-145.
35. Shaik, S.; Hirao, H.; Kumar, D., Reactivity of high-valent iron-oxo species in enzymes and synthetic reagents: A tale of many states. *Acc. Chem. Res.* **2007,** 40, (7), 532-542.
36. Shiota, Y.; Yoshizawa, K., A Spin-Orbit Coupling Study on the Spin Inversion Processes in the Direct Methane-to-Methanol Conversion by FeO^+. *J. Chem. Phys.* **2003,** 118, (13), 5872-5879.
37. Schröder, D.; Schwarz, H.; Clemmer, D. E.; Chen, Y.; Armentrout, P. B.; Baranov, V.; Bohme, D. K., Activation of Hydrogen and Methane by Thermalized FeO^+ in the Gas Phase as Studied by Multiple Mass Spectrometric Techniques. *Int. J. Mass Spectrom. Ion Proc.* **1997,** 161, 175-191.
38. Kellogg, C. B.; Irikura, K. K., Gas-phase Thermochemistry of Iron Oxides and Hydroxides: Portrait of a Super-efficient Flame Suppressant. *J. Phys. Chem. A* **1999,** 103, (8), 1150-1159.
39. Glukhovtsev, M. N.; Bach, R. D.; Nagel, C. J., Performance of the B3LYP/ECP DFT Calculations of Iron-Containing Compounds. *J. Phys. Chem. A* **1997,** 101, 316-323.
40. Feller, D., *Ab Initio* Study of M^+:18-Crown-6 Microsolvation. *J. Phys. Chem. A* **1997,** 101, 2723-2731.
41. Metz, R. B.; Nicolas, C.; Ahmed, M.; Leone, S. R., Direct Determination of the Ionization Energies of FeO and CuO with VUV Radiation. *J. Chem. Phys.* **2005,** 123, 114313.
42. Armentrout, P. B.; Kickel, B. L., Gas-Phase Thermochemistry of Transition Metal Ligand Systems: Reassessment of Values and Periodic Trends. In *Organometallic Ion Chemistry*, Freiser, B. S., Ed. Kluwer Academic Publishers: Dordrecht, The Netherlands, 1994; pp 1-45.
43. Lu, W. Y.; Wong, T. H.; Sheng, Y.; Lytle, A. T.; Kleiber, P. D., Photodissociation Spectroscopy of Zn^+-Methanol. *J. Phys. Chem. A* **2003,** 107, (7), 984-989.
44. Citir, M.; Altinay, G.; Metz, R. B., Electronic and Vibrational Spectroscopy and Vibrationally Mediated Photodissociation of $V^+(OCO)$. *J. Phys. Chem. A* **2006,** 110, 5051-5057.
45. Okumura, M.; Yeh, L. I.; Meyers, J. D.; Lee, Y. T., Infrared Spectra of the Cluster Ions $H_7O_3^+$-H_2 and $H_9O_4^+$-H_2. *J. Chem. Phys.* **1986,** 85, 2328-2329.

46. Corcelli, S. A.; Kelley, J. A.; Tully, J. C.; Johnson, M. A., Infrared Characterization of the Icosahedral Shell Closing in $Cl^-\cdot H_2O\cdot Ar_n$ ($1 \le n \le 13$) Clusters. *J. Phys. Chem. A* **2002,** 106, 4872-4879.
47. Duncan, M. A., Infrared Spectroscopy to Probe Structure and Dynamics in Metal Ion-molecule Complexes. *Int. Rev. Phys. Chem.* **2003,** 22, (2), 407-435.
48. Vaden, T. D.; Lisy, J. M.; Carnegie, P. D.; Pillai, E. D.; Duncan, M. A., Infrared Spectroscopy of the $Li^+(H_2O)Ar$ complex: the role of internal energy and its dependence on ion preparation. *Phys. Chem. Chem. Phys.* **2006,** 8, (26), 3078-3082.
49. Furuya, A.; Tsuruta, M.; Misaizu, F.; Ohno, K.; Inokuchi, Y.; Judai, K.; Nishi, N., Infrared photodissociation spectroscopy of $Al^+(CH_3OH)_n$ (n=1-4). *J. Phys. Chem. A* **2007,** 111, (27), 5995-6002.
50. Asmis, K. R.; Sauer, J., Mass-selective vibrational spectroscopy of vanadium oxide cluster ions. *Mass Spec. Rev.* **2007,** 26, (4), 542-562.
51. Dopfer, O., Spectroscopic and theoretical studies of CH_3^+-Rg_n clusters (Rg = He, Ne, Ar): From weak intermolecular forces to chemical reaction mechanisms. *Int. Rev. Phys. Chem.* **2003,** 22, (3), 437-495.
52. Hammer, N. I.; Diken, E. G.; Roscioli, J. R.; Johnson, M. A.; Myshakin, E. M.; Jordan, K. D.; McCoy, A. B.; Huang, X.; Bowman, J. M.; Carter, S., The Vibrational Predissociation Spectra of the $H_5O_2^+ \bullet RG_n$ (RG=Ar,Ne) Clusters: Correlation of the Solvent Perturbations in the Free OH and Shared Proton Transitions of the Zundel Ion. *J. Chem. Phys.* **2005,** 122, (24), Art. No. 244301.
53. Tjelta, B. L.; Walter, D.; Armentrout, P. B., Determination of weak Fe^+-L bond energies (L = Ar, Kr, Xe, N-2, and CO_2) by ligand exchange reactions and collision-induced dissociation. *Int. J. Mass Spectrom.* **2001,** 204, (1-3), 7-21.
54. Shimanouchi, T., Molecular Vibrational Frequencies. In *NIST Chemistry WebBook, NIST Standard Reference Database Number 69*, Linstrom, P. J.; Mallard, W. G., Eds. National Institute of Standards and Technology: Gaithersburg MD, 1972.
55. Allison, J.; Ridge, D. P., Reactions of Atomic Metal Ions with Alkyl Halides and Alcohols in the Gas Phase. *J. Am. Chem. Soc.* **1979,** 101, 4998-5009.
56. Chen, Y.-M.; Clemmer, D. E.; Armentrout, P. B., Conversion of CH_4 to CH_3OH: Reactions of CoO^+ with CH_4 and D_2, Co^+ with CH_3OD and D_2O, and $Co^+(CH_3OD)$ with Xe. *J. Am. Chem. Soc.* **1994,** 116, 7815.

CHAPTER 4

VIBRATIONAL SPECTROSCOPY OF INTERMEDIATES IN BENZENE-TO-PHENOL CONVERSION BY FeO^+

4.1 Introduction

Phenol is an important commodity chemical, with 9 million metric tons produced worldwide. It is used to make materials such as polycarbonate, nylon and epoxy resins, drugs such as aspirin and cosmetics such as sunscreens and hair dyes.[1] Industrially, phenol is mainly produced from benzene via the cumene process: benzene → cumene → cumene hydroperoxide → phenol. This three-step process is energy intensive and has a low phenol yield. Thus, *direct* conversion of benzene to phenol has attracted great attention due to its economical and industrial importance. Promising direct benzene-phenol oxidation techniques include Fe-doped ZSM-5 zeolites with N_2O as the oxidant[2, 3] and direct oxidation using O_2 and H_2 through a Pd membrane.[4] Some bacteria can directly convert benzene to phenol under mild conditions using toluene monooxygenases, which have a di-iron active site.[5] The biotoxicity of benzene in mammals is enhanced by its conversion to phenol by cytochrome P450, which has an Fe-heme active site.[6, 7]

Schwarz, Schröder and coworkers showed that, under thermal conditions, several gas-phase metal oxide cations MO^+ react efficiently with benzene to produce phenol with good selectivity (Table1.3)[8] The reaction of FeO^+ has been particularly well-studied. It

primarily produces Fe^+ + phenol (56%) and $Fe(C_5H_6)^+$ + CO (37%).[9] They subsequently produced several $[FeC_6H_6O]^+$ isomers by reacting Fe^+ with different precursors in a chemical ionization source and characterized them using fragmentation patterns observed following collisional activation in a tandem mass spectrometer.[10]

This prototypical arene oxidation reaction has also been studied computationally. Yoshizawa et al. calculated the energetics of reactants, intermediates and transition states for benzene-phenol conversion by FeO^+ using B3LYP hybrid density functional theory.[11] They considered a mechanism in which FeO^+ first binds to the ring, forming a $OFe^+(C_6H_6)$ entrance channel complex, then hydrogen abstraction via transition state TS1 forms the insertion intermediate $HO\text{-}Fe^+\text{-}C_6H_5$. Phenyl or hydroxyl migration through TS2 produces the $Fe^+(C_6H_5OH)$ exit channel complex, which subsequently dissociates to $Fe^+ + C_6H_5OH$. Molecular dynamics simulations on this potential energy surface predict that the reaction is rapid, and that the hydrogen transfer at TS1 leads to O-H stretch excitation in the insertion intermediate.[12] They later also considered two other possible mechanisms. A radical mechanism involving direct H atom abstraction via a Fe-O-H transition state was considered unlikely on energetic grounds. An oxygen insertion mechanism which proceeds via an arenium intermediate $[FeOC_6H_6]^+$ with covalent Fe-O-C bonds was considered to be favorable if the FeO^+ was also ligated.[13] The oxygen insertion mechanism was also studied by Kwapien et. al.[14]

Our group has studied the vibrational and electronic spectroscopy of intermediates of methane to methanol conversion by FeO^+.[15, 16] By extending these studies to benzene-phenol conversion by FeO^+ we can evaluate the effect of the aromatic ring on the reaction mechanism.

4.2 Experimental and Theoretical Methods

Vibrational spectra are measured using a dual time-of-flight reflectron photofragment spectrometer (See chapter 2 for details).[17, 18] Iron cations are generated by laser ablation of an iron rod (Sigma-Aldrich, 99.8% pure). Fe^+ cations react with either 0.01% phenol in helium or a mixture of 2% N_2O and 0.5% benzene in helium to produce the target molecule. The choice of precursors is guided by the collision-induced dissociation (CID) studies of Becker et al.[10] and is discussed in more detail below. Ions produced in the source expand supersonically into vacuum and cool to a rotational temperature of ~10 K.[19] Ions are accelerated to 1800 V kinetic energy, then re-referenced to ground potential before entering the field-free flight tube. Mass-selected ions are photodissociated at the turning point of the reflectron. Energetically, photodissociation of $[HO\text{-}Fe\text{-}C_6H_5]^+$ requires at least four photons in the O-H stretching region. So, vibrational spectra are obtained using infrared multi-photon dissociation (IRMPD) of $[HO\text{-}Fe\text{-}C_6H_5]^+$ and $Fe^+(C_6H_5OH)$. The photodissociation efficiency is greatly improved using a multi-pass mirror arrangement[20] in which the laser makes 21 passes through the ion cloud (See chapter 2 for details). The light source is a Nd:YAG pumped optical parametric oscillator which is tunable from 2 to 5 μm, producing ~10 mJ/pulse near 3600 cm^{-1}. The IR beam path is purged with nitrogen to minimize absorptions by water vapor. The laser wavelength is calibrated using H_2O absorptions. Fragment ions and undissociated parent ions are detected by a dual micro-channel plate detector. The ion signal is amplified, collected on a digital oscilloscope or a gated integrator, and

averaged with a LabView based program. The *photodissociation spectrum* is obtained by monitoring the yield of the fragment ion of interest as a function of wavelength and normalizing to parent ion signal and laser fluence. In this study we separately and simultaneously monitor the Fe^+ and $FeOH^+$ fragments. The photodissociation spectrum is the product of the absorption spectrum and the photodissociation quantum yield. Computations are carried out with the Gaussian 2003 program package.[21] Optimized geometries of the reactants, intermediates, transition states and products are calculated using the Becke Lee-Yang-Parr hybrid HF/DFT method (B3LYP) with the 6-311+G(d,p) basis set. Vibrational frequencies are computed to ensure that all optimized geometries correspond to a local minimum or a first-order saddle point (for transition states). To obtain more accurate energies we calculated single-point energies using the complete basis set CBS-QB3 method, which is optimized for thermodynamics.[22, 23] All energies include zero point energy and correspond to 0 Kelvin values.

4.3 Results and Discussion

4.3.1 Potential Energy Surface for the $FeO^+ + C_6H_6$ Reaction

To establish the accuracy of the computational method used, we compare calculated and accurate experimental results for the sextet-quartet energy splitting in Fe^+, the Fe^+-O bond enthalpy, and the overall exothermicity of the $FeO^+ + C_6H_6 \rightarrow Fe^+ + C_6H_5OH$ reaction. Experimentally, the ground state of Fe^+ is ^6D ($3d^6$ 4s), with the ^4F ($3d^7$) state 23.9 kJ/mol higher. Calculations at the B3LYP/6-311+G(d,p) level incorrectly predict a quartet ground state, 19.8 kJ/mol below the sextet state. This is a well known failure of the B3LYP method.[24, 25] An attractive alternative to rigorous and expensive high level

correlated *ab initio* calculations are hybrid methods developed for accurate thermochemistry, such as the complete basis set CBS-QB3 approach.[22, 23] In CBS-QB3, one first optimizes the geometry and calculates harmonic frequencies at the B3LYP level. Then, from a series of single point energy calculations at various levels of theory and with different basis sets, one extrapolates the result of a large basis set calculation at a very high level of theory. CBS-QB3 thermodynamics have similar accuracy to an extrapolated series of CCSD(T) calculations with very large basis sets, and are significantly more accurate than a single CCSD(T) calculation with a modest basis set.[26] CBS-QB3 calculations correctly predict the ordering of the Fe^+ states, with the quartet 30.1 kJ/mol above the sextet. For the dissociation enthalpy of FeO^+, CBS-QB3 calculations predict 337.8 kJ/mol, in excellent agreement with experiment (340±2 kJ/mol;[27] 335±5 kJ/mol).[28] For the $FeO^+ + C_6H_6 \rightarrow Fe^+ + C_6H_5OH$ reaction enthalpy, CBS-QB3 predicts -88 kJ/mol, in excellent agreement with experiment, -85±2 kJ/mol.[27, 29]

Figure 4.1 shows the potential energy surface for the $FeO^+ + C_6H_6$ reaction calculated using the CBS-QB3 method. Phenol production occurs in a two-step concerted manner through the formation of the hydroxy intermediate $[HO\text{-}Fe\text{-}C_6H_5]^+$. The minimum energy path involves first producing the $OFe^+(C_6H_6)$ entrance channel complex. For the sextet state, the FeO^+ is not centered on the ring, but rather binds to adjacent carbons in a η_2 configuration, with r(Fe-C)=2.34 Å. Quartet FeO^+ is nearly

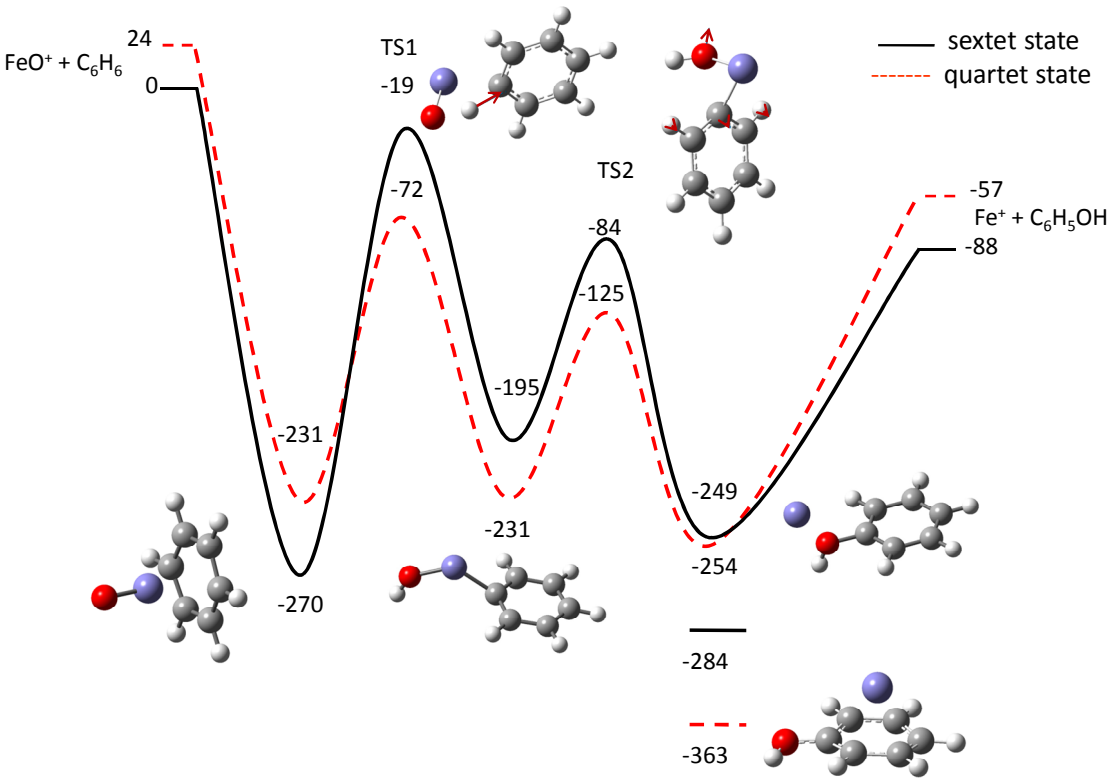

Figure 4.1 Schematic potential energy surface for the $FeO^+ + C_6H_6 \rightarrow Fe^+ + C_6H_5OH$ reaction and structures of intermediates and transition states. Energies (in kJ/mol) are calculated at the CBS-QB3 level of theory. The solid line represents the sextet and dashed line the quartet surface. The imaginary frequencies for transition states TS1 and TS2 are 1930*i* and 390*i* for quartet states and 1916*i* and 352*i* for sextet states, respectively. The corresponding vibrations are shown in the figure. All geometries shown are those of the quartet states.

centered on the ring, with r(Fe-C)=2.32 Å. Hydrogen abstraction via TS1 leads to the key $[HO\text{-}Fe\text{-}C_6H_5]^+$ insertion intermediate. For the quartet state, the Fe-O-H group is perpendicular to the ring, with r(Fe-C)=1.878 Å, r(Fe-O)=1.705 Å and r(O-H)=0.964 Å. In the sextet state, the Fe-O-H group is in the plane of the ring, with slightly longer bonds to iron: with r(Fe-C)=1.908 Å, r(Fe-O)=1.729 Å and r(O-H)=0.961 Å. The FeO^+ reactant and Fe^+ product have sextet ground states.[19] The minimum energy pathway involves quartet intermediates. However, since both sextet TS1 and sextet TS2 lie below the reactants, the reaction can proceed completely along the sextet pathway without changing spin. The overall reaction *efficiency* is determined by the probability that reactants will cross TS1, which can occur in two ways: by crossing sextet TS1, or by changing spin and crossing the low-lying quartet TS1. This is a major difference from the FeO^+ + methane reaction (Ch.3), where sextet TS1 lies above reactants. As a result, FeO^+ reacts with benzene at the collision rate,[9] while it reacts with methane at only ~20% of the collision rate.[30, 31] Once produced, the $[HO\text{-}Fe\text{-}C_6H_5]^+$ insertion intermediate can isomerize via TS2 to form the $Fe^+(C_6H_5OH)$ exit channel complex, which subsequently dissociates to $Fe^+ + C_6H_5OH$. The calculations predict that production of $FeOH^+ + C_6H_5$ is 20 kJ/mol endothermic. So, it is not surprising that is not observed as a product of the $FeO^+ + C_6H_6$ reaction.[9] This is another significant difference with the $FeO^+ + CH_4$ system, where $FeOH^+ + CH_3$ is energetically allowed, is a significant product at thermal energies, and dominates at high collision energy.[31] Manganese is the only first-row transition metal for which MOH^+ is observed as a product of the MO^+ + benzene reaction.[8] The calculations predict two isomers of the

$Fe^+(C_6H_5OH)$ exit channel complex. A σ-complex in which the Fe^+ binds to the oxygen lone pair, and a π-complex, where the Fe^+ binds to the ring. The π-complex is predicted to lie lower in energy, at -284 kJ/mol (sextet state) and -363 kJ/mol (quartet state), relative to $FeO^+ + C_6H_6$. In the σ-complex, the Fe^+ is not in the plane of the ring, and is 1.952 Å from the oxygen for the quartet state. The Fe-O distance is substantially longer for the sextet state, at 2.071 Å. The quartet π-complex has a very interesting geometry. The carbons *ortho* and *meta* to the –OH group pucker towards the Fe^+, leading to η_4 coordination, with r(Fe-C)=2.20 Å. Sextet Fe^+ binds much more weakly and leads to much less distortion of the ring. The Fe^+ is slightly displaced towards a *meta* carbon, with r(Fe-C)=2.53 Å. The electron in the large 4s orbital leads to much weaker non-covalent interactions for sextet Fe^+ ($3d^6$ 4s electron configuration) than for quartet Fe^+ ($3d^7$ configuration). Our potential energy surface for the $FeO^+ + C_6H_6$ reaction is similar to one calculated by Yoshizawa et al. at the B3LYP/6-311+G(d,p) level.[11] One key difference is that the B3LYP calculations predict that the $[HO\text{-}Fe\text{-}C_6H_5]^+$ insertion intermediates are ~20 kJ/mol more stable relative to reactants. As a result, TS1 and TS2 are also predicted to be ~20 kJ/mol lower. Previous studies of the $FeO^+ + C_6H_6$ reaction have also considered two other mechanisms: a radical and an oxygen insertion mechanism.[13, 14] We measure the spectra of $[FeC_6H_6O]^+$ intermediates in the O-H stretching region. The C-H stretches are weak and they are not distinctive for different intermediates. We did not carry out calculations on the intermediates in the alternate mechanisms as they do not contain an O-H bond. In addition, as our experiments measure spectra in the O-H stretching region, we are not sensitive to the presence of other likely intermediates such as the $OFe^+(C_6H_6)$ entrance channel complex or the key

arenium intermediate $[FeOC_6H_6]^+$ in the proposed oxygen insertion mechanism, as these species do not contain O-H bonds.

4.3.2 IRMPD Spectroscopy of $[FeC_6H_6O]^+$

A major challenge in studies of intermediates of ion-molecule reactions is to find suitable precursors and reaction conditions to selectively produce specific intermediates. The identity of the intermediates produced is deduced from their vibrational spectrum and dissociation pathways. Vibrational spectra of $[HO\text{-}Fe\text{-}C_6H_5]^+$ and $Fe^+(C_6H_5OH)$ in the O-H stretching region were measured using photofragment spectroscopy. A challenge in obtaining vibrational spectra using photofragment spectroscopy is that absorption of a photon needs to lead to bond breaking. One photon in the O-H stretching region only has ~43 kJ/mol of energy, so photodissociation of $[HO\text{-}Fe\text{-}C_6H_5]^+$ or $Fe^+(C_6H_5OH)$ requires at least four photons. So, vibrational spectra were measured using infrared multi-photon dissociation (IRMPD). We previously used IRMPD to measure vibrational spectra of the $[HO\text{-}Fe\text{-}CH_3]^+$ and $Fe^+(CH_3OH)$ intermediates of the $FeO^+ + CH_4 \rightarrow Fe^+ + CH_3OH$ reaction (Chapter 3).[15] They are not ideal candidates for IRMPD due to the high binding energy and small size of the molecules, which leads to relatively slow intramolecular vibrational redistribution (IVR) of energy. Intermediates of the $FeO^+ + C_6H_6$ reaction are much better suited to IRMPD studies, and we observe higher dissociation yields and significantly narrower spectra for the larger system.

In this study, we find that reacting ablated Fe^+ with phenol or benzene + N_2O produces $[HO\text{-}Fe\text{-}C_6H_5]^+$ and $Fe^+(C_6H_5OH)$, with the relative amounts depending on the

precursor. IRMPD of ions generated by reacting Fe^+ with 0.01% phenol in helium primarily produces Fe^+ and $FeOH^+$ photofragments. Along with a small amount of $Fe^+(C_6H_4) + H_2O$, trace amounts of $Fe^+(C_5H_6) + CO$ and $Fe^+(C_5H_5) + HCO$ are also observed. The maximum dissociation yield is ~15%. Figure 4.2 (top) shows IRMPD spectra obtained by monitoring Fe^+ (blue) and $FeOH^+$ (red). The two channels give completely different vibrational spectra, indicating that two or more intermediates are produced in the source, and each channel monitors a different intermediate or group of intermediates. The $Fe^+(C_6H_4)$ and Fe^+ channels have a similar wavelength dependence. Photodissociation of $[FeC_6H_6O]^+$ ions produced using 0.5% benzene and 2% N_2O in helium also gives Fe^+ and $FeOH^+$ as the major fragments. Again, spectra obtained by monitoring Fe^+ and $FeOH^+$ are different (Figure 2, bottom). The observed dissociation products and vibrational frequencies (see below) indicate that IRMPD of $Fe^+(C_6H_5OH)$ produces $Fe^+ + C_6H_5OH$ while IRMPD of $[HO\text{-}Fe\text{-}C_6H_5]^+$ forms $FeOH^+ + C_6H_5$. Becker et al. generated several $[FeC_6H_6O]^+$ isomers by reacting Fe^+ produced by electron bombardment of $Fe(CO)_5$ with organic molecules in a chemical ionization source and characterized them by collisional activation (CA).[10] CA of $Fe^+(C_6H_5OH)$ primarily leads to $Fe^+(C_6H_4) + H_2O$ and Fe^+ + phenol, while $Fe^+(C_5H_6) + CO$ and $FeOH^+ + C_6H_5$ are major products in CA of $[HO\text{-}Fe\text{-}C_6H_5]^+$. So, the fragment ions observed by CA and IRMPD are similar.

In the O-H stretching region, IRMPD of $[FeC_6H_6O]^+$ produced by reacting Fe^+ with phenol in helium generates $FeOH^+ + C_6H_5$ or $Fe^+ + C_6H_5OH$, depending on wavelength. The spectrum of $Fe^+(C_6H_5OH)$, obtained by monitoring Fe^+, consists of a 45 cm^{-1} FWHM peak at 3598 cm^{-1}. This is 59 cm^{-1} red shifted from the O-H stretch in bare phenol (3657 cm^{-1}).[32] Under the same conditions, the $FeOH^+$ channel gives a much less intense, 50 cm^{-1} FWHM peak at ~3700 cm^{-1}. Dissociating $[FeC_6H_6O]^+$ formed by reacting Fe^+ with N_2O/benzene in helium also produces Fe^+ and $FeOH^+$. The relative intensity of the $FeOH^+$ channel increases eight fold (figure 2 bottom), but its peak position and shape are unchanged. This is consistent with reaction of Fe^+ with N_2O and benzene producing more $[HO\text{-}Fe\text{-}C_6H_5]^+$ than reaction of Fe^+ with phenol. The peak obtained by monitoring Fe^+ is slightly narrower for the N_2O/benzene precursor than for phenol. This suggests that more than one isomer or spin state of $Fe^+(C_6H_5OH)$ contributes to the spectrum or, more likely, that the ions have slightly different vibrational temperatures in the two cases. IRMPD spectra are more sensitive to internally excited molecules than one-photon spectroscopies, as fewer photons may be required to dissociate hot molecules.

To help assign the spectra, we calculated geometries, energies and frequencies of the quartet and sextet states of insertion intermediate $[HO\text{-}Fe\text{-}C_6H_5]^+$ and exit channel complexes $Fe^+(C_6H_5OH)$ (Table 4.1). Calculations were carried out using the B3LYP hybrid density functional with the 6-311+G(d,p) basis set. Calculated harmonic frequencies are scaled by 0.954, which is the ratio of the experimental to calculated O-H stretching frequencies in bare phenol.

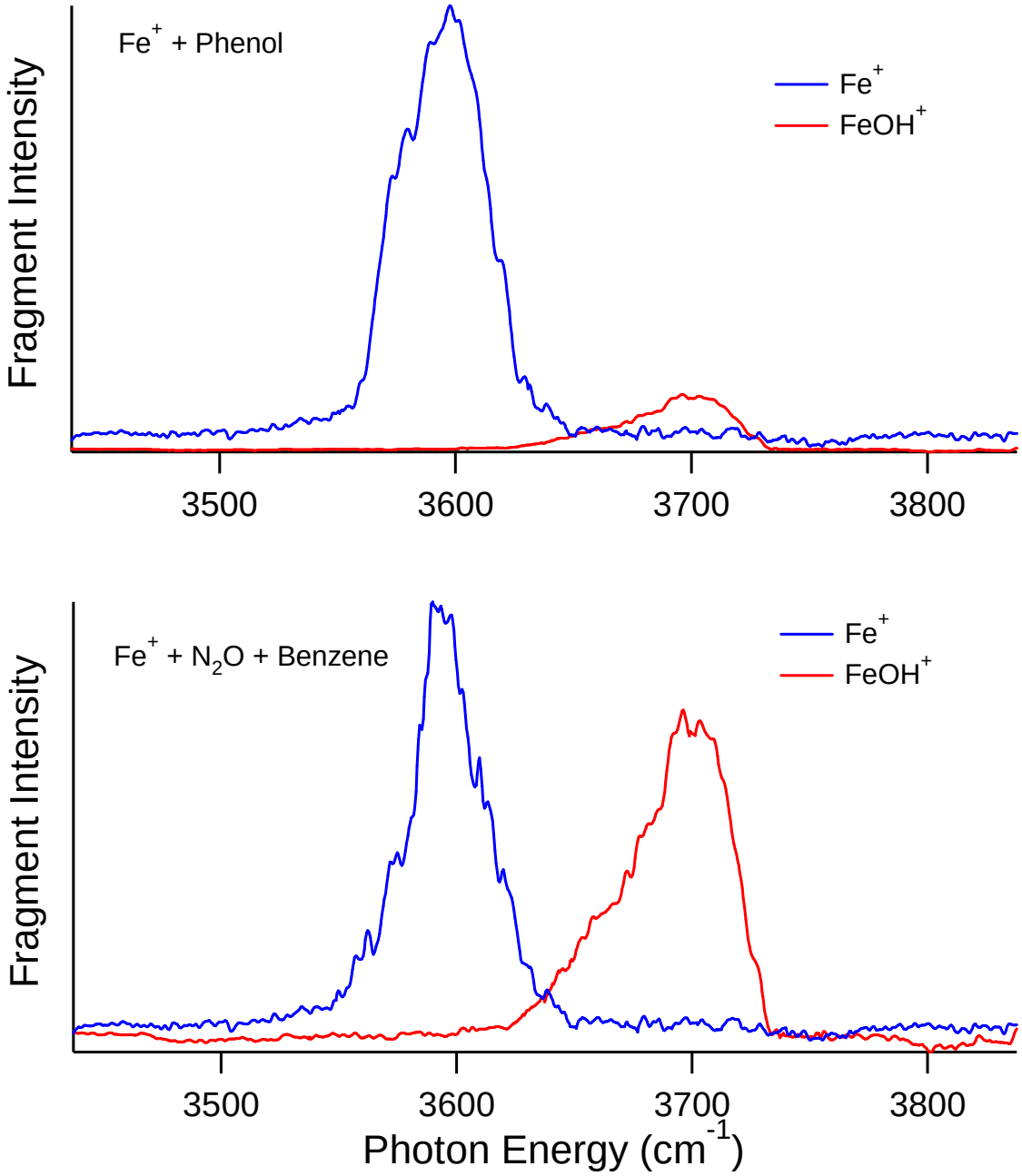

Figure 4.2 Vibrational spectra of $[FeC_6H_6O]^+$ in the O-H stretching region. Spectra are obtained by IRMPD of ions produced by reacting Fe^+ with C_6H_5OH (top) and by reacting Fe^+ with N_2O and C_6H_6 (bottom). Spectra obtained by monitoring Fe^+ and $FeOH^+$ are in blue and red, respectively. The two product channels are formed by dissociation of different $[FeC_6H_6O]^+$ isomers, and the relative amounts of these isomers depends on the precursor.

4.3.3 Vibrational Spectroscopy of the $[HO\text{-}Fe\text{-}C_6H_5]^+$ Insertion Intermediate

IRMPD of the $[HO\text{-}Fe\text{-}C_6H_5]^+$ insertion intermediate produces $FeOH^+ + C_6H_5$. Reacting laser-ablated Fe^+ with N_2O and benzene produces significantly more $[HO\text{-}Fe\text{-}C_6H_5]^+$ than does reaction with phenol. Both precursors lead to a vibrational spectrum with a peak at ~3700 cm^{-1} and a shoulder at ~3670 cm^{-1} (red traces in Figs. 4.2 and 4.3).

The calculations predict O-H stretch vibrations at 3700 cm^{-1} and 3674 cm^{-1} for the sextet and quartet states of the insertion intermediate, respectively. The sextet has somewhat higher oscillator strength, while the quartet is predicted to lie 36 kJ/mol lower in energy. Both spin states appear to contribute to the spectrum: the peak at 3700 cm^{-1} is due to the sextet state, and the quartet state is responsible for the shoulder at ~3670 cm^{-1}. In our study of the insertion intermediate for the $FeO^+ + CH_4$ reaction, we also found that both spin states contribute to the vibrational spectrum. IRMPD of $[HO\text{-}Fe\text{-}CH_3]^+$ gives an asymmetrical peak at 3623 cm^{-1} with a shoulder at 3576 cm^{-1}, which were assigned to the sextet and quartet states, respectively.[15] Adding argon atoms to $[HO\text{-}Fe\text{-}CH_3]^+$ removes charge from the metal center and leads to progressively larger blue shifts in the O-H stretch frequencies. The O-H stretch in *neutral* $HO\text{-}Fe\text{-}CH_3$ shows an even larger blue shift, to 3745 cm^{-1}.[33, 34] Mulliken population analysis shows a charge of +0.77 for the Fe-O-H moiety in $[HO\text{-}Fe\text{-}CH_3]^+$, which drops to 0.56 in $[HO\text{-}Fe\text{-}C_6H_5]^+$. Relative to $[HO\text{-}Fe\text{-}CH_3]^+$, the O-H stretches of $[HO\text{-}Fe\text{-}C_6H_5]^+$ exhibit a ~80 cm^{-1} blue shift. Thus, this system continues a trend we observed previously: removing charge from the Fe-O-H group blue-shifts the O-H stretch frequency.

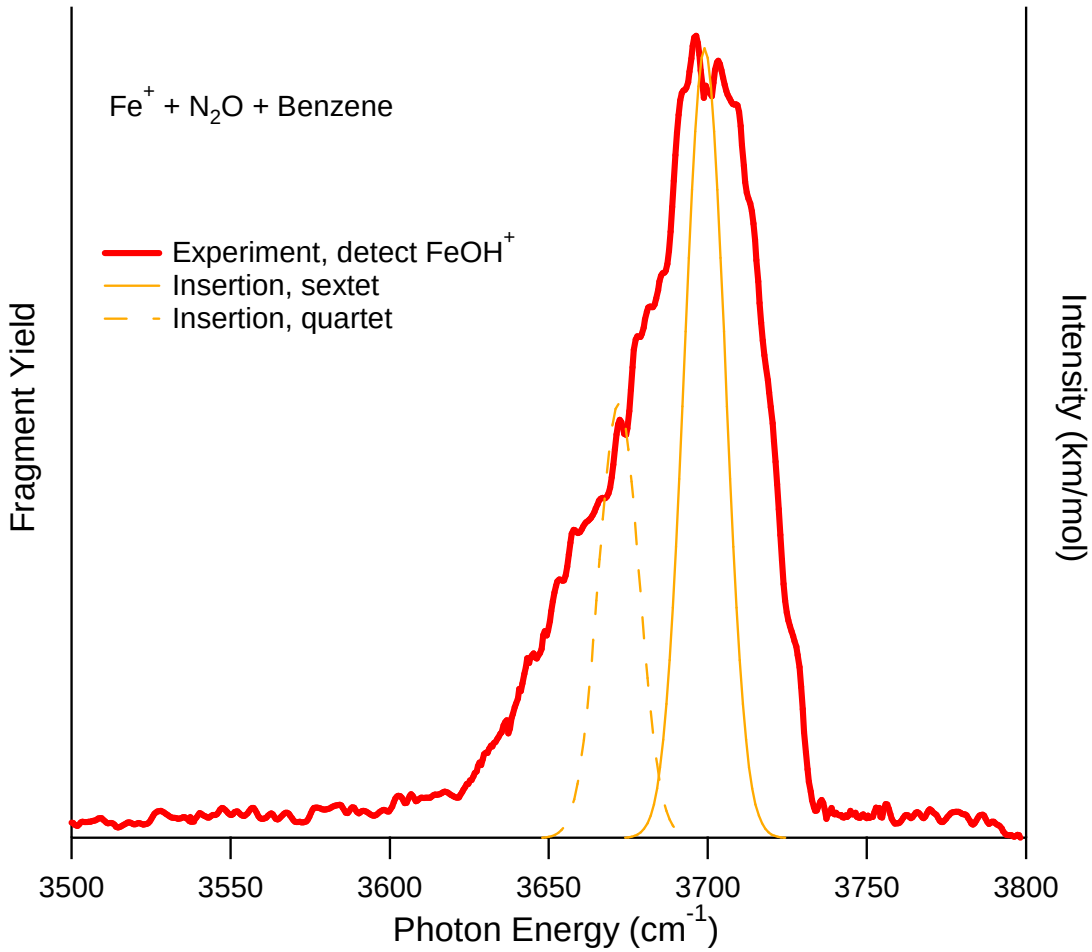

Figure 4.3. Experimental and calculated vibrational spectra of $[HO\text{-}Fe\text{-}C_6H_5]^+$ in the O-H stretching region. The experimental spectrum is obtained by IRMPD of ions produced by reacting Fe^+ with N_2O and C_6H_6 and monitoring $FeOH^+$ fragments (red). Calculated spectra (right axis) are at the B3LYP/6-311+G(d,p) level, with frequencies scaled by 0.954. For the simulations, solid lines represent sextet states and dashed lines quartet states.

	O-H stretches (cm^{-1})	C-H stretches (cm^{-1})
C_6H_5OH	3657(61)	3049***(4)***, 3042***(17)***, 3029***(17)***, 3003***(14)***
$OFe^+(C_6H_6)$ quartet	-	3063***(0)***, 3058***(42)***, 3050***(0)***, 3049***(0)***, 3044***(0)***,
$OFe^+(C_6H_6)$ sextet	-	3064***(5)***, 3057***(13)***, 3053***(9)***, 3048***(3)***, 3045***(3)***, 3037***(0)***,
$[HO\text{-}Fe\text{-}C_6H_5]^+$ quartet	3674***(467)***	3056***(2)***, 3050***(3)***, 3041***(1)***, 3027***(5)***,
$[HO\text{-}Fe\text{-}C_6H_5]^+$ sextet	3700***(849)***	3058***(1)***, 3052***(0)***, 3041***(0)***, 3027***(0)***, 3016***(0)***
$Fe^+(C_6H_5OH)$ quartet π-structure	3619***(158)***	3063***(3)***, 3059***(10)***, 3052***(1)***, 3047***(0)***, 3032**(1)**
$Fe^+(C_6H_5OH)$ sextet π-structure	3617***(175)***	3065***(7)***, 3058***(14)***, 3051***(3)***, 3046***(1)***, 3033***(2)***
$Fe^+(C_6H_5OH)$ quartet σ-structure	3605***(195)***	3060***(0)***, 3054***(0)***, 3046***(1)***, 3039***(0)***, 3037***(1)***
$Fe^+(C_6H_5OH)$ sextet σ-structure	3562***(173)***	3061***(0)***, 3056***(0),*** 3048***(0)***, 3042***(1)***, 3039***(7)***

Table 4.1 Harmonic vibrational frequencies for intermediates of the $FeO^+ + C_6H_6 \rightarrow Fe^+ + C_6H_5OH$ reaction at the B3LYP/6-311+G(d,p) level. IR intensities (km/mol) in parentheses. Frequencies are scaled by 0.954.

Our spectroscopic observation that reaction of Fe^+ with N_2O and benzene produces $[HO\text{-}Fe\text{-}C_6H_5]^+$ is a bit surprising in light of collisional activation (CA) and ion cyclotron resonance (ICR) studies which find no clear evidence for the $[HO\text{-}Fe\text{-}C_6H_5]^+$ intermediate in the $FeO^+ + C_6H_6$ reaction.[8-10] A possible explanation is that this reaction can occur via several mechanisms and the different conditions in our laser ablation source and in the ICR favor different reaction pathways. Our IRMPD results do not address whether other intermediates, such as the $OFe^+(C_6H_6)$ entrance channel complex or intermediates proposed for the oxygen insertion mechanism,[13, 14] are also present. These intermediates do not contain an O-H bond and thus would not be detected in our study. Another possibility is that in our laser ablation source $[HO\text{-}Fe\text{-}C_6H_5]^+$ is not produced by

$$Fe^+ + N_2O \rightarrow FeO^+ + N_2 \qquad (4.1)$$

followed by reaction of FeO^+ with benzene, but rather is formed by

$$Fe^+ + C_6H_6 \rightarrow Fe^+(C_6H_6) \qquad (4.2)$$

followed by reaction of $Fe^+(C_6H_6)$ with N_2O. Although we use a 4:1 N_2O:C_6H_6 ratio, kinetics favors reaction (4.2). The high-pressure limiting bimolecular rate k_2 is 1.2×10^{-9} $cm^3molecule^{-1}sec^{-1}$ for Co^+ and should be similar for Fe^+.[8] At thermal energies reaction (4.1) is much slower:[35] $k_1=3.1 \times 10^{-11}$ $cm^3molecule^{-1}sec^{-1}$. However, CID and ICR reaction studies[36] as well as flow tube studies[37] show that the $Fe^+(C_6H_6) + N_2O$ reaction produces $OFe^+(C_6H_6)$ (the entrance channel complex in Fig. 4.1) rather than the insertion intermediate. Our spectroscopic results show that reacting laser-ablated Fe^+ with N_2O and benzene produces $[HO\text{-}Fe\text{-}C_6H_5]^+$. However, our experiments do not

determine whether $[HO\text{-}Fe\text{-}C_6H_5]^+$ is formed by reaction of FeO^+ with benzene, or by reaction of Fe^+(benzene) with N_2O.

4.3.4 Vibrational Spectroscopy of the $Fe^+(C_6H_5OH)$ Exit Channel Complex

The $Fe^+(C_6H_5OH)$ exit channel complexes are predicted to have the lowest O-H stretching frequencies, with two different possible geometries. The Fe^+ can bind above the benzene ring (π-complex) or to the oxygen lone pair (σ-complex). The CBS-QB3 calculations predict that the lowest energy structure is clearly the quartet state of the π-complex, which is predicted to be bound by 275 kJ/mol relative to sextet Fe^+ + phenol. The sextet π-complex is bound by 196 kJ/mol, while the quartet and sextet σ-complexes are bound by 166 and 161 kJ/mol, respectively. The preference for Fe^+ to bind to the aromatic ring rather than to oxygen is consistent with the greater measured binding energy for Fe^+-benzene (207±10 kJ/mol) than for Fe^+-H_2O (128±5 kJ/mol).[38] The quartet and sextet π-complexes and quartet σ-complex are predicted to have very similar O-H stretching frequencies. All are in excellent agreement with the observed O-H stretch at 3598 cm^{-1} (Figure 4.4). The O-H stretch for the sextet σ-complex is predicted to lie well below the observed peak.

The O-H stretching frequency in Fe^+(phenol) is 3598 cm^{-1}, which is 59 cm^{-1} below the O-H stretch in bare phenol (3657 cm^{-1}).[32] Vaden and Lisy measured vibrational spectra of M^+(phenol)(Ar) (M=Na, K) in the O-H stretching region, monitoring argon loss.[39] For K^+ they observed a narrow, symmetric peak at 3636 cm^{-1}, which was assigned to the π-complex. The spectrum of the Na^+ complex consists of a peak at 3641 cm^{-1} with a clear shoulder at 3632 cm^{-1}, which were assigned to the σ- and π-complexes,

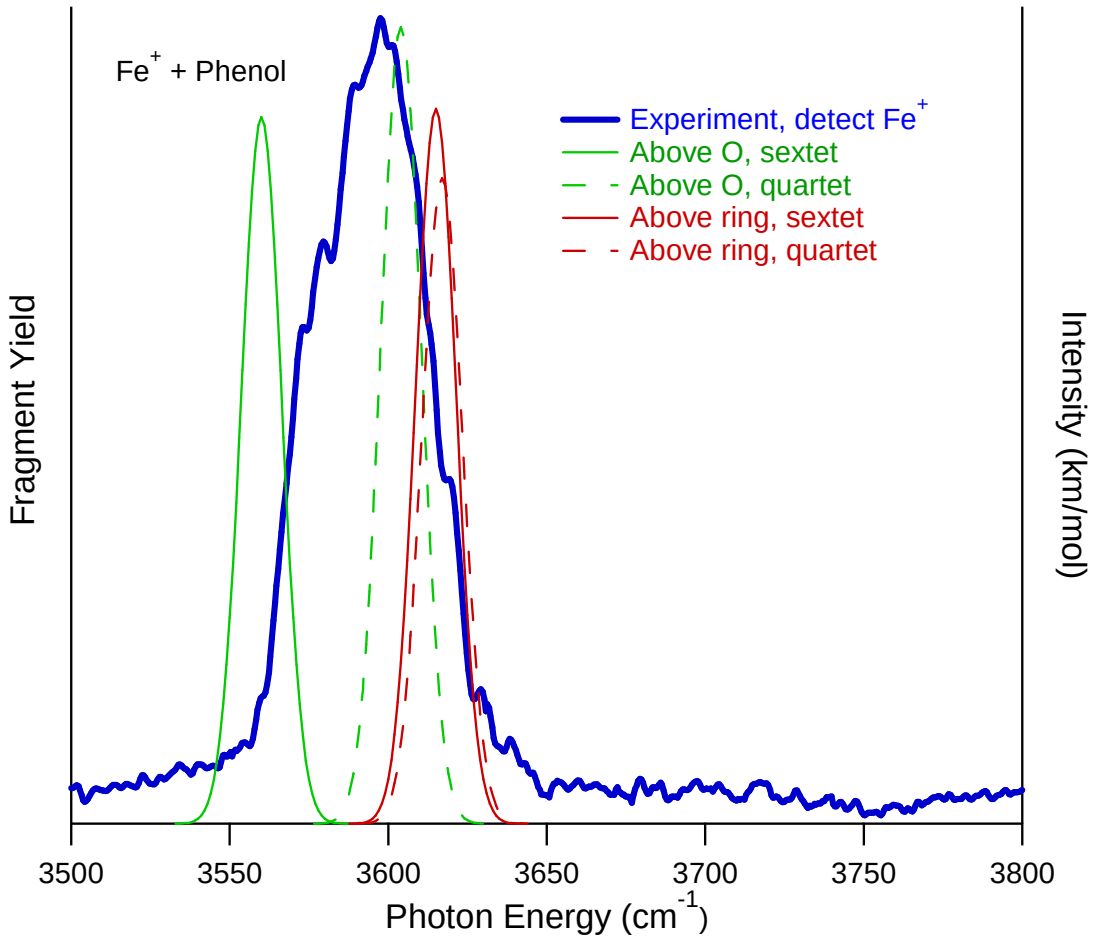

Figure 4.4 Experimental and calculated vibrational spectra of $Fe^+(C_6H_5OH)$ in the O-H stretching region. The experimental spectrum is obtained by IRMPD of ions produced by reacting Fe^+ with C_6H_5OH and monitoring Fe^+ fragments (blue). Calculated spectra (right axis) are at the B3LYP/6-311+G(d,p) level, with frequencies scaled by 0.954. Spectra of Fe^+(phenol) with Fe^+ bound to the oxygen (σ-complex) and above the ring (π-complex) are shown. For the simulations, solid lines represent sextet states and dashed lines quartet states.

respectively. So, binding to Na^+ or K^+ leads to a ~20 cm^{-1} red shift in the O-H stretching frequency of bare phenol, significantly smaller than the 59 cm^{-1} red shift due to Fe^+ binding. The observed red shifts correlate with the binding energies of M^+(phenol), which are measured[40] to be 74 kJ/mol for K^+, 102 kJ/mol for Na^+ and calculated to be 275 kJ/mol for Fe^+.

4.4 Conclusions

Vibrational spectra of two intermediates of the gas-phase $FeO^+ + C_6H_6 \rightarrow Fe^+ + C_6H_5OH$ reaction have been measured in the O-H stretching region. Spectra of the quartet and sextet states of $[HO\text{-}Fe\text{-}C_6H_5]^+$, the key insertion intermediate, are obtained from IRMPD, monitoring the $FeOH^+$ fragment. With the aid of B3LYP/6-311+G(d,p) calculations the main peak observed at 3700 cm^{-1} is assigned to the sextet state and the shoulder at ~3670 cm^{-1} to the quartet state. IRMPD of the $Fe^+(C_6H_5OH)$ exit channel complex primarily produces $Fe^+ + C_6H_5OH$; $Fe^+(C_6H_4) + H_2O$ is a minor product. The spectrum consists of a peak at 3598 cm^{-1}. Calculations suggest that quartet and sextet states of the $Fe^+(C_6H_5OH)$ π-complex and the quartet σ-complex could contribute. The spectrum of ions produced by reacting Fe^+ with N_2O and benzene is narrower than that obtained using Fe^+ + phenol. This could be due to different populations of the isomers or to different vibrational temperatures in the two cases. In addition, a potential energy surface for the reaction has been calculated at the CBS-QB3 level.

4.5 References

1. DeSelms, R. H. *UV-Active Phenol Ester Compounds*; Washington, DC, 2008.
2. Panov, G. I., Advances in Oxidation Catalysis: Oxidation of Benzene to Phenol by Nitrous Oxide *Cattech* **2000,** 4, 18-31.
3. Taboada, J. B., *Direct Oxidation of Benzene to Phenol: Investigation of the active iron species in [Fe,Al]MFI catalysts by ^{57}Fe Mössbauer spectroscopy*. Delft University Press: Amsterdam, 2006; p 172.
4. Niwa, S.; Eswaramoorthy, M.; Nair, J.; Raj, A.; Itoh, N.; Shoji, H.; Namba, T.; Mizukami, F., A one-step conversion of benzene to phenol with a palladium membrane. *Science* **2002,** 295, 105-107.
5. Tao, Y.; Fishman, A.; Bentley, W. E.; Wood, T. K., Oxidation of benzene to phenol, catechol, and 1,2,3-trihydroxybenzene by toluene 4-monooxygenase of Pseudomonas mendocina KR1 and toluene 3-monooxygenase of Ralstonia pickettii PKO1. *Appl. Environ. Microbiol.* **2004,** 70, 3814-3820.
6. Schlosser, P. M.; Bond, J. A.; Medinsky, M. A., Benzene and Phenol Metabolism by Mouse and Rat-Liver Microsomes. *Carcinogenesis* **1993,** 14, 2477-2486.
7. Ortiz de Montellano, P. R., *Cytochrome P450: Structure, Mechanism, and Biochemistry*. Third ed.; Kluwer Academic/Plenum Publishers: New York, 2004.
8. Ryan, M. F.; Stockigt, D.; Schwarz, H., Oxidation of Benzene Mediated by First-Row Transition-Metal Oxide Cations - the Reactivity of ScO^+ through NiO^+ in Comparison. *J. Am. Chem. Soc.* **1994,** 116, 9565-9570.
9. Schröder, D.; Schwarz, H., Benzene Oxidation By 'Bare' FeO^+ in the Gas Phase. *Helv. Chim. Acta* **1992,** 75, 1281-1287.
10. Becker, H.; Schröder, D.; Zummack, W.; Schwarz, H., Generation, Fragmentation, and Interconversion Processes of $[Fe,C_6,H_6,O]^+$ Isomers Relevant for the Oxygenation of Aromatic Hydrocarbons. *J. Am. Chem. Soc.* **1994,** 116, 1096-1100.
11. Yoshizawa, K.; Shiota, Y.; Yamabe, T., Reaction pathway for the direct benzene hydroxylation by iron-ore species. *J. Am. Chem. Soc.* **1999,** 121, 147-153.
12. Yoshizawa, K.; Shiota, Y.; Kagawa, Y.; Yamabe, T., Femtosecond Dynamics of the Methane-Methanol and Benzene-Phenol Conversions by an Iron-Oxo Species. *J. Phys. Chem. A* **2000,** 104, 2552-2561.
13. Shiota, Y.; Suzuki, K.; Yoshizawa, K., Mechanism for the direct oxidation of benzene to phenol by FeO+. *Organometallics* **2005,** 24, 3532-3538.
14. Kwapien, K.; Broclawik, E., Interaction of FeO^+ cation with benzene, aniline, and 3-methylaniline: DFT study of oxygen insertion mechanism. *Int. J. Quantum Chem.* **2008,** 108, 2016-2022.
15. Altinay, G.; Citir, M.; Metz, R. B., Vibrational Spectroscopy of Intermediates in Methane-to-Methanol Conversion by FeO^+. *J. Phys. Chem. A* **2010,** 114, 5104-5112.
16. Aguirre, F.; Husband, J.; Thompson, C. J.; Stringer, K. L.; Metz, R. B., Electronic Spectroscopy of Intermediates Involved in the Conversion of Methane to Methanol by FeO^+. *J. Chem. Phys.* **2002,** 116, 4071-4078.
17. Metz, R. B., Photofragment Spectroscopy of Covalently Bound Transition Metal Complexes: A Window into C-H and C-C Bond Activation by Transition Metal Ions. *Int. Rev. Phys. Chem.* **2004,** 23, 79-108.

18. Husband, J.; Aguirre, F.; Ferguson, P.; Metz, R. B., Vibrationally Resolved Photofragment Spectroscopy of FeO^+. *J. Chem. Phys.* **1999,** 111, 1433-1437.
19. Aguirre, F.; Husband, J.; Thompson, C. J.; Stringer, K. L.; Metz, R. B., The Low-Lying Electronic States of FeO^+: Rotational Analysis of the Resonance Enhanced Photodissociation Spectra of the $^6\Pi_{7/2} <-- {}^6\Sigma^+$ System. *J. Chem. Phys.* **2003,** 119, 10194-10201.
20. Kaur, D.; Desouza, A. M.; Wanna, J.; Hammad, S. A.; Mercorelli, L.; Perry, D. S., Multipass Cell for Molecular-Beam Absorption-Spectroscopy. *Appl. Optics* **1990,** 29, 119-124.
21. Frisch, M. J.; Trucks, G. W.; Schlegel, H. B.; Scuseria, G. E.; Robb, M. A.; Cheeseman, J. R.; Montgomery Jr., J. A.; Vreven, T.; Kudin, K. N.; Burant, J. C.; Millam, J. M.; Iyengar, S. S.; Tomasi, J.; Barone, V.; Mennucci, B.; Cossi, M.; Scalmani, G.; Rega, N.; Petersson, G. A.; Nakatsuji, H.; M.Hada; Ehara, M.; Toyota, K.; Fukuda, R.; Hasegawa, J.; Ishida, M.; Nakajima, T.; Honda, Y.; Kitao, O.; Nakai, H.; Klene, M.; Li, X.; Knox, J. E.; Hratchian, H. P.; Cross, J. B.; Adamo, C.; Jaramillo, J.; Gomperts, R.; Stratmann, R. E.; Yazyev, O.; Austin, A. J.; Cammi, R.; Pomelli, C.; Ochterski, J. W.; Ayala, P. Y.; Morokuma, K.; Voth, G. A.; Salvador, P.; Dannenberg, J. J.; Zakrzewski, V. G.; Dapprich, S.; Daniels, A. D.; Strain, M. C.; Farkas, O.; Malick, D. K.; Rabuck, A. D.; Raghavachari, K.; Foresman, J. B.; Ortiz, J. V.; Cui, Q.; Baboul, A. G.; Clifford, S.; Cioslowski, J.; Stefanov, B. B.; Liu, G.; Liashenko, A.; Piskorz, P.; Komaromi, I.; Martin, R. L.; Fox, D. J.; Keith, T.; Al-Laham, M. A.; Peng, C. Y.; Nanayakkara, A.; Challacombe, M.; Gill, P. M. W.; Johnson, B.; Chen, W.; Wong, M. W.; Gonzalez, C.; Pople, J. A. *Gaussian 03*, Gaussian, Inc.: Pittsburgh PA, Wallingford CT, 2004.
22. Montgomery Jr, J. A.; Frisch, M. J.; Ochterski, J. W.; Petersson, G. A., A complete basis set model chemistry. VI. Use of density functional geometries and frequencies. *J. Chem. Phys.* **1999,** 110, 2822-2827.
23. Montgomery Jr, J. A.; Frisch, M. J.; Ochterski, J. W.; Petersson, G. A., A complete basis set model chemistry. Use of the minimum population localization method. *J. Chem. Phys.* **2000,** 112, 6532-6542.
24. Kellogg, C. B.; Irikura, K. K., Gas-phase Thermochemistry of Iron Oxides and Hydroxides: Portrait of a Super-efficient Flame Suppressant. *J. Phys. Chem. A* **1999,** 103, 1150-1159.
25. Glukhovtsev, M. N.; Bach, R. D.; Nagel, C. J., Performance of the B3LYP/ECP DFT Calculations of Iron-Containing Compounds. *J. Phys. Chem. A* **1997,** 101, 316-323.
26. Feller, D., *Ab Initio* Study of M^+:18-Crown-6 Microsolvation. *J. Phys. Chem. A* **1997,** 101, 2723-2731.
27. Metz, R. B.; Nicolas, C.; Ahmed, M.; Leone, S. R., Direct Determination of the Ionization Energies of FeO and CuO with VUV Radiation. *J. Chem. Phys.* **2005,** 123, 114313.
28. Armentrout, P. B.; Kickel, B. L., Gas-Phase Thermochemistry of Transition Metal Ligand Systems: Reassessment of Values and Periodic Trends. In *Organometallic Ion Chemistry*, Freiser, B. S., Ed. Kluwer Academic Publishers: Dordrecht, The Netherlands, 1994; pp 1-45.

29. Lias, S. G.; Bartmess, J. E.; Liebman, J. F.; Holmes, J. L.; Levin, R. D.; Mallard, W. G., Gas-Phase Ion and Neutral Thermochemistry. *J. Phys. Chem. Ref. Data* **1988,** 17, 1-861.
30. Schröder, D.; Schwarz, H., FeO^+ Activates Methane. *Angew. Chem. Intl. Ed. Engl.* **1990,** 29, 1433-1434.
31. Schröder, D.; Schwarz, H.; Clemmer, D. E.; Chen, Y.; Armentrout, P. B.; Baranov, V.; Bohme, D. K., Activation of Hydrogen and Methane by Thermalized FeO^+ in the Gas Phase as Studied by Multiple Mass Spectrometric Techniques. *Int. J. Mass Spectrom. Ion Proc.* **1997,** 161, 175-191.
32. Yamada, Y.; Ebata, T.; Kayano, M.; Mikami, N., Picosecond IR-UV pump-probe spectroscopic study of the dynamics of the vibrational relaxation of jet-cooled phenol. I. Intramolecular vibrational energy redistribution of the OH and CH stretching vibrations of bare phenol. *J. Chem. Phys.* **2004,** 120, 7400-7409.
33. Park, M.; Hauge, R. H.; Kafafi, Z. H.; Margrave, J. L., Activation of O-H and C-O Bonds of Methanol by Photoexcited Iron Atoms. *J. Chem. Soc. Chem. Comm.* **1985**, 1570-1571.
34. Wang, G. J.; Chen, M. H.; Zhou, M. F., Matrix Isolation Infrared Spectroscopic and Theoretical Studies on the Reactions of Manganese and Iron Monoxides with Methane. *J. Phys. Chem. A* **2004,** 108, 11273-11278.
35. Baranov, V.; Javahery, G.; Hopkinson, A. C.; Bohme, D. K., Intrinsic Coordination Properties of Iron in FeO^+: Kinetics at 294 ± 3 K for Gas-Phase Reactions of the Ground States of Fe^+ and FeO^+ with Inorganic Ligands Containing Hydrogen, Nitrogen, and Oxygen. *J. Am. Chem. Soc.* **1995,** 117, 12801-12809.
36. Stockigt, D.; Schwarz, H., Reactivity Tuning by Ligand Effects - Gas-Phase Reactions of $Fe(C_6H_6)O^+$ Versus Bare FeO^+. *Chemische Berichte* **1994,** 127, 2499-2503.
37. Baranov, V.; Bohme, D. K., Reactions of Fe^+ Coordinated to the Pi-Donating Ligands C_2H_4, c-C_5H_5, C_6H_6 and C_{60} with N_2O and CO - Probing the Bonding in $(C_{60})Fe^+$. *Int. J. Mass Spectrom. Ion Process.* **1995,** 149, 543-553.
38. Meyer, F.; Khan, F. A.; Armentrout, P. B., Thermochemistry of Transition-Metal Benzene Complexes - Binding-Energies of $M(C_6H_6)(X)^+$ (X=1, 2) for M=Ti to Cu. *J. Am. Chem. Soc.* **1995,** 117, 9740-9748.
39. Vaden, T. D.; Lisy, J. M., Characterization of Hydrated Na^+(Phenol) and K^+(Phenol) Complexes using Infrared Spectroscopy. *J. Chem. Phys.* **2004,** 120, 721-730.
40. Amunugama, R.; Rodgers, M. T., The influence of substituents on cation-pi interactions. 4. Absolute binding energies of alkali metal cation - Phenol complexes determined by threshold collision-induced dissociation and theoretical studies. *J. Phys. Chem. A* **2002,** 106, 9718-9728.

CHAPTER 5

COMPARISON OF IRMPD, Ar-TAGGING AND IRLAPS FOR VIBRATIONAL SPECTROSCOPY OF $Ag^+(CH_3OH)$

5.1 Introduction

Vibrational spectroscopy is widely used to measure structure and bonding of gas-phase ions.[1-5] Due to low density of ions in most cases, direct absorption is not applicable. Thus photofragment spectroscopy is a nice tool to get the desired information. The primary challenge in applying photofragment spectroscopy to measuring vibrational spectra is that light absorption needs to lead to bond breaking. For many ions, one photon in the IR does not have enough energy to break a bond. Common techniques to overcome this problem are infrared multiple photon dissociation, messenger spectroscopy, and two-color techniques such as vibrationally mediated photodissociation. These techniques have been discussed in Chapter 1. They are useful methods but each has some drawbacks. In this chapter we focus on developing a method to get better vibrational spectra, especially for strongly bound ions. The method is called infrared laser assisted photodissociation spectroscopy (IRLAPS). In IRLAPS a tunable IR laser excites a vibration. The vibrationally excited ions absorb several photons from a second infrared laser and dissociate.[6-10]

The application of IRLAPS to spectra of $Ag^+(CH_3OH)$ is shown schematically in figure 5.1. A tunable IR laser system excites the O-H stretch vibration via one-photon

absorption. Vibrationally excited molecules then selectively sequentially absorb several photons in the C-O stretching region from a high-power pulsed CO_2 laser and dissociate. In principle, vibrationally mediated photodissociation (VMP) and IRLAPS can be used to measure vibrational spectra of unperturbed ions with laser-limited resolution. These techniques require careful spatial and, in some cases, temporal overlap of both lasers with the ion cloud. In addition, one-laser background can interfere with the desired two-laser signal. Lee and coworkers first applied IRLAPS in their study of the O-H stretching vibrations of hydrated hydronium ions $H_3O^+(H_2O)_n$ (n=1-3).[6] Eyler and coworkers used a tunable, pulsed CO_2 laser to excite ions and a second, continuous wave (cw) CO_2 laser to dissociate them, measuring the spectra of $C_3F_6^+$ and $C_2H_5Cl^+$. They also quantified the two-laser signal dependence on the laser power, irradiation time, and time delay between the lasers.[7] Dopfer, Maitre and coworkers observed very low signals in IRMPD of Ag^+(phenol) using a free electron laser. Combining the free electron laser with subsequent cw CO_2 laser irradiation greatly increased the fragment ion yield, allowing them to measure the vibrational spectrum.[11] The most extensive application of IRLAPS is by Rizzo and coworkers, who have used the technique to study vibrational overtone spectra of neutral molecules such as CH_3OH and CF_3H.[8, 9] In this paper, we compare vibrational spectra of $Ag^+(CH_3OH)$ obtained using IRMPD, IRLAPS and Ar tagging. This allows us to compare the suitability of these techniques for measuring vibrational spectra of a strongly-bound ion produced in a laser ablation-molecular beam source.

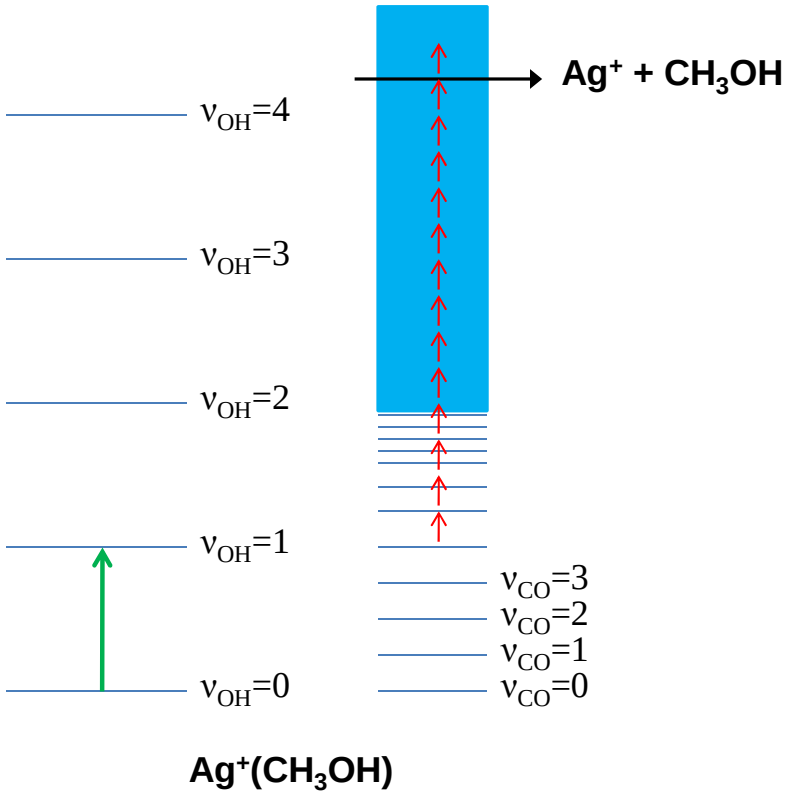

Figure 5.1 Schematic representation of the two-laser infrared laser assisted photodissociation spectroscopy of $Ag^+(CH_3OH)$. Molecules are vibrationally excited in the O-H stretching region, near 3600 cm^{-1}. Vibrationally excited molecules sequentially absorb several 929 cm^{-1} photons and dissociate.

5.2 Experimental and Theoretical Methods

Vibrational spectra are measured using a dual time-of-flight reflectron photofragment spectrometer described in detail in Chapter 2.[12, 13] Silver cations are generated by laser ablation of a silver rod (Sigma-Aldrich, 99.8% pure). Ag^+ cations interact with a pulse of 0.5% methanol in helium or argon at a stagnation pressure of 4-5 atm. from a pulsed piezoelectric valve to produce $Ag^+(CH_3OH)$ and $Ag^+(CH_3OH)(Ar)$ respectively. Ions produced in the source expand supersonically into vacuum and cool to a rotational temperature of ~10 K.[14] Ions are accelerated to 1800 V kinetic energy, then re-referenced to ground potential before entering the field-free flight tube. Mass-selected ions are photodissociated at the turning point of the reflectron. Energetically, photodissociation of $Ag^+(CH_3OH)$ requires at least four photons in the O-H stretching region. So, vibrational spectra are obtained using infrared laser-assisted photodissociation spectroscopy (IRLAPS) and infrared multiple photon dissociation (IRMPD). In the O-H stretching region, the light source is a Nd:YAG pumped optical parametric oscillator/optical parametric amplifier (OPO/OPA, Laservision Inc.) which is tunable from 2 to 5 μm, producing ~15 mJ/pulse near 3600 cm^{-1}, with a beam diameter of 5 mm. The photodissociation efficiency is greatly improved by using a multi-pass mirror arrangement[15, 16] in which light from the OPO makes 21 passes through the ion cloud. The IRLAPS experiments also use a TEA-CO_2 laser to dissociate vibrationally excited molecules via multiple photon excitation of the C-O stretch. The CO_2 laser (InfraLight SP, Optosystems, Ltd.) is line-tunable from 929.0-1086.8 cm^{-1}, producing up to 50-500 mJ in a 100 ns pulse, depending on the line. It makes one pass

through the ion beam. The CO_2 laser beam is approximately rectangular, 4 mm x 8 mm. It is not focused. The OPO wavelength is calibrated using H_2O absorptions and CO_2 laser emission lines are calibrated using NH_3 absorptions. In the IRLAPS experiment, the OPO fires ~30 ns before the CO_2 laser. The IR beam path is purged with nitrogen to minimize absorptions by water vapor.

Fragment ions and undissociated parent ions are detected by a dual micro-channel plate detector. The ion signal is amplified, collected on a gated integrator, and averaged with a LabView based program. The photodissociation spectrum is obtained by monitoring the yield of the fragment ion of interest as a function of wavelength and normalizing to parent ion signal and laser fluence. In IRLAPS and IRMPD of $Ag^+(CH_3OH)$, the only fragment observed is Ag^+. As expected, photodissociation of $Ag^+(CH_3OH)(Ar)$ leads solely to loss of argon.

Computations are carried out with the Gaussian 2003 program package.[17] The optimized geometries of $Ag^+(CH_3OH)$ and $Cu^+(CH_3OH)$ are calculated using the Becke Lee-Yang-Parr hybrid HF/DFT method (B3LYP) with the SDD relativistic effective core potential and basis set on the metal and 6-311+G(d,p) basis set on the remaining atoms. Vibrational frequencies are computed to ensure that optimized geometries correspond to a local minimum. Anharmonic frequency calculations use the *opt=verytight* and *int=ultrafine* keywords. Anharmonic frequencies are not scaled. All energies include zero-point energy and correspond to 0 Kelvin values.

5.3 Results and Discussion

The $Ag^+(CH_3OH)$ ion is a promising candidate for an IRLAPS study for several reasons. First, it is relatively small and strongly bound, so simple IRMPD is expected to be inefficient. The O-H stretch is a strong IR chromophore that is also sensitive to the bonding in the molecule. The C-O stretch in bare methanol is a good IR absorber in the rather limited CO_2 laser tuning range. The Ag^+ cation has a $4d^{10}$, ^1S ground state. As a result, $Ag^+(CH_3OH)$ is the only stable isomer. In our calculations, we were unable to optimize an inserted $[HO\text{-}Ag\text{-}CH_3]^+$ structure; all attempts rearrange to $Ag^+(CH_3OH)$. This is in contrast to the open shell metal system we studied such as, Fe^+ and Co^+. In addition, the first excited state of Ag^+ ($4d^95s$, ^3D) lies 470 kJ/mol above the ground state, so only singlet $Ag^+(CH_3OH)$ contributes to the vibrational spectrum. This is in contrast to the iron system, where the quartet and sextet spin states of the $[HO\text{-}Fe\text{-}CH_3]^+$ and $Fe^+(CH_3OH)$ isomers are at similar energies and can contribute to the spectrum, depending on how the ions are produced (Chapter 3).[18]

For bare CH_3OH, the calculated anharmonic frequencies are ν_{OH}=3670 cm^{-1} and ν_{CO}=1015 cm^{-1}. These are very slightly below the experimental values ν_{OH}=3681 cm^{-1} and ν_{CO}=1033 cm^{-1}.[19] The calculations predict that Ag^+ binds to CH_3OH at $r_{Ag\text{-}O}$ = 2.21 Å. Binding to the metal lengthens the O-H bond by 0.004 Å, to 0.965 Å and lengthens the C-O bond by 0.040 Å, to 1.464 Å. As a result, the calculated anharmonic O-H stretching frequency is predicted to drop to 3644 cm^{-1} and the C-O stretching frequency drops to 927 cm^{-1}. This is slightly below the 929 cm^{-1} lower limit of our CO_2 laser. The

calculated Ag^+-CH_3OH dissociation energy is 145 kJ/mol. Thus, for IRMPD in the O-H stretching region, at least four photons are required to break the bond. Using the CO_2 laser alone, 13 photons need to be absorbed to dissociate the molecule. In the IRLAPS experiment, after absorbing one photon in the O-H stretch region, dissociation requires 9 additional CO_2 photons.

5.3.1 IRLAPS of $Ag^+(CH_3OH)$

We measure the vibrational spectrum of $Ag^+(CH_3OH)$ molecules using three techniques: IRLAPS, IRMPD, and argon-tagging, and the results are compared. In infrared laser assisted photodissociation spectroscopy (IRLAPS) one vibrationally excites the molecules using a tunable laser. Vibrationally excited molecules are then selectively photodissociated using a high-power laser such as a CO_2 laser (Figure 5.1). Ideally, the molecules are vibrationally excited to an energy where the density of vibrational states is sufficiently high that they form a quasi-continuum, and they absorb CO_2 laser photons much more readily than vibrationally unexcited molecules. In this ideal case, fragmentation is only observed when both lasers are present, and there is no background from either laser alone. This has been observed in studies by Rizzo and coworkers, where it is achieved by exciting vibrational overtones, so that one reaches the quasi-continuum, even for small molecules.[8, 9, 20] Background from the CO_2 laser is minimized by tuning the CO_2 laser to the red of the resonant absorption for vibrationally unexcited molecules and decreasing the CO_2 laser power until it induces negligible

dissociation alone. Vibrational absorptions are shifted to the red for vibrationally excited molecules due to vibrational cross-anharmonicities.[20]

Figure 5.2 shows the IRLAPS spectrum of the O-H stretching fundamental in $Ag^+(CH_3OH)$. This is obtained with 50 mJ/pulse at the 10P(36) CO_2 laser transition, at 929.0 cm^{-1}, and with ~16 mJ/pulse at 3600-3700 cm^{-1}. In this experiment, there is significant one-laser background. Each laser alone dissociates ~4% of the ions. As a result, we measure the normalized fragment ion yield with both lasers on (brown trace) and subtract from it the fragment yield measured from each laser alone (green trace). The result is the IRLAPS spectrum, shown in blue. It consists of a slightly asymmetric peak at 3660 cm^{-1}, with full-width half-max (FWHM) of 50 cm^{-1}. The anharmonic calculations predict an O-H frequency of 3644 cm^{-1}, in good agreement with our experimental result.

To optimize the signal to background in the IRLAPS experiment, we measured the dependence of the one-laser background and two-laser signal on the OPO and CO_2 laser power and CO_2 laser wavelength. The one-laser IRMPD background and two-laser IRLAPS signal were measured at OPO/OPA laser powers of 5 to 16 mJ/pulse and CO_2 laser powers of 25 to 50 mJ/pulse. The IRMPD fragment yield depends on (OPO laser power)$^{1.7}$ and on (CO_2 laser power)$^{1.9}$. The IRLAPS signal depends linearly on the OPO laser power and depends on (CO_2 laser power)$^{1.6}$. As expected, IRLAPS is favored at lower power from each laser, but the effect is small. This is in contrast to power dependencies measured by Rizzo and coworkers in IRLAPS studies of methanol overtones, where the threshold for IRLAPS is significantly lower than that for IRMPD.[10] As a result, they were able to select laser powers at which they could obtain

reasonable IRLAPS signal with negligible one-color background. There are two likely reasons for our having to use such high CO_2 laser power: the choice of CO_2 laser wavenumber, and whether the vibrationally excited molecule is in the quasi-continuum region.

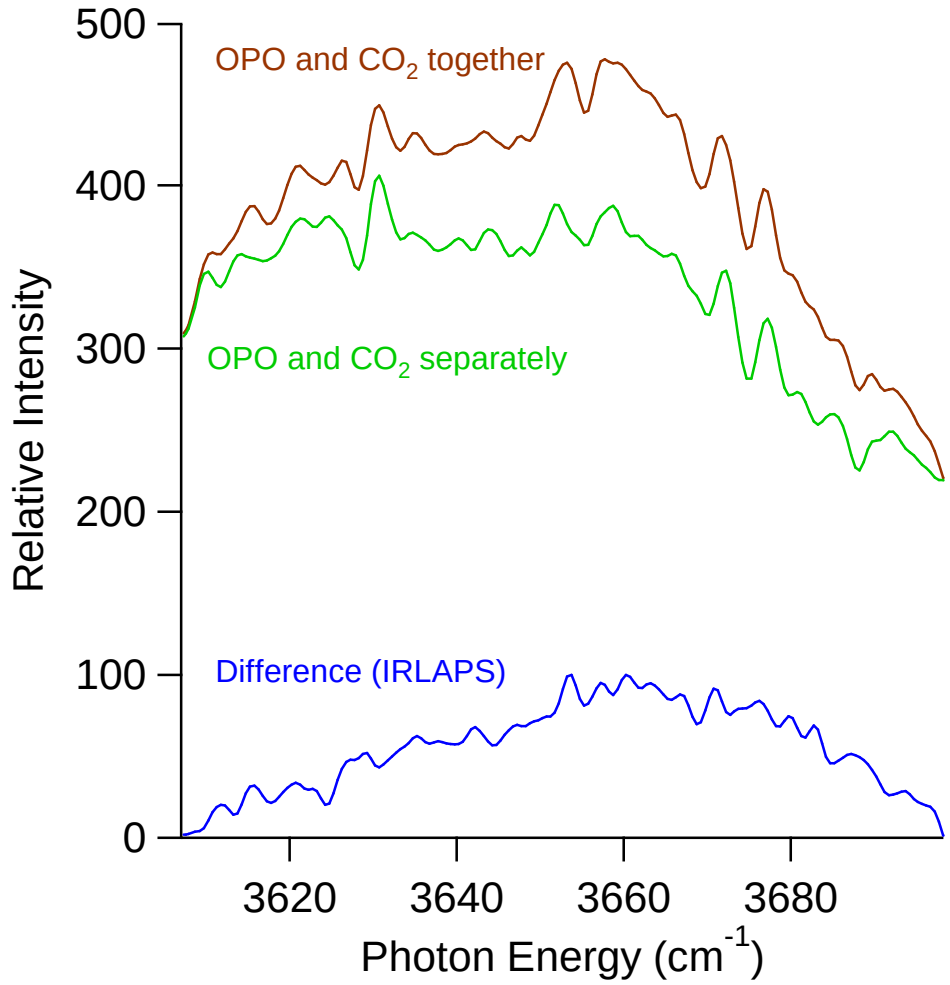

Figure 5.2 IRLAPS spectrum of $Ag^+(CH_3OH)$ in the O-H stretching region. In addition to the two-color signal, there is significant one-color background. This background is shown in the green trace, which is the sum of the Ag^+ fragment yield, normalized to laser power, from the CO_2 laser (which is not scanned) alone and from IRMPD by the tunable OPO alone. The brown trace shows the normalized signal with both lasers on. The enhanced dissociation yield (the difference between the brown and green traces) is the net IRLAPS signal, and is shown in blue. The dips in the spectra are due to loss of laser power due to absorption by trace atmospheric water.

To optimize IRLAPS signal and minimize CO_2 laser background, Rizzo and coworkers tune the CO_2 laser to the red of the transition in the vibrationally unexcited molecule. The anharmonic calculations predict that the C-O stretch in $Ag^+(CH_3OH)$ lies at 927 cm^{-1}. We find that the fragment ion yield for both IRLAPS and IRMPD improves with decreasing CO_2 laser wavenumber. Unfortunately, the limited tuning range of the CO_2 laser does not allow us to explore wavenumbers significantly to the red of the C-O stretch. The 929 cm^{-1} transition used is the lowest available for our laser. We also tried to measure ν_{OH} in $Cu^+(CH_3OH)$ via IRLAPS. Although each laser produced photofragments, no net IRLAPS signal was observed. The anharmonic frequency calculations predict ν_{CO}=908 cm^{-1} in $Cu^+(CH_3OH)$, significantly lower than the value in $Ag^+(CH_3OH)$, and well below the CO_2 laser tuning range. Large red-shifts in ν_{CO} upon binding to metal cations have also been quantified by Dietrich et al. for $Au_n^+(CH_3OH)_m$ using IRMPD with a CO_2 laser.[21] Clusters with fewer methanol molecules show progressively larger red shifts. The C-O stretch frequency lies below 929 cm^{-1} even for $Au^+(CH_3OH)_2$.

Rizzo and coworkers also observe that the threshold CO_2 laser power required for IRLAPS is lower for more highly vibrationally excited CH_3OH. This is a result of the steep increase in vibrational density of states ρ_{vib} with increasing internal energy. At higher initial vibrational energies, the molecules are more likely to be in the quasi-continuum region and to sequentially absorb CO_2 laser photons more readily. Also, fewer CO_2 photons are required to dissociate the molecule. For $Ag^+(CH_3OH)$, we calculate that ρ_{vib}=50 states/cm^{-1} at ν_{OH}=1. This is not quite in the quasi-continuum, and may make CO_2 laser absorption less efficient. This effect was also noted by Lee and

coworkers in their study of $H_3O^+(H_2O)_n$. For $H_5O_2^+$, at v_{OH}=1, ρ_{vib} is only 38 states/cm^{-1}, so they observe less efficient absorption of CO_2 photons than for $H_7O_3^+$ and $H_9O_4^+$, which have much higher densities of states at the same energy.[22] In summary, both conditions-not tuning significantly to the red of ν_{CO} in the unexcited molecule and the low density of states at v_{OH}=1- are responsible for the significant one-color background.

5.3.2 IRMPD of $Ag^+(CH_3OH)$

In the O-H stretching region, IRMPD of $Ag^+(CH_3OH)$ requires at least four photons. Using the multipass mirror arrangement, we observe ~4% dissociation near 3635 cm^{-1}. The only fragment observed is Ag^+. The IRMPD spectrum is shown in figure 5.3 (green trace). It consists of a peak at 3635 cm^{-1}, with a width of 180 cm^{-1}. This is 25 cm^{-1} red-shifted and significantly broader than the peak observed using IRLAPS. The O-H stretches of several other $M^+(CH_3OH)$ systems have also been measured using IRMPD. Those spectra show similarly broad features. Weinheimer and Lisy[23] observe a peak at 3663 cm^{-1} (108 cm^{-1} FWHM) for $Cs^+(CH_3OH)$. For $Mg^+(CH_3OH)$, Machinaga et al.[24] obtain a 200 cm^{-1} wide peak at 3520 cm^{-1}, and Furuya et al. measure a 130 cm^{-1} wide peak at 3490 cm^{-1} for $Al^+(CH_3OH)$.[25]

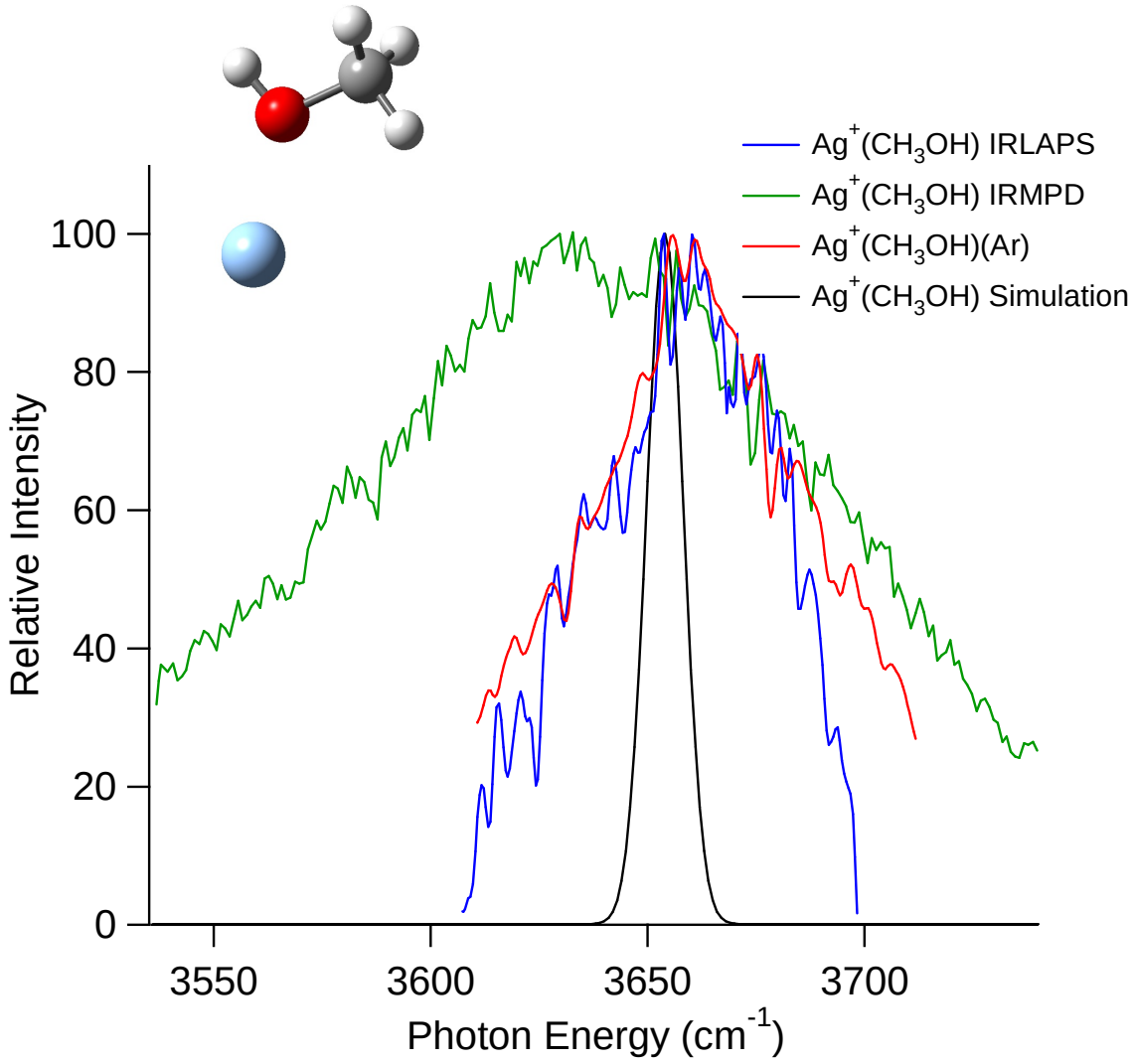

Figure 5.3 Comparison of vibrational spectra of $Ag^+(CH_3OH)$ in the O-H stretching region. The spectra obtained using IRLAPS (blue) and argon tagging (red) are similar. The IRMPD spectrum is significantly broader, especially to lower wavenumber.

5.3.3 Argon-Tagged $Ag^+(CH_3OH)$

Photodissociation of $Ag^+(CH_3OH)(Ar)$ provides another means to measure the O-H stretching frequency. The computed argon binding energy is 24 kJ/mol (2000 cm^{-1}), so one photon in the O-H stretching region can break the bond. Ar tagging is calculated to blue-shift the O-H stretching frequency by 3 cm^{-1}. Experimentally, loss of argon is the only photodissociation fragment observed. The resulting photodissociation spectrum is shown in red in Figure 5.3. It consists of a peak at 3660 $cm^{-1}$with a width of 60 cm^{-1}. This is narrower than the IRMPD spectrum, but is slightly broader than that obtained by IRLAPS. There is no significant shift between the Ar-tagging and IRLAPS spectra. The photodissociation spectrum of $Ag^+(CH_3OH)(Ar)$ is broader than is typically observed for Ar-tagged ions. Much of the width of the Ar-tagged and IRLAPS spectra is likely due to sequence bands from vibrationally excited ions. Attachment of Ag^+ to CH_3OH is 145 kJ/mol exothermic. Ideally, collisions with the carrier gas in the ablation source and subsequent expansion remove this energy. However, molecular beams cool vibrations much less efficiently than rotations. As a result, the $Ag^+(CH_3OH)$ can be vibrationally excited, particularly in the low-frequency intermolecular vibrations and CH_3OH torsion. A similar effect is expected for $Ag^+(CH_3OH)(Ar)$, except the 2000 cm^{-1} Ar binding energy limits the vibrational energy.

Several groups have measured the O-H stretching frequencies of $M^+(CH_3OH)$ complexes using IRMPD and Ar-tagging. Binding to the metal lowers ν_{OH} from its value in bare methanol (3681 cm^{-1}). For many metals, this red shift is small. For example, Weinheimer and Lisy measure ν_{OH}=3663 cm^{-1} in $Cs^+(CH_3OH)$,[23] and 3659 cm^{-1} in $Na^+(CH_3OH)_2$ (the value for $Na^+(CH_3OH)$ is likely to be similar, as there is little

shift in going from $Na^+(CH_3OH)_n$, n=4 to 2).[26] We measure ν_{OH}=3660 cm^{-1} in $Ag^+(CH_3OH)$. Previously, we observed ν_{OH}=3630 cm^{-1} in $Fe^+(CH_3OH)$ via Ar-tagging (Ch.3).[18] Hirabayashi et al. measured O-H stretches for $Ni_n^+(CH_3OH)$, obtaining ν_{OH}=3634 cm^{-1} for n=3 and 3645 cm^{-1} for n=4.[27] They measure similar values for $Co_n^+(CH_3OH)$.[28] There are two metals which give much larger red shifts. For $Mg^+(CH_3OH)$, Machinaga et al. measure a broad peak at 3520 cm^{-1} using IRMPD and a much narrower peak at 3560 cm^{-1} using Ar tagging.[24] $Al^+(CH_3OH)$ shows a further red shift, to ν_{OH}=3490 (IRMPD) and ν_{OH}=3495 (Ar tagged), as measured by Furuya et al.[25]

5.4 Summary and Conclusion

IRLAPS gives the narrowest vibrational spectrum of $Ag^+(CH_3OH)$ in the O-H stretching region. The spectrum obtained via Ar-tagging is slightly broader and shows no significant shift. In contrast, IRMPD leads to a peak that is three times as broad, is 25 cm^{-1} shifted to the red, and exhibits significant tailing to the red. With the same laser ablation source, for larger molecules, we find that IRMPD can give narrower peaks. For example, IRMPD of Fe^+(phenol) gives a peak at 3598 cm^{-1}, with 45 cm^{-1} FWHM (Ch.4).[16] This is despite the fact that Fe^+(phenol) is more strongly bound than $Fe^+(CH_3OH)$. The narrower spectrum is likely due to the greater IVR rate in Fe^+(phenol), which allows for efficient sequential multiple photon absorption by rapidly transferring energy out of the O-H stretch vibration. This also suggests that IRLAPS may be more efficient and give narrower features for larger molecules, as one O-H quantum is sufficient to reach the quasi-continuum region, facilitating subsequent absorption of CO_2 laser photons.

5.5 References

1. Duncan, M. A., Frontiers in the Spectroscopy of Mass-Selected Molecular Ions. *Int. J. Mass Spectrom.* **2000,** 200, 545-569.
2. Metz, R. B., Spectroscopy of the Potential Energy Surfaces for C-H and C-O Bond Activation by Transition Metal and Metal Oxide Cations. *Adv. Chem. Phys.* **2008,** 138, 331-373.
3. Bieske, E. J.; Dopfer, O., High-Resolution Spectroscopy of Cluster Ions. *Chem. Rev.* **2000,** 100, 3963-3998.
4. MacAleese, L.; Maitre, P., Infrared spectroscopy of organometallic ions in the gas phase: From model to real world complexes. *Mass Spectrom. Rev.* **2007,** 26, 583-605.
5. Oomens, J.; Sartakov, B. G.; Meijer, G.; Von Helden, G., Gas-Phase Infrared Multiple Photon Dissociation Spectroscopy of Mass-Selected Molecular Ions. *Int. J. Mass Spectrom.* **2006,** 254, 1-19.
6. Yeh, L. I.; Okumura, M.; Meyers, J. D.; Price, J. M.; Lee, Y. T., Vibrational Spectroscopy of the Hydrated Hydronium Cluster Ions $H_3O^+ \cdot (H_2O)_n$ (n=1,2,3). *J. Chem. Phys.* **1989,** 91, 7319-7330.
7. Watson, C. H.; Zimmerman, J. A.; Bruce, J. E.; Eyler, J. R., Resonance-Enhanced Two-Laser Infrared Multiple Photon Dissociation of Gaseous Ions. *J. Phys. Chem.* **1991,** 95, 6081-6086.
8. Boyarkin, O. V.; Settle, R. D. F.; Rizzo, T. R., Vibrational Overtone Spectra of Jet-Cooled CF_3H by Infrared-Laser Assisted Photofragment Spectroscopy. *Ber. Bunsen-Ges. Phys. Chem. Chem. Phys.* **1995,** 99, 504-513.
9. Boyarkin, O. V.; Lubich, L.; Settle, R. D. F.; Perry, D. S.; Rizzo, T. R., Intramolecular energy transfer in highly vibrationally excited methanol.1. Ultrafast dynamics. *J. Chem. Phys.* **1997,** 107, 8409-8422.
10. Boyarkin, O. V.; Rizzo, T. R.; Rueda, D. S.; Quack, M.; Seyfang, G., Nonlinear Intensity Dependence in the Infrared Multiphoton Excitation of Methanol Preexcited to Different Energies. *J. Chem. Phys.* **2002,** 117, 9793-9805.
11. A. Lagutschenkov; R.J. Sinha; P. Maitre; O. Dopfer, Structure and infrared spectrum of the Ag^+-phenol ionic complex. *submitted to J. Phys. Chem. A* **2010**.
12. Metz, R. B., Photofragment Spectroscopy of Covalently Bound Transition Metal Complexes: A Window into C-H and C-C Bond Activation by Transition Metal Ions. *Int. Rev. Phys. Chem.* **2004,** 23, 79-108.
13. Husband, J.; Aguirre, F.; Ferguson, P.; Metz, R. B., Vibrationally Resolved Photofragment Spectroscopy of FeO^+. *J. Chem. Phys.* **1999,** 111, 1433-1437.
14. Aguirre, F.; Husband, J.; Thompson, C. J.; Stringer, K. L.; Metz, R. B., The Low-Lying Electronic States of FeO^+: Rotational Analysis of the Resonance Enhanced Photodissociation Spectra of the $^6\Pi_{7/2} \leftarrow\!\!- {}^6\Sigma^+$ System. *J. Chem. Phys.* **2003,** 119, 10194-10201.
15. Kaur, D.; Desouza, A. M.; Wanna, J.; Hammad, S. A.; Mercorelli, L.; Perry, D. S., Multipass Cell for Molecular-Beam Absorption-Spectroscopy. *Appl. Optics* **1990,** 29, 119-124.
16. Altinay, G.; Metz, R. B., Vibrational Spectroscopy of Intermediates in Benzene-to-Phenol Conversion by FeO^+. *J. Am. Soc. Mass Spectrom.* **2010,** 21, 750-757.

17. Frisch, M. J.; Trucks, G. W.; Schlegel, H. B.; Scuseria, G. E.; Robb, M. A.; Cheeseman, J. R.; Montgomery Jr., J. A.; Vreven, T.; Kudin, K. N.; Burant, J. C.; Millam, J. M.; Iyengar, S. S.; Tomasi, J.; Barone, V.; Mennucci, B.; Cossi, M.; Scalmani, G.; Rega, N.; Petersson, G. A.; Nakatsuji, H.; M.Hada; Ehara, M.; Toyota, K.; Fukuda, R.; Hasegawa, J.; Ishida, M.; Nakajima, T.; Honda, Y.; Kitao, O.; Nakai, H.; Klene, M.; Li, X.; Knox, J. E.; Hratchian, H. P.; Cross, J. B.; Adamo, C.; Jaramillo, J.; Gomperts, R.; Stratmann, R. E.; Yazyev, O.; Austin, A. J.; Cammi, R.; Pomelli, C.; Ochterski, J. W.; Ayala, P. Y.; Morokuma, K.; Voth, G. A.; Salvador, P.; Dannenberg, J. J.; Zakrzewski, V. G.; Dapprich, S.; Daniels, A. D.; Strain, M. C.; Farkas, O.; Malick, D. K.; Rabuck, A. D.; Raghavachari, K.; Foresman, J. B.; Ortiz, J. V.; Cui, Q.; Baboul, A. G.; Clifford, S.; Cioslowski, J.; Stefanov, B. B.; Liu, G.; Liashenko, A.; Piskorz, P.; Komaromi, I.; Martin, R. L.; Fox, D. J.; Keith, T.; Al-Laham, M. A.; Peng, C. Y.; Nanayakkara, A.; Challacombe, M.; Gill, P. M. W.; Johnson, B.; Chen, W.; Wong, M. W.; Gonzalez, C.; Pople, J. A. *Gaussian 03*, Gaussian, Inc.: Pittsburgh PA, Wallingford CT, 2004.
18. Altinay, G.; Citir, M.; Metz, R. B., Vibrational Spectroscopy of Intermediates in Methane-to-Methanol Conversion by FeO^+. *J. Phys. Chem. A* **2010,** 114, 5104-5112.
19. Shimanouchi, T., Molecular Vibrational Frequencies. In *NIST Chemistry WebBook, NIST Standard Reference Database Number 69*, Linstrom, P. J.; Mallard, W. G., Eds. National Institute of Standards and Technology: Gaithersburg MD, 1972.
20. Boyarkin, O. V.; Kowalczyk, M.; Rizzo, T. R., Collisionally Enhanced Isotopic Selectivity in Multiphoton Dissociation of Vibrationally Excited CF_3H. *J. Chem. Phys.* **2003,** 118, 93-103.
21. Dietrich, G.; Kruckeberg, S.; Lutzenkirchen, K.; Schweikhard, L.; Walther, C., The interaction of gold clusters with methanol molecules: Infrared photodissociation of mass-selected $Au_n^+(CH_3OH)_m$. *J. Chem. Phys.* **2000,** 112, 752-760.
22. Okumura, M.; Yeh, L. I.; Meyers, J. D.; Lee, Y. T., Infrared Spectra of the Cluster Ions $H_7O_3^+$-H_2 and $H_9O_4^+$-H_2. *J. Chem. Phys.* **1986,** 85, 2328-2329.
23. Weinheimer, C. J.; Lisy, J. M., Hydrogen bonding in metal ion solvation: Vibrational spectroscopy of $Cs^+(CH_3OH)_{1-6}$ in the 2.8 μm region. *Int. J. Mass Spectrom. Ion Process.* **1996,** 159, 197-208.
24. Machinaga, H.; Ohashi, K.; Inokuchi, Y.; Nishi, N.; Sekiya, H., Infrared photodissociation spectra and solvation structures of $Mg^+(CH_3OH)_n$ (n=1-4). *Chem. Phys. Lett.* **2004,** 391, 85-90.
25. Furuya, A.; Tsuruta, M.; Misaizu, F.; Ohno, K.; Inokuchi, Y.; Judai, K.; Nishi, N., Infrared photodissociation spectroscopy of $Al^+(CH_3OH)_n$ (n=1-4). *J. Phys. Chem. A* **2007,** 111, 5995-6002.
26. Weinheimer, C. J.; Lisy, J. M., Gas-phase cluster ion vibrational spectroscopy of $Na^+(CH_3OH)_{(2-7)}$. *J. Phys. Chem.* **1996,** 100, 15305-15308.
27. Hirabayashi, S.; Okawa, R.; Ichihashi, M.; Kondow, T., Detection of OH stretching mode of CH_3OH chemisorbed on Ni_3^+ and Ni_4^+ by infrared photodissociation spectroscopy. *Journal of Physical Chemistry A* **2007,** 111, 7664-7669.
28. Hirabayashi, S.; Okawa, R.; Ichihashi, M.; Kawazoe, Y.; Kondow, T., Structures and reactions of methanol molecules on cobalt cluster ions studied by infrared photodissociation spectroscopy. *J. Chem. Phys.* **2009,** 130, 164304.

CHAPTER 6

RECOMMENDATIONS FOR FUTURE WORK

6.1 Additional vibrational studies of $FeO^+ + CH_4$ reaction intermediates

There are several directions in which we can extend the studies described in chapter 3 to gain addition information on the intermediates of the $FeO^+ + CH_4$ reaction.

6.1.1 Spectroscopy of $OFe^+(CH_4)$

The initial step in the $FeO^+ + CH_4$ reaction is formation of the $OFe^+(CH_4)$ entrance channel complex. The vibrational spectroscopy of the $OFe(CH_4)^+$ entrance channel complex should be investigated to provide complete picture of the vibrational information for all the $FeO^+ + CH_4$ reaction intermediates.

Binding to FeO^+ weakens the C-H bonds in CH_4, and vibrational spectroscopy is a sensitive probe of this effect. Figure 6.1 shows the calculated IR spectra of two possible $OFe^+(CH_4)$ complexes and of bare methane. Note that binding to FeO^+ leads to substantial IR intensity for the IR-inactive symmetric stretch band in methane. Many electrostatically bound compounds have several possible structures with similar energies. We know that vibrational spectroscopy is really sensitive to the structure of the molecule. To find the ground state, we have to combine vibrational spectroscopy with electronic structure calculations of vibrational frequencies. In Figure 6.1, this situation is demonstrated by showing that the C-H stretching spectrum of η^3

coordinated $OFe^+(H_3CH)$ is considerably different from that of the η^2 $OFe^+(H_2CH_2)$ complex.

The biggest challenge to create $OFe^+(CH_4)$ is finding a suitable precursor. Reasonable candidates are reacting Fe^+ with N_2O and CH_4 in a specific ratio, or to use a mineral, e.g. hematite, to create FeO^+ by ablation, which then reacts with the CH_4.

6.1.2 VMP studies of reaction intermediates

A major challenge in characterizing the intermediates of an ion-molecule reaction is that the intermediates are all isomers and thus cannot be separated in a mass spectrometer. One way to circumvent this problem is through the use of different precursors to selectively prepare specific intermediates. In some cases, this works quite well – see, for example, intermediates of the FeO^+ + benzene reaction discussed in chapter 4. However, for systems like the FeO^+ + CH_4 reaction intermediates we have yet to find a chemical precursor and reaction conditions that produce only $Fe^+(CH_3OH)$; it is always accompanied by $[HO\text{-}Fe\text{-}CH_3]^+$. One way to distinguish isomers is via a double resonance experiment. The electronic spectra of the intermediates differ. By combining electronic spectroscopy with vibrational spectroscopy we could selectively measure vibrational spectra of specific intermediates.

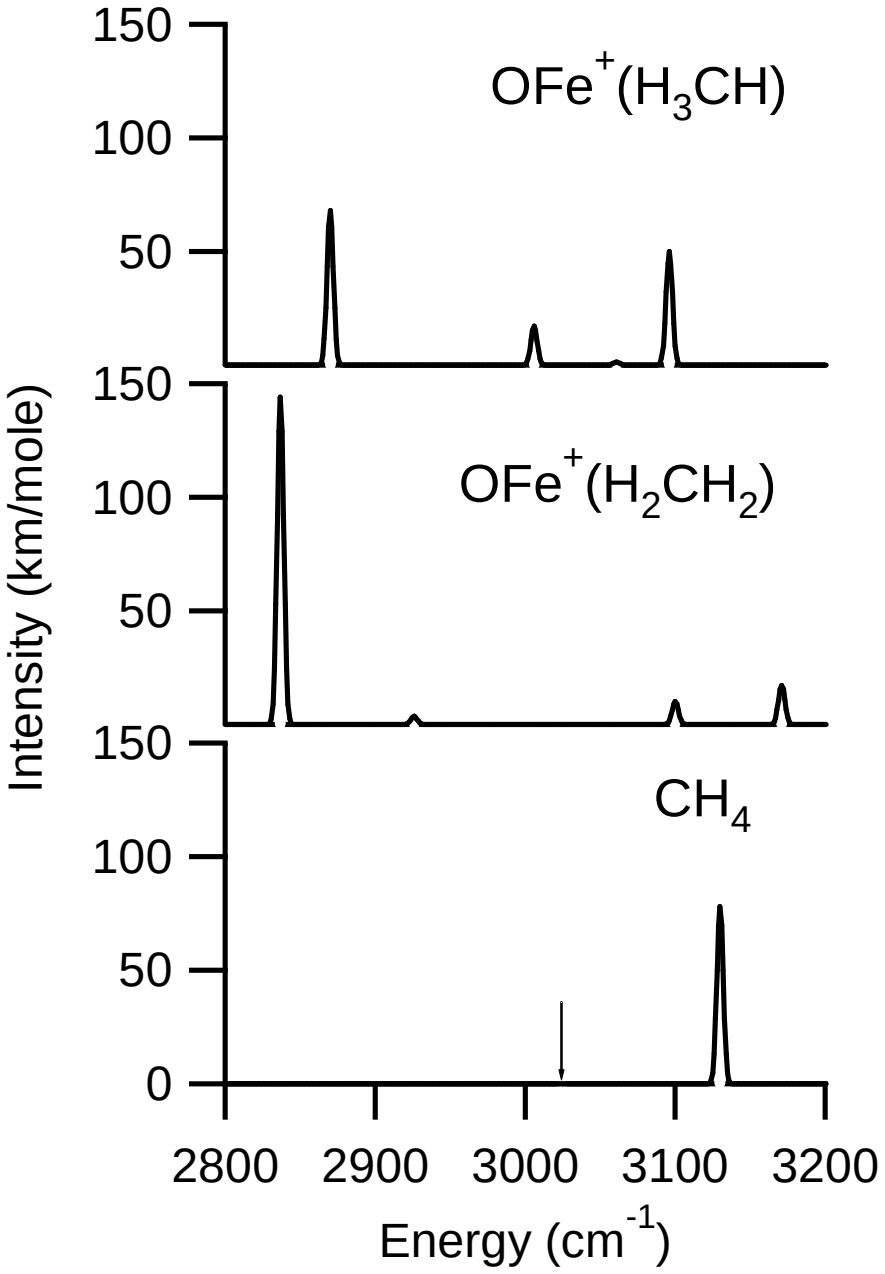

Figure 6.1 Calculated IR spectra of CH_4 and η^2 and η^3 isomers of $FeO^+(CH_4)$. Calculations at the B3LYP/6-311+G(d,p) level. The arrow indicates the position of the IR-inactive symmetric stretch in CH_4.

Vibrationally mediated photodissociation (VMP) could be used to measure vibrational spectra of isomer- and spin-state selected $[HO\text{-}Fe\text{-}CH_3]^+$ with laser-limited resolution. In VMP, a laser vibrationally excites the molecules; a second laser selectively promotes vibrationally excited molecules to an excited electronic state, from which they dissociate. We have used VMP to measure the antisymmetric OCO stretch in $V^+(OCO)$, partially resolving rotational structure[1] and to measure the O-H stretching vibrations in $Co^+(H_2O)$. In order for VMP to work, the electronic photodissociation spectrum of vibrationally excited molecules must be significantly different from that of the vibrationally unexcited ones. Also, to measure spectra of specific intermediates, the electronic photodissociation of the vibrationally excited intermediate of interest must be much more efficient than that of other intermediates present. The quartet state of the insertion intermediate has a structured photodissociation spectrum in the 300-325 nm region (figure 6.2). Follow-up experiments could thus selectively characterize the O-H and C-H stretches of bare quartet $[HO\text{-}Fe\text{-}CH_3]^+$ using VMP.

6.1.3 Vibrational spectra in the fingerprint region

Measuring vibrations directly involving the metal center would give much more information on bonding in intermediates such as $[HO\text{-}Fe\text{-}CH_3]^+$. We used electronic spectroscopy to measure the Fe-C and Fe-O stretches, and the O-Fe-C bend in an excited electronic state of $[HO\text{-}Fe\text{-}CH_3]^+$ (Fig 6.2).[2] We would like to characterize the corresponding vibrations in the ground electronic state. These vibrations are calculated to lie at 776 cm^{-1} (Fe-O stretch), 397 cm^{-1} (Fe-C stretch) and 130 cm^{-1} (O-Fe-C bend) in

quartet $[HO\text{-}Fe\text{-}CH_3]^+$ and at 771cm^{-1} (Fe-O stretch), 480 cm^{-1} (Fe-C stretch) and 130 cm^{-1} (O-Fe-C bend) in sextet $[HO\text{-}Fe\text{-}CH_3]^+$. The Fe-C stretch frequency could be used to identify the spin state.

Measuring these vibrations is more challenging than measuring O-H stretches. Laboratory lasers produce ~10 mJ/pulse in the O-H stretching region, but <0.1 mJ/pulse near 800 cm^{-1}. In addition, IRMPD in the fingerprint region requires substantially more photons than in the O-H stretch region, as each photon has only ~25% the energy. Spectra of molecules such as protonated benzene, protonated toluene[3] and $X^-(H_2O)$ (X=OH, O, F, Cl, Br)[4] have been measured in the fingerprint region. Another possibility is to use VMP to selectively detect vibrationally excited molecules.

An alternate approach is to use a light source with substantially more intensity in the fingerprint region. The free electron lasers at FELIX (Netherlands) [5] and CLIO (France)[6] have been used for IRMPD studies of vibrational spectra of a huge number of ions,[7-10] as they are broadly tunable and produce ~30 mJ/macropulse down to ~600 cm^{-1}.

6.2 Studies of intermediates of methane and benzene activation by other MO^+

As was discussed in chapter 1, there are several MO^+ which convert methane to methanol, with varying efficiencies and selectivities. Thus, it is of interest to study the spectroscopy of intermediates of the $MO^+ + CH_4$ reaction for a range of metals, and attempt to correlate the photofragment pathways and the vibrational and electronic spectroscopy of the intermediates with the reactivity patterns. The CoO^+ and PtO^+

systems are particularly interesting, as they show very different efficiencies and selectivities (CoO^+ shows 0.5% efficiency, but 100% selectivity for methanol, while PtO^+ shows 100% efficiency, but only 25% selectivity for methanol, see table 1.1).

I have measured the electronic and vibrational spectra of the $[HO\text{-}Co\text{-}CH_3]^+$ insertion intermediate and $Co^+(CH_3OH)$ exit channel complex. Photodissociation of $[HO\text{-}Co\text{-}CH_3]^+$ in the visible produces only $Co^+ + CH_3OH$. This is in sharp contrast to $[HO\text{-}Fe\text{-}CH_3]^+$, which dissociates to produce similar amounts of $Fe^+ + CH_3OH$ and $FeOH^+ + CH_3$. The observed photodissociation pathways mirror the bimolecular reaction results. Figure 6.2 compares a portion of the electronic photodissociation spectra of $[HO\text{-}Co\text{-}CH_3]^+$ and $[HO\text{-}Fe\text{-}CH_3]^+$. They both show resolved vibrational progressions in the excited electronic state, particularly an extended progression in the metal-C stretch (335 cm^{-1} and 478 cm^{-1} respectively). Calculations agree with the experimental findings, predicting that electronic excitation leads to lengthening of the M-C bond and slight contraction of the M-O bond. Figure 6.3 shows the vibrational spectra of $[HO\text{-}Co\text{-}CH_3]^+$ and $[HO\text{-}Fe\text{-}CH_3]^+$ in the O-H stretching region, measured using argon-tagging. The spectra are very similar.

A great deal could be learnt by extending these studies to intermediates of the $MO^+ + CH_4$ reaction for M=Pt, Ni, Mn, as they show interesting reactivities (table 1.1). In addition, it would be instructive to study MO^+ + benzene intermediates for these metals, as well as Co.

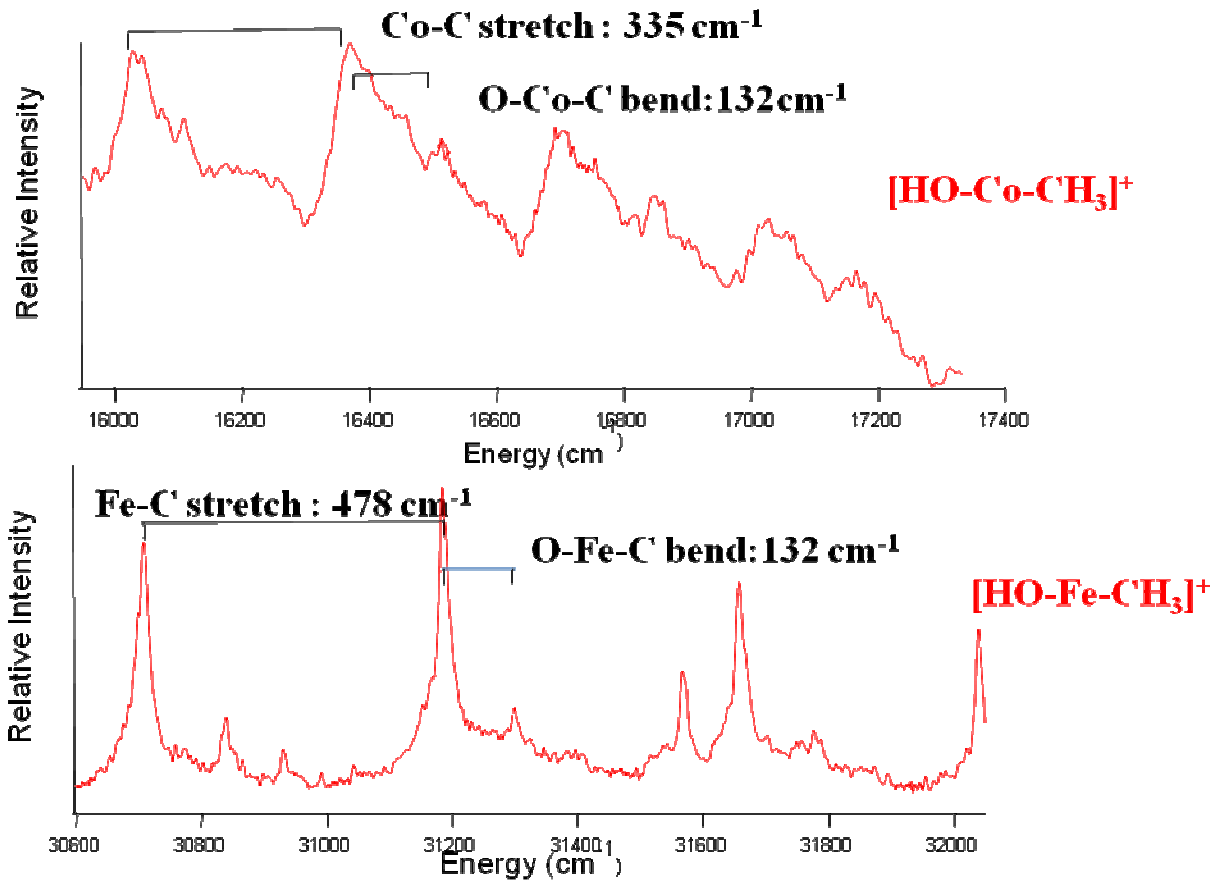

Figure 6.2 Electronic photodissociation spectra of $[HO\text{-}Fe\text{-}CH_3]^+$ and $[HO\text{-}Co\text{-}CH_3]^+$. M^+ loss is detected.

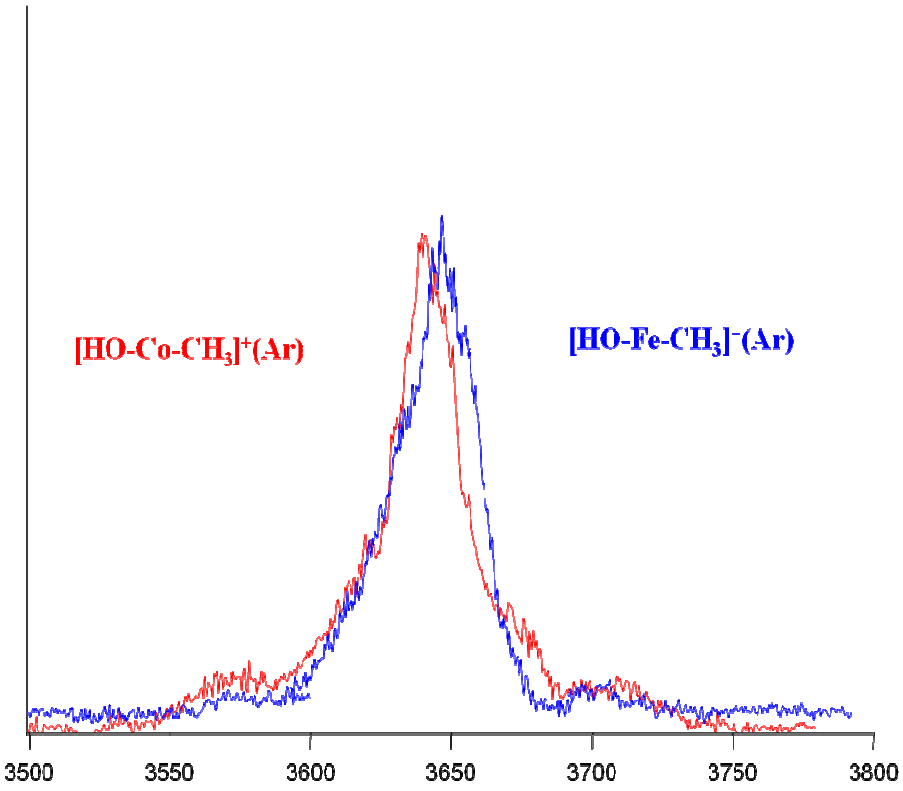

Figure 6.3 Infrared photodissociation spectra of $[HO\text{-}Fe\text{-}CH_3]^+(Ar)$ and $[HO\text{-}Co\text{-}CH_3]^+(Ar)$ in the O-H stretching region. Argon loss is detected.

6.3 Spectroscopy of intermediates of $M^+ + C_3H_8$ reactions

Alkanes are unusually stable compounds and they are also among the most abundant organic compounds in nature. The abundance of the alkanes makes them important raw materials for chemical synthesis. On the other hand the stability of the alkanes makes transformations into other compounds difficult. Therefore, the selective activation of alkane carbon-hydrogen and carbon-carbon bonds is a challenge to organic chemists.

Certain gas-phase transition-metal ions M^+ are chemically interesting for their ability to activate C-H and C-C bonds of saturated alkanes. A summary of the observed reactions of the first row M^+ with C_3H_8 at thermal energies is shown in Table 6.1.[11] Parentheses indicate the minor product in cases where both C-C and C-H activation are observed. At low kinetic energy V^+ and Ti^+ react exothermically with linear alkanes to yield primarily H_2 elimination products, e.g.:

$$Ti^+ + C_3H_8 \rightarrow TiC_3H_6^+ + H_2 \qquad (6.1)$$

On the other hand, exothermic reactions of Sc^+, Fe^+, Co^+ and, Ni^+ with larger alkanes branch between H_2 and CH_4 elimination.[11] e.g.;

$$Fe^+ + C_3H_8 \rightarrow FeC_3H_6^+ + H_2 \qquad (6.2)$$

$$Fe^+ + C_3H_8 \rightarrow FeC_2H_4^+ + CH_4 \qquad (6.3)$$

It is obvious that the first-row transition metal cations do not react uniformly with hydrocarbons. Why do some (Sc^+, $Ti,^+$ V^+ and Co^+) give predominately C-H activation, others (Fe^+ and Ni^+) give predominantly C-C activation, while still others ($Cr,^+$ Mn^+, Cu^+ and $Zn^{+)}$ are unreactive? Asymptotic studies of the reactants and products have suggested correlations between electron configuration and reactivity.[11, 12] For example the lack of reactivity of $Cr,^+$ Mn^+, Cu^+ and Zn^+ has been attributed to these ions having filled, or half filled d-orbitals. Other models have been based on conservation of spin during the reaction, the need for empty M^+ orbitals of suitable symmetry into which the alkane can back-donate electron density, and non-adiabatic effects.

The mechanism for the gas phase reaction is basically simple: on collision the reactants form an adduct, $[M{\cdot}RH]^+$, which can dissociate back to reactants or go on to products. Tonkyn *et al.* observed that the reaction of M^+ with propane in helium buffer gas forms $M^+(C_3H_8)$ adducts for most M^+.[11] In crossed-beam studies Weisshaar's group found that the $Co^+ + C_3H_8$ reaction forms an adduct that lives for $\geq$8 μs at 0.01-0.21eV collision energy.[13] These mass spectrometric studies were not able to characterize the structure of the $M^+(C_3H_8)$ adducts. Knowing the structure of the adduct is of immense help in characterizing the mechanism for the reaction. For example, comparing the structure of the adduct isolated for $Cu^+ + C_3H_8$ with that for $Fe^+ + C_3H_8$ would show why the Cu^+ adduct reverts to $Cu^+ + C_3H_8$ while the Fe^+ adduct proceeds to $FeC_2H_4^+ + CH_4$.

Sc^+	Ti^+	V^+	Cr^+	Mn^+	Fe^+	Co^+	Ni^+	Cu^+	Zn^+
Ground Electronic State Configuration									
$3d\ 4s$	$3d^2\ 4s$	$3d^4$	$3d^5$	$3d^5\ 4s$	$3d^6\ 4s$	$3d^8$	$3d^9$	$3d^{10}$	$3d^{10}\ 4s$
^3D	^4F	^5D	^6S	^7S	^6D	^3F	^2D	^1S	^2S
Reaction with propane;[11] C ⇒ C-C activation, H ⇒ C-H activation									
H,(C)	H	H	None	None	C,(H)	H,(C)	C,(H)	None	None
Excited Electronic States and their Energies (cm^{-1})[14]									
4s → 3d									
$3d^2$	$3d^3$			$3d^6$	$3d^7$				
4803 (^3F)	908 (^4F)			14326 (^5D)	1873 (^4F)				
12074 (^3P)	9364 (^4P)				13474 (^4P)				
3d → 4s									
$4s^2$	$3d\ 4s^2$	$3d^3\ 4s$	$3d^4\ 4s$	$3d^4\ 4s^2$	$3d^5 4s^2$	$3d^7\ 4s$	$3d^8\ 4s$	$3d^9\ 4s$	$3d^9\ 4s^2$
11736 (^1S)	24961 (^2D)	2605 (^5F)	11962 (^6D)	54846 (^5D)	23318 (^6S)	3351 (^5F)	8394 (^4F)	21929 (^3D)	62722 (^2D)
		13512 (^5P)				9818 (^3F)	13550 (^2F)	26265 (^1D)	

Table 6.1 Ground and low-lying electronic states of first row M^+ and reactivity with propane

Depending on the nature of M^+ and RH, possible forms for these adducts range from simple cluster ions, $[M^+ \cdot RH]$ held together by only electrostatic forces, to C-H, and C-C insertion forms $[H\text{-}M^+\text{-}R]$ $[H_3C\text{-}M^+\text{-}R']$ or rearrangement intermediates such as $[H_2\text{-}M^+\text{-}R'']$ exhibiting new chemical bonds. Long-range attractive forces, of the type ion - induced dipole, exist between all M^+-RH pairs. These forces will stabilize the adduct relative to both reactants and products.

It would be interesting to study the vibrational spectroscopy of the adducts arising from reaction of the 3d transition metals with small alkanes such as propane to gain structural and thermochemical information on these molecules. The first systems could be $M^+(C_3H_8)$ where M= Fe, Co, Ni. These metals show both C-H and C-C activation at thermal energies. Elegant crossed beam studies by the Weisshaar group find that, at low collision energy Co^+ + propane produces predominantly H_2 elimination products in preference to CH_4 elimination products.[13] This contrasts sharply with the behavior of Fe^+ and Ni^+, its two nearest neighbors, both of which produce predominantly CH_4.[15-18] Also, there have been high quality computational studies of the reactions of Fe^+, Co^+, Ni^+ with small alkanes using DFT which have examined all important stationary points on the ground state surfaces.[13, 15]

A preliminary IRMPD spectrum of $Fe^+(C_3H_8)_2$ in the C-H stretching region is shown in figure 6.4. The peak at 2970 cm^{-1} corresponds to stretching vibrations of C-H pointing away from the metal. This is similar to frequency observed in bare C_3H_8. The enhanced dissociation near 2750 cm^{-1} could be due to C-H stretches of C-H proximate to the metal.

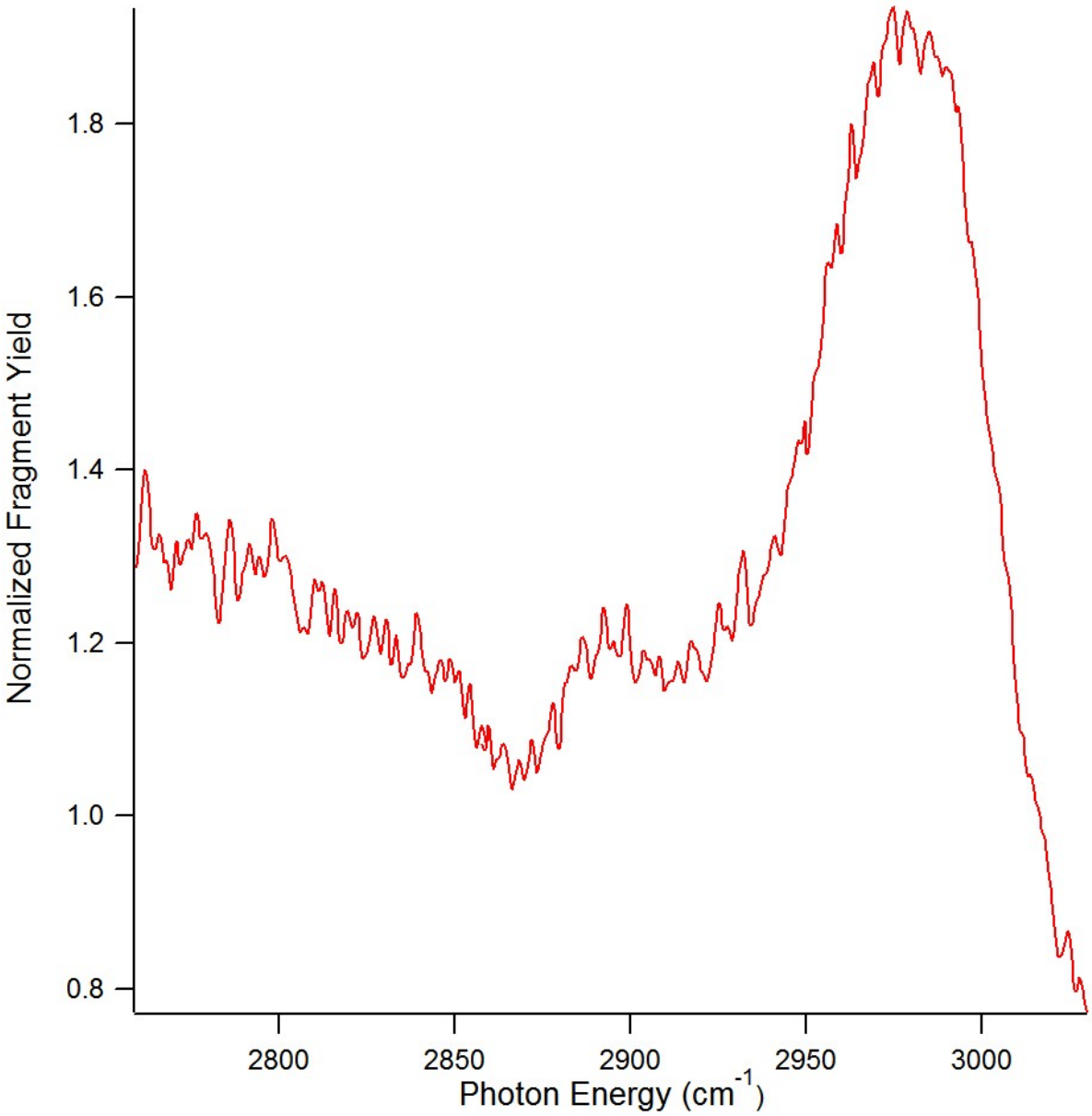

Figure 6.4 IRMPD spectrum of $Fe^{+}(C_3H_8)_2$ in the C-H stretching region.

6.4 References

1. Citir, M.; Altinay, G.; Metz, R. B., Electronic and Vibrational Spectroscopy and Vibrationally Mediated Photodissociation of $V^+(OCO)$. *J. Phys. Chem. A* **2006,** 110, 5051-5057.
2. Aguirre, F.; Husband, J.; Thompson, C. J.; Stringer, K. L.; Metz, R. B., Electronic Spectroscopy of Intermediates Involved in the Conversion of Methane to Methanol by FeO^+. *J. Chem. Phys.* **2002,** 116, 4071-4078.
3. Douberly, G. E.; Ricks, A. M.; Schleyer, P. V. R.; Duncan, M. A., Infrared spectroscopy of gas phase benzenium ions: Protonated benzene and protonated toluene, from 750 to 3400 cm^{-1}. *J. Phys. Chem. A* **2008,** 112, (22), 4869-4874.
4. Roscioli, J. R.; Diken, E. G.; Johnson, M. A.; Horvath, S.; McCoy, A. B., Prying apart a water molecule with anionic H-bonding: A comparative spectroscopic study of the X-center dot H_2O (X = OH, O, F, Cl, and Br) binary complexes in the 600-3800 cm^{-1} region. *J. Phys. Chem. A* **2006,** 110, (15), 4943-4952.
5. Valle, J. J.; Eyler, J. R.; Oomens, J.; Moore, D. T.; van der Meer, A. F. G.; von Helden, G.; Meijer, G.; Hendrickson, C. L.; Marshall, A. G.; Blakney, G. T., Free electron laser-Fourier transform ion cyclotron resonance mass spectrometry facility for obtaining infrared multiphoton dissociation spectra of gaseous ions. *Review of Scientific Instruments* **2005,** 76, (2).
6. Maitre, P.; Le Caer, S.; Simon, A.; Jones, W.; Lemaire, J.; Mestdagh, H. N.; Heninger, M.; Mauclaire, G.; Boissel, P.; Prazeres, R.; Glotin, F.; Ortega, J. M., Ultrasensitive Spectroscopy of Ionic Reactive Intermediates in the Gas Phase Performed with the First Coupling of an IR FEL with an FTICR-MS. *Nucl. Instrum. Meth. A* **2003,** 507, (1-2), 541-546.
7. Duncan, M. A., Frontiers in the Spectroscopy of Mass-Selected Molecular Ions. *Int. J. Mass Spectrom.* **2000,** 200, 545-569.
8. Dunbar, R. C., Photodissociation of Trapped Ions. *Int. J. Mass Spectrom.* **2000,** 200, (1-3), 571-589.
9. Simon, A.; Jones, W.; Ortega, J. M.; Boissel, P.; Lemaire, J.; Maitre, P., Infrared Multiphoton Dissociation Spectroscopy of Gas-Phase Mass-Selected Hydrocarbon-Fe^+ Complexes. *J. Am. Chem. Soc.* **2004,** 126, (37), 11666-11674.
10. MacAleese, L.; Maitre, P., Infrared spectroscopy of organometallic ions in the gas phase: From model to real world complexes. *Mass Spectrom. Rev.* **2007,** 26, (4), 583-605.
11. Tonkyn, R.; Ronan, M.; Weisshaar, J. C., Multicollision Chemistry of Gas-Phase Transition Metal Ions with Small Alkanes. *J. Phys. Chem.* **1988,** 92, 92.
12. Armentrout, P. B., Electronic State-Specific M^+ chemistry. *Ann. Rev. Phys. Chem.* **1990,** 41, 313.
13. Yi, S. S.; Reichert, E. L.; Holthausen, M. C.; Koch, W.; Weisshaar, J. C., Crossed-Beam Study of $Co^+(^3F_4)$ + Propane: Experiment and Density Functional Theory. *Chem.-Eur. J.* **2000,** 6, (12), 2232-2245.

14. Moore, C. E., *Atomic Energy Levels, Circular 467; National Bureau of Standards*
Washington, DC, 1949.
15. Noll, R. J.; Yi, S. S.; Weisshaar, J. C., Bimolecular Ni^+ ($^2D_{5/2}$) + C_3H_8 Reaction Dynamics in Real Time. *J. Phys. Chem. A* **1998,** 102, 386-394.
16. van Koppen, P. A. M.; Bowers, M. T.; Haynes, C. L.; Armentrout, P. B., Reactions of Ground-State Ti^+ and V^+ with Propane: Factors that Govern C-H and C-C Bond Cleavage Product Branching Ratios. *J. Am. Chem. Soc.* **1998,** 120, (23), 5704-5712.
17. Jacobson, D. B.; Freiser, B. S., Studies of the Reactions of Group-8 Transition-Metal Ions Fe+, Co+, and Ni+ with Linear Alkanes - Determination of Reaction-Mechanisms and $MCnH_{2n}^+$ Ion Structures Using Fourier-Transform Mass-Spectrometry Collision-Induced Dissociation. *J. Am.Chem. Soc.* **1983,** 105, (16), 5197-5206.
18. Georgiadis, R.; Fisher, E. R.; Armentrout, P. B., Neutral and Ionic Metal Hydrogen and Metal-Carbon Bond-Energies - Reactions of Co^+, Ni^+, and Cu^+ with Ethane, Propane, Methylpropane, and Dimethylpropane. *J. Am. Chem. Soc.* **1989,** 111, (12), 4251-4262.

BIBLIOGRAPHY

Abusen, R.; Bennett, F. R.; Cox, S. G.; McNab, I. R.; Sharp, D. N.; Shiell, R. C.; Smith, F. E.; Walley, J. M., Hyperfine-resolved spectrum of the molecular dication DCl^{2+}. *Phys. Rev. A* **2000,** 61, 050501.

Aguirre, F.; Husband, J.; Thompson, C. J.; Metz, R. B., Gas-Phase Photodissociation of $AuCH_2^+$: the Dissociation Threshold of Jet-Cooled and Rotationally Thermalized Ions. *Chem. Phys. Lett.* **2000,** 318, 466-470.

Aguirre, F.; Husband, J.; Thompson, C. J.; Stringer, K. L.; Metz, R. B., Electronic Spectroscopy of Intermediates Involved in the Conversion of Methane to Methanol by FeO^+. *J. Chem. Phys.* **2002,** 116, 4071-4078.

Aguirre, F.; Husband, J.; Thompson, C. J.; Stringer, K. L.; Metz, R. B., The Low-Lying Electronic States of FeO^+: Rotational Analysis of the Resonance Enhanced Photodissociation Spectra of the $^6\Pi_{7/2} \leftarrow\!\!- {}^6\Sigma^+$ System. *J. Chem. Phys.* **2003,** 119, 10194-10201.

Allison, J.; Ridge, D. P., Reactions of Atomic Metal Ions with Alkyl Halides and Alcohols in the Gas Phase. *J. Am. Chem. Soc.* **1979,** 101, 4998-5009.

Altinay, G.; Citir, M.; Metz, R. B., Vibrational Spectroscopy of Intermediates in Methane-to-Methanol Conversion by FeO^+. *J. Phys. Chem. A* **2010,** 114, 5104-5112.

Altinay, G.; Metz, R. B., Vibrational Spectroscopy of Intermediates in Benzene-to-Phenol Conversion by FeO^+. *J. Am. Soc. Mass Spectrom.* **2010,** 21, 750-757.

Amunugama, R.; Rodgers, M. T., The influence of substituents on cation-pi interactions. Absolute binding energies of alkali metal cation - Phenol complexes determined by threshold collision-induced dissociation and theoretical studies. *J. Phys. Chem. A* **2002,** 106, 9718-9728.

Andrews, D. L.; Demidov, A. A., *An Introduction to Laser Spectroscopy* second ed.; Kluwer Academic/Plenum Publishers: New York, **2002**.

Armentrout, P. B., Electronic State-Specific M^+ chemistry. *Ann. Rev. Phys. Chem.* **1990,** 41, 313.

Armentrout, P. B.; Kickel, B. L., Gas-Phase Thermochemistry of Transition Metal Ligand Systems: Reassessment of Values and Periodic Trends. In *Organometallic Ion Chemistry*, Freiser, B. S., Ed. Kluwer Academic Publishers: Dordrecht, The Netherlands, **1994**; pp 1-45.

Asmis, K. R.; Sauer, J., Mass-selective vibrational spectroscopy of vanadium oxide cluster ions. *Mass Spec. Rev.* **2007,** 26, 542-562.

Baik, M. H.; Newcomb, M.; Friesner, R. A.; Lippard, S. J., Mechanistic Studies on the Hydroxylation of Methane by Methane Monooxygenease. *Chem. Rev.* **2003,** 103, 2385.

Baranov, V.; Bohme, D. K., Reactions of Fe^+ Coordinated to the Pi-Donating Ligands C_2H_4, c-C_5H_5, C_6H_6 and C_{60} with N_2O and CO - Probing the Bonding in $(C_{60})Fe^+$. *Int. J. Mass Spectrom. Ion Process.* **1995,** 149, 543-553.

Baranov, V.; Javahery, G.; Hopkinson, A. C.; Bohme, D. K., Intrinsic Coordination Properties of Iron in FeO^+: Kinetics at 294 ± 3 K for Gas-Phase Reactions of the Ground States of Fe^+ and FeO^+ with Inorganic Ligands Containing Hydrogen, Nitrogen, and Oxygen. *J. Am. Chem. Soc.* **1995,** 117, 12801-12809.

Barton, D. H. R., The Invention of Chemical Reactions. *Aldrichim. Acta* **1990,** 23, 3-10.

Becker, H.; Schröder, D.; Zummack, W.; Schwarz, H., Generation, Fragmentation, and Interconversion Processes of $[Fe,C_6,H_6,O]^+$ Isomers Relevant for the Oxygenation of Aromatic Hydrocarbons. *J. Am. Chem. Soc.* **1994,** 116, 1096-1100.

Bieske, E. J.; Dopfer, O., High-Resolution Spectroscopy of Cluster Ions. *Chem. Rev.* **2000,** 100, 3963-3998.

Bohme, D. K.; Schwarz, H., Gas-Phase Catalysis by Atomic and Cluster Metal Ions: The Ultimate Single-Site Catalysts. *Angew. Chem. Int. Ed. Engl.* **2005,** 44, 2336-2354.

Boyarkin, O. V.; Kowalczyk, M.; Rizzo, T. R., Collisionally Enhanced Isotopic Selectivity in Multiphoton Dissociation of Vibrationally Excited CF_3H. J. Chem. Phys. 2003, 118, 93-103.

Boyarkin, O. V.; Lubich, L.; Settle, R. D. F.; Perry, D. S.; Rizzo, T. R., Intramolecular energy transfer in highly vibrationally excited methanol.1. Ultrafast dynamics. *J. Chem. Phys.* **1997,** 107, 8409-8422.

Boyarkin, O. V.; Rizzo, T. R.; Rueda, D. S.; Quack, M.; Seyfang, G., Nonlinear Intensity Dependence in the Infrared Multiphoton Excitation of Methanol Preexcited to Different Energies. *J. Chem. Phys.* **2002,** 117, 9793-9805.

Boyarkin, O. V.; Settle, R. D. F.; Rizzo, T. R., Vibrational Overtone Spectra of Jet-Cooled CF_3H by Infrared-Laser Assisted Photofragment Spectroscopy. *Ber. Bunsen-Ges. Phys. Chem. Chem. Phys.* **1995,** 99, 504-513.

Chackerian, C.; Chance, K.; Coudert, L.H.; Dana, V.; Devi, V. M.; Flaud, J.M.; Gamache, R.R.; Goldman, A.; Hartmann, J.M.; Jucks, K.W.; Maki, A.G.; Mandin, J.Y.; Massie, S.T.; Orphal, J.; Perrin, A.; Rinsland, C.P.; Smith, M.A.H.; Tennyson, J.; Tolchenov, R.N.; Toth, R.A.; Vander Auwera, J.; Varanasi, P.; Wagner, G., The HITRAN 2004 Molecular Spectroscopic Database *J. Quant. Spec. Radiat. Transfer* **2005,** 96, 139.

Chen, M. S.; White, M. C., A predictably selective aliphatic C-H oxidation reaction for complex molecule synthesis. *Science* **2007,** 318, 783-787.

Chen, Y.-M.; Clemmer, D. E.; Armentrout, P. B., Conversion of CH_4 to CH_3OH: Reactions of CoO^+ with CH_4 and D_2, Co^+ with CH_3OD and D_2O, and $Co^+(CH_3OD)$ with Xe. *J. Am. Chem. Soc.* **1994,** 116, 7815.

Citir, M.; Altinay, G.; Metz, R. B., Electronic and Vibrational Spectroscopy and Vibrationally Mediated Photodissociation of $V^+(OCO)$. *J. Phys. Chem. A* **2006,** 110, 5051-5057.

Corcelli, S. A.; Kelley, J. A.; Tully, J. C.; Johnson, M. A., Infrared Characterization of the Icosahedral Shell Closing in $Cl^-\cdot H_2O\cdot Ar_n$ ($1 \leq n \leq 13$) Clusters. *J. Phys. Chem. A* **2002,** 106, 4872-4879.

Cornett, D. S.; Peschke, M.; Laitting, K.; Cheng, P. Y.; Willey, K. F.; Duncan, M. A., Reflectron Time-of-Flight Mass Spectrometer for Laser Photodissociation. *Rev. Sci. Instrum.* **1992,** 63, 2177.

Crabtree, R. H., Aspects of Methane Chemistry. *Chem. Rev.* **1995,** 95, 987-1007.

Crim, F. F., Vibrationally Mediated Photodissociation: Exploring Excited-State Surfaces and Controlling Decomposition Pathways. *Annu. Rev. Phys. Chem.* **1993,** 44, 397.

Danovich, D.; Shaik, S., Spin-orbit coupling in the oxidative activation of H-H by FeO+. Selection rules and reactivity effects. *J. Am. Chem. Soc.* **1997,** 119, 1773.

Demtröder, W., *Laser Spectroscopy : Basic Concepts and Instrumentation*. third ed.; Springer: Berlin ; New York, **2003**.

DeSelms, R. H. *UV-Active Phenol Ester Compounds*; Washington, DC, **2008**.

Dietrich, G.; Kruckeberg, S.; Lutzenkirchen, K.; Schweikhard, L.; Walther, C., The interaction of gold clusters with methanol molecules: Infrared photodissociation of mass-selected Au_n^+ $(CH_3OH)_m$. J. Chem. Phys. **2000**, 112, 752-760.

Dolg, M.; Wedig, U.; Stoll, H.; Preuss, H., Abinitio Pseudopotential Study of the 1st Row Transition-Metal Monoxides and Iron Monohydride. *J. Chem. Phys.* **1987,** 86, 2123-2131.

Dopfer, O., Spectroscopic and theoretical studies of CH_3^+-Rg_n clusters (Rg = He, Ne, Ar): From weak intermolecular forces to chemical reaction mechanisms. *Int. Rev. Phys. Chem.* **2003,** 22, 437-495.

Douberly, G. E.; Ricks, A. M.; Schleyer, P. V. R.; Duncan, M. A., Infrared spectroscopy of gas phase benzenium ions: Protonated benzene and protonated toluene, from 750 to 3400 cm^{-1}. *J. Phys. Chem. A* **2008,** 112, 4869-4874.

Dunbar, R. C., Photodissociation of Trapped Ions. *Int. J. Mass Spectrom.* **2000,** 200, 571-589.

Duncan, M. A., Frontiers in the Spectroscopy of Mass-Selected Molecular Ions. *Int. J. Mass Spectrom.* **2000,** 200, 545-569.

Duncan, M. A., Infrared Spectroscopy to Probe Structure and Dynamics in Metal Ion-molecule Complexes. *Int. Rev. Phys. Chem.* **2003,** 22, 407-435.

Eller, K.; Schwarz, H., Organometallic Chemistry in the Gas Phase. *Chem. Rev.* **1991,** 91, 1121-1177.

Feller, D., *Ab Initio* Study of M^+:18-Crown-6 Microsolvation. *J. Phys. Chem. A* **1997,** 101, 2723-2731.

Frisch, M. J.; Trucks, G. W.; Schlegel, H. B.; Scuseria, G. E.; Robb, M. A.; Cheeseman, J. R.; Montgomery Jr., J. A.; Vreven, T.; Kudin, K. N.; Burant, J. C.; Millam, J. M.; Iyengar, S. S.; Tomasi, J.; Barone, V.; Mennucci, B.; Cossi, M.; Scalmani, G.; Rega, N.; Petersson, G. A.; Nakatsuji, H.; M.Hada; Ehara, M.; Toyota, K.; Fukuda, R.; Hasegawa, J.; Ishida, M.; Nakajima, T.; Honda, Y.; Kitao, O.; Nakai, H.; Klene, M.; Li, X.; Knox, J. E.; Hratchian, H. P.; Cross, J. B.; Adamo, C.; Jaramillo, J.; Gomperts, R.; Stratmann, R. E.; Yazyev, O.; Austin, A. J.; Cammi, R.; Pomelli, C.; Ochterski, J. W.; Ayala, P. Y.; Morokuma, K.; Voth, G. A.; Salvador, P.; Dannenberg, J. J.; Zakrzewski, V. G.; Dapprich, S.; Daniels, A. D.; Strain, M. C.; Farkas, O.; Malick, D. K.; Rabuck, A. D.; Raghavachari, K.; Foresman, J. B.; Ortiz, J. V.; Cui, Q.; Baboul, A. G.; Clifford, S.; Cioslowski, J.; Stefanov, B. B.; Liu, G.; Liashenko, A.; Piskorz, P.; Komaromi, I.; Martin, R. L.; Fox, D. J.; Keith, T.; Al-Laham, M. A.; Peng, C. Y.; Nanayakkara, A.; Challacombe, M.; Gill, P. M. W.; Johnson, B.; Chen, W.; Wong, M. W.; Gonzalez, C.; Pople, J. A. *Gaussian 03*, Gaussian, Inc.: Pittsburgh PA, Wallingford CT, **2004**.

Furuya, A.; Tsuruta, M.; Misaizu, F.; Ohno, K.; Inokuchi, Y.; Judai, K.; Nishi, N., Infrared photodissociation spectroscopy of $Al^+(CH_3OH)_n$ (n=1-4). *J. Phys. Chem. A* **2007,** 111, 5995-6002.

Georgiadis, R.; Fisher, E. R.; Armentrout, P. B., Neutral and Ionic Metal Hydrogen and Metal-Carbon Bond-Energies - Reactions of Co^+, Ni^+, and Cu^+ with Ethane, Propane, Methylpropane, and Dimethylpropane. *J. Am. Chem. Soc.* **1989,** 111, 4251-4262.

Glukhotsev, M.; Bach, R. D.; Pross, A.; Radom, L., "The Performance of B3-LYP Density Functional Theory in Describing S_N2 Reactions at Saturated Carbon," *Chem. Phys. Lett.* **1996,** 260, 558-564.

Glukhovtsev, M. N.; Bach, R. D.; Nagel, C. J., Performance of the B3LYP/ECP DFT Calculations of Iron-Containing Compounds. *J. Phys. Chem. A* **1997,** 101, 316-323.

Goeppert, A.; Prakash, G. K. S., *Beyond Oil and Gas: The Methanol Economy*. Wiley: Weinheim, **2006**.

Hall, C.; Perutz, R. N., Transition metal alkane complexes. *Chem. Rev.* **1996,** 96, 3125-3146.

Hammer, N. I.; Diken, E. G.; Roscioli, J. R.; Johnson, M. A.; Myshakin, E. M.; Jordan, K. D.; McCoy, A. B.; Huang, X.; Bowman, J. M.; Carter, S., The Vibrational Predissociation Spectra of the $H_5O_2^+ \bullet RG_n$ (RG=Ar,Ne) Clusters: Correlation of the Solvent Perturbations in the Free OH and Shared Proton Transitions of the Zundel Ion. *J. Chem. Phys.* **2005,** 122, Art. No. 244301.

Hirabayashi, S.; Okawa, R.; Ichihashi, M.; Kawazoe, Y.; Kondow, T., Structures and reactions of methanol molecules on cobalt cluster ions studied by infrared photodissociation spectroscopy. J. Chem. Phys. **2009**, 130, 164304.

Hirabayashi, S.; Okawa, R.; Ichihashi, M.; Kondow, T., Detection of OH stretching mode of CH3OH chemisorbed on Ni3+ and Ni4+ by infrared photodissociation spectroscopy. Journal of Physical Chemistry A. **2007**, 111, 7664-7669.

Honovich, J. P.; Dunbar, R. C., Vibrational Spectroscopy and Photo-Dissociation Properties of Ions as Determined by Two-Laser Photo-Dissociation Techniques. *J. Phys. Chem.* **1983,** 87, 3755-3758.

Husband, J.; Aguirre, F.; Ferguson, P.; Metz, R. B., Vibrationally Resolved Photofragment Spectroscopy of FeO^+. *J. Chem. Phys.* **1999,** 111, 1433-1437.

Jacobson, D. B.; Freiser, B. S., Studies of the Reactions of Group-8 Transition-Metal Ions Fe^+, Co^+, and Ni^+ with Linear Alkanes - Determination of Reaction-Mechanisms and $MC_nH_{2n}^+$ Ion Structures Using Fourier-Transform Mass-Spectrometry Collision-Induced Dissociation. *J. Am.Chem. Soc.* **1983,** 105, 5197-5206.

Kaur, D.; Desouza, A. M.; Wanna, J.; Hammad, S. A.; Mercorelli, L.; Perry, D. S., Multipass Cell for Molecular-Beam Absorption-Spectroscopy. *Appl. Optics* **1990,** 29, 119-124.

Kellogg, C. B.; Irikura, K. K., Gas-phase Thermochemistry of Iron Oxides and Hydroxides: Portrait of a Super-efficient Flame Suppressant. *J. Phys. Chem. A* **1999,** 103, 1150-1159.

Kulik, H. J.; Marzari, N., A self-consistent Hubbard U density-functional theory approach to the addition-elimination reactions of hydrocarbons on bare FeO^+. *J. Chem. Phys.* **2008,** 129, 134314.

Kwapien, K.; Broclawik, E., Interaction of FeO^+ cation with benzene, aniline, and 3-methylaniline: DFT study of oxygen insertion mechanism. *Int. J. Quantum Chem.* **2008,** 108, 2016-2022.

Lagutschenkov, A.; Sinha, R.K.; Maitre, P.; Dopfer, O., Structure and Infrared Spectrum of the Ag^+-Phenol Ionic Complex. submitted to J. Phys. Chem. A. **2010**.

Lias, S. G.; Bartmess, J. E.; Liebman, J. F.; Holmes, J. L.; Levin, R. D.; Mallard, W. G., Gas-Phase Ion and Neutral Thermochemistry. *J. Phys. Chem. Ref. Data* **1988,** 17, 1-861.

Lieberman, R. L.; Rosenzweig, A. C., Crystal Structure of a Membrane-Bound Metalloenzyme that Catalyses the Biological Oxidation of Methane. *Nature* **2005,** 434, 177-182.

Lu, W. Y.; Wong, T. H.; Sheng, Y.; Lytle, A. T.; Kleiber, P. D., Photodissociation Spectroscopy of Zn^+-Methanol. *J. Phys. Chem. A* **2003,** 107, 984-989.

Lunsford, J. H., Catalytic Conversion of Methane to more Useful Chemicals and Fuels: a Challange for the 21st Century. *Catal. Today* **2000,** 63, 165-174.

MacAleese, L.; Maitre, P., Infrared spectroscopy of organometallic ions in the gas phase: From model to real world complexes. Mass Spectrom. Rev. **2007**, 26, 583-605.

Machinaga, H.; Ohashi, K.; Inokuchi, Y.; Nishi, N.; Sekiya, H., Infrared photodissociation spectra and solvation structures of $Mg^+(CH_3OH)_n$ (n=1-4). Chem. Phys. Lett. **2004**, 391, 85-90.

Maitre, P.; Le Caer, S.; Simon, A.; Jones, W.; Lemaire, J.; Mestdagh, H. N.; Heninger, M.; Mauclaire, G.; Boissel, P.; Prazeres, R.; Glotin, F.; Ortega, J. M., Ultrasensitive Spectroscopy of Ionic Reactive Intermediates in the Gas Phase Performed with the First Coupling of an IR FEL with an FTICR-MS. *Nucl. Instrum. Meth. A* **2003,** 507, 541-546.

Metz, R. B., Photofragment Spectroscopy of Covalently Bound Transition Metal Complexes: A Window into C-H and C-C Bond Activation by Transition Metal Ions. *Int. Rev. Phys. Chem.* **2004,** 23, 79-108.

Metz, R. B., Spectroscopy of the Potential Energy Surfaces for C-H and C-O Bond Activation by Transition Metal and Metal Oxide Cations. *Adv. Chem. Phys.* **2008,** 138, 331-373.

Metz, R. B.; Nicolas, C.; Ahmed, M.; Leone, S. R., Direct Determination of the Ionization Energies of FeO and CuO with VUV Radiation. *J. Chem. Phys.* **2005,** 123, 114313.

Meyer, F.; Khan, F. A.; Armentrout, P. B., Thermochemistry of Transition-Metal Benzene Complexes - Binding-Energies of $M(C_6H_6)(X)^+$ (X=1, 2) for M=Ti to Cu. *J. Am. Chem. Soc.* **1995,** 117, 9740-9748.

Montgomery Jr, J. A.; Frisch, M. J.; Ochterski, J. W.; Petersson, G. A., A complete basis set model chemistry. Use of the minimum population localization method. *J. Chem. Phys.* **2000,** 112, 6532-6542.

Montgomery Jr, J. A.; Frisch, M. J.; Ochterski, J. W.; Petersson, G. A., A complete basis set model chemistry. VI. Use of density functional geometries and frequencies. *J. Chem. Phys.* **1999,** 110, 2822-2827.

Moore, C. E., *Atomic Energy Levels, Circular 467; National Bureau of Standards.* **1953,** 2.

Niwa, S.; Eswaramoorthy, M.; Nair, J.; Raj, A.; Itoh, N.; Shoji, H.; Namba, T.; Mizukami, F., A one-step conversion of benzene to phenol with a palladium membrane. *Science* **2002,** 295, 105-107.

Noll, R. J.; Yi, S. S.; Weisshaar, J. C., Bimolecular Ni^+ ($^2D_{5/2}$) + C_3H_8 Reaction Dynamics in Real Time. *J. Phys. Chem. A* **1998,** 102, 386-394.

Okumura, M.; Yeh, L. I.; Meyers, J. D.; Lee, Y. T., Infrared Spectra of the Cluster Ions $H_7O_3^+$-H_2 and $H_9O_4^+$-H_2. *J. Chem. Phys.* **1986,** 85, 2328-2329.

Olah, G. A., Electrophilic Methane Conversion. *Acc. Chem. Res.* **1987,** 20, 422.

Olah, G. A.; Raja, R.; Ratnasamy, P., Direct Conversion of Methane to Methanol. *Appl. Catal. A General* **1997,** 158, L7-L15.

Oomens, J.; Sartakov, B. G.; Meijer, G.; Von Helden, G., Gas-Phase Infrared Multiple Photon Dissociation Spectroscopy of Mass-Selected Molecular Ions. *Int. J. Mass Spectrom.* **2006,** 254, 1-19.

Ortiz de Montellano, P. R., *Cytochrome P450: Structure, Mechanism, and Biochemistry*. Third ed.; Kluwer Academic/Plenum Publishers: New York, 2004.

Otsuka, K.; Wang, Y., Direct Conversion of Methane into Oxygenates. *Appl. Catal. A* **2001,** 222, 145.

Panov, G. I., Advances in Oxidation Catalysis: Oxidation of Benzene to Phenol by Nitrous Oxide *Cattech* **2000,** 4, 18-31.

Park, M.; Hauge, R. H.; Kafafi, Z. H.; Margrave, J. L., Activation of O-H and C-O Bonds of Methanol by Photoexcited Iron Atoms. *J. Chem. Soc. Chem. Comm.* **1985**, 1570-1571.

Periana, R. A.; Taube, D. J.; Gamble, S.; Taube, H.; Satoh, T.; Fujii, H., Platinum Catalysts for the High-Yield Oxidation of Methane to a Methanol Derivative. *Science* **1998,** 280, 560-564.

Roscioli, J. R.; Diken, E. G.; Johnson, M. A.; Horvath, S.; McCoy, A. B., Prying apart a water molecule with anionic H-bonding: A comparative spectroscopic study of the X-center dot H_2O (X = OH, O, F, Cl, and Br) binary complexes in the 600-3800 cm^{-1} region. *J. Phys. Chem. A* **2006,** 110, 4943-4952.

Rosenwaks, S. Z., *Vibrationally Mediated Photodissociation*. The Royal Society of Chemistry: Cambridge, 2009.

Rothman, L.S.; Jacquemart, D.; Barbe, A.; Benner, D.C.; Birk, M.; Brown, L.R.; Carleer, M.R. Chackerian C.; Chance K.; Dana V.; Devi V.M.; Flaud J-M.; Gamache R.R.; Goldman A.; Hartmann J-M.; Jucks K.W.; Maki A.G.; Mandin J-Y.; Massie S.T.; Orphal J.; Perrin A.; Rinsland C.P.; Smith M.A.H.; Tennyson J.; Tolchenov R.N.; Toth R.A.; Vander A.J.; Varanasi P.; Wagner G. The HITRAN 2004 Molecular Spectroscopy Database, *J. Quant. Spec. Radiat. Transfer* **2004**.

Ryan, M. F.; Stockigt, D.; Schwarz, H., Oxidation of Benzene Mediated by First-Row Transition-Metal Oxide Cations - the Reactivity of ScO^+ through NiO^+ in Comparison. *J. Am. Chem. Soc.* **1994,** 116, 9565-9570.

Schlosser, P. M.; Bond, J. A.; Medinsky, M. A., Benzene and Phenol Metabolism by Mouse and Rat-Liver Microsomes. *Carcinogenesis* **1993,** 14, 2477-2486.

Schröder, D.; Fiedler, A.; Hrusák, J.; Schwarz, H., Experimental and Theoretical Studies Toward a Characterization of Conceivable Intermediates Involved in the Gas-Phase Oxidation of Methane by Bare FeO^+. Generation of Four Distinguishable $[Fe,C,H_4,O]^+$ Isomers. *J. Am. Chem. Soc.* **1992,** 114, 1215-1222.

Schröder, D.; Schwarz, H., Benzene Oxidation By 'Bare' FeO^+ in the Gas Phase. *Helv. Chim. Acta* **1992,** 75, 1281-1287.

Schröder, D.; Schwarz, H., C-H and C-C Bond Activation by Bare Transition-Metal Oxide Cations in the Gas Phase. *Angew. Chem. Int. Ed. Engl.* **1995,** 34, 1973-1995.

Schröder, D.; Schwarz, H., FeO^+ Activates Methane. *Angew. Chem. Intl. Ed. Engl.* **1990,** 29, 1433-1434.

Schroder, D.; Schwarz, H., Gas-phase activation of methane by ligated transition-metal cations. *Proc. Nat. Acad. Sci.* **2008,** 105, 18114-18119.

Schröder, D.; Schwarz, H.; Clemmer, D. E.; Chen, Y.; Armentrout, P. B.; Baranov, V.; Bohme, D. K., Activation of Hydrogen and Methane by Thermalized FeO^+ in the Gas Phase as Studied by Multiple Mass Spectrometric Techniques. *Int. J. Mass Spectrom. Ion Proc.* **1997,** 161, 175-191.

Schröder, D.; Schwarz, H.; Shaik, S., Characterization, Orbital Description, and Reactivity Patterns of Transition-Metal Oxo Species in the Gas Phase. *Struct. Bonding* **2000,** 97, 91-123.

Schröder, D.; Shaik, S.; Schwarz, H., Two-State Reactivity as a New Concept in Organometallic Chemistry. *Acc. Chem. Res.* **2000,** 33, 139-145.

Shaik, S.; Hirao, H.; Kumar, D., Reactivity of high-valent iron-oxo species in enzymes and synthetic reagents: A tale of many states. *Acc. Chem. Res.* **2007,** 40, 532-542.

Shilov, A. E.; Shul'pin, G. B., Activation of C-H bonds by metal complexes. *Chem. Rev.* **1997,** 97, 2879-2932.

Shimanouchi, T., Molecular Vibrational Frequencies. In NIST Chemistry WebBook, NIST Standard Reference Database Number 69, Linstrom, P. J.; Mallard, W. G., Eds. National Institute of Standards and Technology: Gaithersburg MD, 1972.

Shiota, Y.; Suzuki, K.; Yoshizawa, K., Mechanism for the Direct Oxidation of Benzene to Phenol by FeO^+. *Organometallics* **2005,** 24, 3532-3538.

Shiota, Y.; Yoshizawa, K., A Spin-Orbit Coupling Study on the Spin Inversion Processes in the Direct Methane-to-Methanol Conversion by FeO^+. *J. Chem. Phys.* **2003,** 118, 5872-5879.

Shiota, Y.; Yoshizawa, K., Methane-to-Methanol Conversion by First-Row Transition-Metal Oxide Ions: ScO^+, TiO^+, VO^+, CrO^+, MnO^+, FeO^+, CoO^+, NiO^+, and CuO^+. *J. Am. Chem. Soc.* **2000,** 122, 12317-12326.

Simon, A.; Jones, W.; Ortega, J. M.; Boissel, P.; Lemaire, J.; Maitre, P., Infrared Multiphoton Dissociation Spectroscopy of Gas-Phase Mass-Selected Hydrocarbon-Fe^+ Complexes. *J. Am. Chem. Soc.* **2004,** 126, 11666-11674.

Solca, N.; Dopfer, O., Microsolvation of the Phenol Cation (Ph^+) in Nonpolar Environments: Infrared Spectra of Ph^+-L_n (L=He, Ne, Ar, N_2, CH_4). *J. Phys. Chem. A* **2001,** 105, 5637-5645.

Stockigt, D.; Schwarz, H., Reactivity Tuning by Ligand Effects - Gas-Phase Reactions of $Fe(C_6H_6)O^+$ Versus Bare FeO^+. *Chemische Berichte* **1994,** 127, 2499-2503.

Taboada, J. B., *Direct Oxidation of Benzene to Phenol: Investigation of the active iron species in [Fe,Al]MFI catalysts by ^{57}Fe Mössbauer spectroscopy*. Delft University Press: Amsterdam, **2006**; p 172.

Tao, Y.; Fishman, A.; Bentley, W. E.; Wood, T. K., Oxidation of benzene to phenol, catechol, and 1,2,3-trihydroxybenzene by toluene 4-monooxygenase of Pseudomonas mendocina KR1 and toluene 3-monooxygenase of Ralstonia pickettii PKO1. *Appl. Environ. Microbiol.* **2004,** 70, 3814-3820.

Tjelta, B. L.; Walter, D.; Armentrout, P. B., Determination of weak Fe^+-L bond energies (L = Ar, Kr, Xe, N-2, and CO_2) by ligand exchange reactions and collision-induced dissociation. *Int. J. Mass Spectrom.* **2001,** 204, 7-21.

Tonkyn, R.; Ronan, M.; Weisshaar, J. C., Multicollision Chemistry of Gas-Phase Transition Metal Ions with Small Alkanes. *J. Phys. Chem.* **1988,** 92, 92.

Vaden, T. D.; Lisy, J. M., Characterization of Hydrated Na^+(Phenol) and K^+(Phenol) Complexes using Infrared Spectroscopy. *J. Chem. Phys.* **2004,** 120, 721-730.

Vaden, T. D.; Lisy, J. M.; Carnegie, P. D.; Pillai, E. D.; Duncan, M. A., Infrared Spectroscopy of the $Li^+(H_2O)Ar$ complex: the role of internal energy and its dependence on ion preparation. *Phys. Chem. Chem. Phys.* **2006,** 8, 3078-3082.

Valle, J. J.; Eyler, J. R.; Oomens, J.; Moore, D. T.; van der Meer, A. F. G.; von Helden, G.; Meijer, G.; Hendrickson, C. L.; Marshall, A. G.; Blakney, G. T., Free electron laser-Fourier transform ion cyclotron resonance mass spectrometry facility for obtaining infrared multiphoton dissociation spectra of gaseous ions. *R.S.I.* **2005,** 76.

Van Koppen, P. A. M.; Bowers, M. T.; Haynes, C. L.; Armentrout, P. B., Reactions of Ground-State Ti^+ and V^+ with Propane: Factors that Govern C-H and C-C Bond Cleavage Product Branching Ratios. *J. Am. Chem. Soc.* **1998,** 120, 5704-5712.

Wang, G. J.; Chen, M. H.; Zhou, M. F., Matrix Isolation Infrared Spectroscopic and Theoretical Studies on the Reactions of Manganese and Iron Monoxides with Methane. *J. Phys. Chem. A* **2004,** 108, 11273-11278.

Wang, G. J.; Zhou, M. F., Probing the intermediates in the MO + CH_4 --> M + CH_3OH reactions by matrix isolation infrared spectroscopy. *Int. Rev. Phys. Chem.* **2008,** 27, 1-25.

Wang, Y.; Otsuka, K., Catalytic Oxidation of Methane to Methanol Initiated in a Gas Mixture of Hydrogen and Oxygen. *J. Chem. Soc. Chem. Commun.* **1994**, 2209.

Watson, C. H.; Zimmerman, J. A.; Bruce, J. E.; Eyler, J. R., Resonance-Enhanced Two-Laser Infrared Multiple Photon Dissociation of Gaseous Ions. *J. Phys. Chem.* **1991,** 95, 6081-6086.

Weinheimer, C. J.; Lisy, J. M., Gas-phase cluster ion vibrational spectroscopy of $Na^+(CH_3OH)_{(2-7)}$. J. Phys. Chem. **1996**, 100, 15305-15308.

Weinheimer, C. J.; Lisy, J. M., Hydrogen bonding in metal ion solvation: Vibrational spectroscopy of $Cs^+(CH_3OH)1$-6 in the 2.8 μm region. Int. J. Mass Spectrom. Ion Process. **1996**, 159, 197-208.

Weisshaar, J. C., Bare Transition Metal Atoms in the Gas Phase: Reactions of M, M^+ and M^{+2} with Hydrocarbons. *Acc. Chem. Res.* **1993,** 26, 213-219.

Yamada, Y.; Ebata, T.; Kayano, M.; Mikami, N., Picosecond IR-UV pump-probe spectroscopic study of the dynamics of the vibrational relaxation of jet-cooled phenol. I. Intramolecular vibrational energy redistribution of the OH and CH stretching vibrations of bare phenol. *J. Chem. Phys.* **2004,** 120, 7400-7409.

Yeh, L. I.; Okumura, M.; Meyers, J. D.; Price, J. M.; Lee, Y. T., Vibrational Spectroscopy of the Hydrated Hydronium Cluster Ions $H_3O^+ \cdot (H_2O)_n$ (n=1,2,3). J. Chem. Phys. **1989**, 91, 7319-7330.

Yi, S. S.; Reichert, E. L.; Holthausen, M. C.; Koch, W.; Weisshaar, J. C., Crossed-Beam Study of $Co^+(^3F_4)$ + Propane: Experiment and Density Functional Theory. *Chem.-Eur. J.* **2000,** 6, 2232-2245.

Yoshizawa, K.; Shiota, Y.; Kagawa, Y.; Yamabe, T., Femtosecond Dynamics of the Methane-Methanol and Benzene-Phenol Conversions by an Iron-Oxo Species. *J. Phys. Chem. A* **2000,** 104, 2552-2561.

Yoshizawa, K.; Shiota, Y.; Yamabe, T., Methane-Methanol Conversion by MnO^+, FeO^+, and CoO^+: A Theoretical Study of Catalytic Activity. *J. Am. Chem. Soc.* **1998,** 120, 564-572.

Yoshizawa, K.; Shiota, Y.; Yamabe, T., Reaction pathway for the direct benzene hydroxylation by iron-ore species. *J. Am. Chem. Soc.* **1999,** 121, 147-153.